Root microbiota functions in mitigating abiotic and biotic stresses in *Arabidopsis*

Inaugural – Dissertation

Zur

Erlangung des Doktorgrades

der Mathematisch-Naturwissenschaftlichen Fakultät

der Universität zu Köln

vorgelegt von

Shiji Hou

aus Yantai, China

Köln, Oct. 2020

Berichterstatter: Prof. Dr. Paul Schulze-Lefert

Prof. Dr. Ute Höcker

Prüfungsvorsitz: Prof. Dr. Gunther Döhlemann

Tag der Disputation: 11. Jan. 2021

MAX-PLANCK-GESELLSCHAFT

Die vorliegende Arbeit wurde am Max-Planck-Institut für Pflanzenzüchtungsforschung in Köln in der Abteilung für Pflanzen-Mikroben Interaktionen (Direktor Prof. Dr. Paul Schulze-Lefert) angefertigt.

Abstract

In nature, plants face both biotic and abiotic stresses while at the same time engaging in complex interactions with a vast diversity of commensal microorganisms comprising bacteria, fungi, and oomycetes. This so-called plant microbiota is thought to promote resistance to pathogens and tolerance to specific environmental constraints, likely driving local adaptation in natural plant populations. Reductionist approaches with synthetic microbial communities assembled from microbial culture collections and gnotobiotic plant systems now allow detailed dissection of microbiota-plant-stress interactions under strictly controlled laboratory conditions. Mechanistic understanding into how the root microbiota promotes mineral nutrition and pathogen protection in plants is now emerging. However, whether belowground response to microbial root commensals and aboveground response to abiotic stresses are connected remains largely unexplored. By reconstituting a synthetic, multi-kingdom root microbiota with different microbial input ratios in two gnotobiotic systems (the calcined-clay system and the FlowPot system) (Chapter I), I first showed that distinct input ratios of bacteria, fungi, and oomycetes converge into a similar output community composition, with stable effects on *Arabidopsis* growth. By testing different abiotic and biotic stresses in three gnotobiotic plant systems (the FlowPot system, the calcined-clay system, and the white sand system) (Chapter I), I provided evidence that salt, drought, and shade stresses negatively affected plant growth across all three systems, whereas nutritional stress affected on plant performance in a system-dependent manner. Moreover, I demonstrated that a synthetic multi-kingdom root microbiota rescued *Arabidopsis* growth under salt, drought and light limitation stresses in the FlowPot system and the white sand system (Chapter I). Given the importance of light for plant growth, in chapter II, I further dissected the extent to which response to the synthetic root microbiota and light are interconnected. By manipulating light conditions (low photosynthetically active radiation, LP; end of day far red-light treatment, EODFR) in the FlowPot system, I demonstrated that microbial root commensals confer *Arabidopsis* tolerance to light limitation stresses and that reciprocally, modification in aboveground light condition shifts the composition of root microbial communities. Notably, this shift in the structure of root bacterial community significantly explains the microbiota-induced growth rescue under LP. *Arabidopsis*

transcriptome analysis revealed that immune responses in root and systemic defense responses in shoot were induced in the presence of the root microbiota under normal light conditions. These host responses were largely shut down under light limiting conditions and were correlated with increased susceptibility to unrelated leaf pathogens, implying that root microbiota-induced systemic defense responses were modulated by light. Through an extensive *Arabidopsis* mutant screen, I demonstrated that root microbiota-mediated plant survival under LP depends on jasmonic acid biosynthesis and signaling, cryptochromes and brassinosteroids. Furthermore, I present genetic evidence that orchestration of this light-dependent growth-defense trade-off requires the transcriptional regulator MYC2. The data suggest that plants can take advantage of root commensals to activate either growth or defense depending on aboveground light conditions.

Zusammenfassung

In der Natur sind Pflanzen sowohl biotischem als auch abiotischem Stress ausgesetzt. Gleichzeitig interagieren sie in einer komplexen Weise mit einer großen Vielfalt von Mikroorganismen, darunter Bakterien, Pilze und Oomyzeten die die Planzen-Mikrobiota ausmachen. Von diesen wird angenommen, dass sie die Resistenz gegen Krankheitserreger und die Toleranz gegenüber spezifischen Umwelteinflüssen fördern und so wahrscheinlich die lokale Anpassung in natürlichen Pflanzenpopulationen voran treiben. Reduktionistische Ansätze mit synthetischen mikrobiellen Lebensgemeinschaften, die aus Sammlungen mikrobieller Kulturen zusammengestellt wurden, und gnotobiotischen Pflanzensystemen ermöglichen nun die detailierte Sezierung von Wechselwirkungen zwischen Mikrobiota und Pflanzen unter Stress unter streng kontrollierten Laborbedingungen. Ein mechanistisches Verständnis darüber, wie Wurzel-Mikrobiota die Ernährung mit Mineralien und den Schutz vor Krankheitserregern bei Pflanzen fördern, zeichnet sich jetzt ab. Ob allerdings die unterirdische Reaktion auf Wurzelmikroben und die oberirdische Antwort auf abiotischen Stress zusammenhängen, ist weitgehend unerforscht und Thema der vorliegenden Arbeit.

Durch Rekonstituierung synthetischer Wurzel-Mikrobiota, bestehend aus Bakterien, Pilzen und Oomyzeten mit unterschiedlichen Input-Verhältnissen, und unter Verwendung von zwei gnotobiotischen Systemen (System mit kalziniertem Ton und FlowPot-System), zeigte ich zuerst, dass unterschiedliche Input-Verhältnisse von Bakterien, Pilzen und Oomyzeten zu einer ähnlichen Zusammensetzung der Output-Gemeinschaften konvergieren, mit stabilen Auswirkungen auf das Wachstum von *Arabidopsis*. Durch Testen verschiedener abiotischer und biotischer Belastungen in drei gnotobiotischen Pflanzensystemen (dem FlowPot-System, dem System mit kalziniertem Ton und dem System mit weißem Sand) konnte ich zeigen, dass Belastungen durch Salz, Trockenheit und Schatten das Pflanzenwachstum in allen drei Systemen beeinträchtigte, wogegen Ernährungsstress systemabhängig das Pflanzenwachstum hemmte. Außerdem konnte ich zeigen, dass synthetische Wurzel-Mikrobiota, bestehend aus Bakterien, Pilzen und Oomyzeten, das Wachstum von *Arabidopsis* unter Salzstress, Trockenheit und Lichtlimitierung im FlowPot und weißen Sand System unterstützte. Angesichts der Bedeutung des Lichts für das Pflanzenwachstum habe ich weiter untersucht, inwieweit die Reaktionen auf die synthetischen Wurzel-Mikrobiota und das Licht gekoppelt sind. Indem ich im FlowPot System die Lichtbedingungen zu niedriger photosynthetisch aktiver Strahlung (LP) oder „end of day

far red“ (EODFR) veränderte, konnte ich zeigen, dass einerseits das mikrobiologische Wurzelbiom *Arabidopsis* Toleranz gegenüber Lichtknappheit verleiht, und dass umgekehrt eine Veränderung der oberirdischen Lichtverhältnisse die Zusammensetzung des mikrobiellen Wurzelbioms verändert. Insbesondere erklärt diese Verschiebung in der Struktur der Wurzel-Mikrobiota die durch die Mikrobiota induzierte Wiederherstellung des Pflanzenwachstums unter LP Bedingungen. *Arabidopsis* Transkriptom-Analysen ergaben, dass Immunantworten in der Wurzel und systemische Abwehrreaktionen im Spross in Gegenwart der Wurzel-Mikrobiota unter normalen Lichtbedingungen induziert wurden. Unter lichtlimitierenden Bedingungen waren diese Wirtsreaktionen weitgehend abgeschaltet und gingen einher mit erhöhter Empfindlichkeit gegenüber anderen Blattpathogenen. Das impliziert, dass die durch Wurzel-Mikrobiota induzierten systemischen Abwehrreaktionen durch Licht moduliert wurden. Durch ein umfangreiches *Arabidopsis*-Mutanten-Screening konnte ich zeigen, dass das durch Wurzel-Mikrobiota bedingte Überleben von Pflanzen unter LP Bedingungen von der Jasmonsäure-Biosynthese und Jasmonsäure–Signalübertragung, Kryptochromen und Brassinosteroiden abhängt. Darüber hinaus biete ich genetische Beweise die zeigen, dass die Orchestrierung dieses lichtabhängigen Wachstum-gegenüber-Verteidigung Kompromisses den Transkriptionsregulator MYC2 benötigt. Die Daten deuten darauf hin, dass Pflanzen durch das mikrobielle Wurzelbiom profitieren können um in Abhängigkeit von den oberirdischen Lichtverhältnissen entweder das Wachstum oder die Abwehr zu aktivieren.

Abstract I
Zusammenfassung III
Chapter I 1
Effect of microbial input ratio and stress conditions on *A. thaliana* development 1
1. Introduction 1
1.1 The microbiota 1
1.2 Plant microbiota 2
1.3 Gnotobiotic systems and plant microbiota reconstitution 8
1.4 Hypothesis and research questions (Chapter I) 9
2. Experimental setup 10
3. Results 15
3.1 The assemblage of multi-kingdom microbial consortia 15
3.2 The effect of inter-kingdom microbial input ratios on host fitness 20
3.3 The effect of biotic and abiotic stresses on *Arabidopsis* growth in gnotobiotic systems 22
3.4 The effect of microbiota on plant growth under single stress 26
3.5 The effect of single stress on microbial communities in FlowPot system 29
4. DISCUSSION AND CONCLUSIONS 32
5. MATERIALS AND METHODS 35
5.1 Microbial culture collection 35
5.2 FlowPot experimental setup 36
5.3 Calcined-clay experimental setup 37
5.4 Microbial inoculation 37
5.5 Seeds sterilization and plant growth condition 38
5.6 Sample harvesting 39
5.7 Amplicon based microbial community profiling 40
5.8 Data analysis and figure generation 42
References 42
Chapter II 48
Microbiota-root-shoot axis modulation by MYC2 alleviates light limitation stress in *Arabidopsis* 48
1. INTRODUCTION 48
1.1 Plant development in response to aboveground stresses 48
1.2 Aboveground stress modulates plant-associated microbes 53
1.3 Plant-microbiota interaction helps partners cope with aboveground stress 55
1.4 Hypothesis and research questions (Chapter II) 55
2. Experimental setup 56

3. RESULTS 57
3.1 Root microbiota confers *A. thaliana* tolerance to light deficiency 57
3.2 The modification of light modulates root microbiota assembly 59
3.3 Root microbiota triggers plant prioritization of growth over defense under LP 70
3.4 Microbiota-mediated plant growth rescue under LP depends on JA, cryptochromes, and BR. 78
3.5 Shifts in the structure of root bacterial community explain plant growth rescue under LP condition 89
3.6 Priority to microbiota-induced growth over defense under LP requires MYC2 96
4. DISCUSSION 106
5. Conclusions 111
6. MATERIALS AND METHODS 113
6.1 Experimental model 113
6.2 Method Details 114
References 121
Abbreviations 130
Acknowledgement 134
Erklärung zur Dissertation 135
Curriculum vitae 136

Chapter I

Effect of microbial input ratio and stress conditions on *A. thaliana* development

1. Introduction

1.1 The microbiota

A staggering diversity of microbes colonize internal or external surfaces of any eukaryotic hosts and form ecological communities called the microbiota (**NIH HMP Working Group, 2009**). The host-associated microbiota includes archaea, bacteria, fungi, protists and viruses. Depending on the relationship with its host, microbiota members can include symbiotic, pathogenic and commensal microbes. During the course of the evolution, some microbes and their associated hosts build up synergistic relationship. In 1991, Margulis first used the holobiont concept to describe the host plants and its associated microbial symbionts as an ecological unit (**Margulis L. 1991**). In the holobiont, microbes and host influence each other and the host-associated microbiota is known to provide beneficial functions to the host linked to nutrition, pathogen protection, or immunomodulation (**Mariat et al., 2009**). In plants and animals symbiotic and pathogenic microbes were primarily studied due the fact that they affect positively or negatively host performance, respectively (**Vannier et al., 2019**). Besides symbiotic and pathogenic relationships, most host-associated microbiota members are referred to as “commensals” because they often live benignly in association with their hosts without causing diseases. However, the pathogenic potential of some commensal microorganisms can vary, thereby leading to disease when optimal environmental conditions are altered (**Berendsen et al., 2018**; **Melnyk et al., 2019**). Given the fact that commensal microbes were reported to be necessary for the development and reproductive

fitness of their hosts (**Buffie & Pamer, 2013**), recent efforts have been undertaken to better understand the role of these microbes for host health across plant and animal kingdoms. Recent examples indicate that these commensals have similar beneficial functions across plant and animal hosts, for example, modulation of nutrient uptake (**Castrillo et al., 2017**; **Harbort et al., 2020**), immune system (**Berer et al., 2011**; **Berendsen, 2012**), pathogen protections (**Ivanov, 2013**; **Vannier & Agler, 2019**). Thanks to advances in technology of molecular biology and sequencing technologies, we start to recognize the molecular basis of microbiota function. However, the underlying multiple molecular mechanisms for this phenotype are still missing.

1.2 Plant microbiota

In nature, healthy and asymptomatic plants live in association with a vast diversity of microorganisms including bacteria, fungi, protists and viruses that are collectively called the plant microbiota (**Delmotte et al., 2009**; **Lundberg et al., 2012**; **Bulgarelli et al., 2013**). Plant microbiota members colonize compartment-specific ecological niches including phylloplane, phyllosphere, rhizoplane, rhizosphere and endosphere microbiota (**Lundberg et al., 2012**; **Bulgarelli et al., 2012**; **Rastogi et al., 2013**; **Bulgarelli et al., 2013**). With the advance of next-generation sequencing technologies, culture-independent analyses studies have helped to characterize the diversity and composition of microbial communities that colonize distinct host compartments of various plant species, including the model plant *Arabidopsis thaliana* and relative species, some crop plants such as corn, barley, rice, potato, tomato and soybean, as well as tree species (**Bai et al., 2015**; **Bodenhausen et al., 2013**; **Bulgarelli et al., 2012**; **Delmotte et al., 2009**; **Horton et al., 2014**; **Lundberg et al., 2012**; **Schlaeppi et al., 2014**; **Kembel et al., 2014**; **Bulgarelli et al., 2015**; **Peiffer et al., 2013**; **Edwards et al., 2015**; **Finkel et al., 2011**; **Mendes et al., 2014**). Various studies already demonstrated that the bacterial component dominate the multi-kingdom microbial assemblages in plant-associated microbes, but fungi and other protists are also integral, yet poorly characterized components that also contribute to host health (**Hacquard et al., 2015**; **Kemen 2014**; **Hassani et al., 2018**). In the following sub-chapter paragraphs, I will outline the current knowledge about the establishment of plant microbiota including the source of plant microbiota and the factors affecting the structure of plant microbiota. Meanwhile, I will talk about the community structure of plant microbiota kingdoms including bacteria, fungi and oomycetes.

1.2.1 Plant microbiota establishment

1.2.1.1 Source inoculum of the plant microbiota

Microbes are found almost everywhere on earth, for example in soils, air, plants, animals, ocean (**Burch et al., 2014**). Plant microbiota members can originate from soils, air, seeds and plants and animals around (**Müller et al., 2016**). On earth, soil hosts the most diverse microbial sources and only a subset can colonize plant roots or leaves (**Berg, 2009**; **Burch et al., 2014**; **Thiergart et al., 2020**). This selection process is largely dependent on soil edaphic factors, host genetics, and microbe-microbe interactions (**Bahram et al., 2018**). Other sources include wind, rain or snow, those likely affecting the establishment of leaf microbiota members more than root microbiota members (**Knief et al., 2010**). During plant development, flowering and propagating, many factors, including plant growth environment, plant metabolisms, plant-microbe interactions and microbe-microbe interactions, will trigger and form specific plant microbiota depend on plant growth environment, plant species and so on (**Berg, 2009**). Therefore, plants will propagate different seed banks which contain different seed microbiota. This vertically-inherited seed-associated microbiota is believed to be an important inoculum source for the next generation plant microbiota and therefore, this specific aspect is receiving more and more attention.

1.2.1.2 Factors driving plant microbiota establishment

Environmental factors

In nature, various abiotic factors could affect plant growth and plant-associated microbial growth, either directly and indirectly (**Matthew et al., 2016**; **Bowsher et al., 2020**). The composition of phyllosphere microbial communities was shown to be more dynamic/stochastic compared to endospheric microbial communities since aboveground environmental conditions are known to fluctuate more than below ground environmental conditions. Previous studies found that various factors, above ground factors including UV radiation, rainfall, temperature, could shift the structure of leaf-associated microbial communities (**Bogino et al, 2013**; **Bouasria et al., 2012**; **Copeland et al., 2015**). Belowground factors, salinity, drought and nutrient deficiency in the soil, drive differential microbial communities. Walitang *et al.* revealed salt stress shifts rice endophytic communities and found *Pantoea, Flavobacterium, Microbacterium, Enterobacter, Kosakonia* and *Curtobacterium* are

dominant bacterial groups under salt stress (**Walitang et al., 2018**). In legume plants, phosphate availability is directly related with the colonization-efficiency of arbuscular mycorrhiza (**Oldroyd et al., 2011**). Arbuscular mycorrhiza symbioses improve the host update of phosphate and nitrogen and dive the communities of nitrogen-fixing bacteria (**Parniske et al., 2008**). Stringlis *et al.* showed available iron concentration is related with the structure of root-associated microbial community (**Stringlis et al. 2018**). Besides abiotic factors, some biotic factors also were proved that changing the structure of plant-associated microbial communities (**Kong et al., 2016**). Kong *et al.* found that two weeks whitefly infestation significantly increased the *Pseudomonadale*s population and the class of *Gammaproteobacteria* in plant rhizosphere indicating aboveground insects could modulate the structure of belowground microbial community (**Kong et al., 2016**). Recently, Thiergart et al. found that pH in soil drove bacterial root microbiota assemble and climate primarily drove fungal community differentiation across sites in Europe (**Thiergart et al., 2020**).

Host genetics

Besides the external factors, from the site of plants, plant genotype also influences plant-associated microbiota. Several studies reported that distinct plants host different phyllosphere communities (**Agler et al., 2016; Horton et al., 2014**). The study from Agler *et al.* found different host genotypes host different phyllosphere communities through sampling various *A. thaliana* populations in the field at the same timepoint and manipulating host colonization experiments under strict lab condition (**Agler et al., 2016**). Similarly, Wagner et al. found that the plant genotypes influenced leaf-associated microbiota but not root microbiota through investigating the leaf- and root-associated microbiota of five B. stricta genotypes (**Wagner et al., 2016**). Recently, Xiong et al. demonstrated that maize microbiome assembly was affected more strongly by host species than by environmental factors (**Xiong et al., 2020**).

Microbe-microbe interactions

Another internal factor, microbe-microbe's interactions, also shifts the structure of plant-associated microbial communities (**Hassani et al., 2018**; **Carlström et al. 2019**). Mendes et al. identified *Proteobacteria* bacteria involved in suppression of a fungal root pathogen *Rhizoctonia solani* indicating that plants could hire beneficial bacteria for protection against pathogen infections upon attack by pathogens (**Mendes et al., 2014**). More

recently, Chapelle *et al.* reported that roots infected by the fungal pathogen *Rhizoctonia solani* significantly enriched for *Oxalobacteraceae, Burkholderiaceae, Sphingobacteriaceae* and *Sphingomonadaceae* in the rhizosphere of sugar beet seedlings (**Chapelle et al., 2016**). Given the fact that individual bacterial, fungal and oomycetal strains can be isolated and cultivated under laboratory conditions (**Bai et al., 2015**; **Durán et al., 2018**), it becomes possible to test the extent to which interactions between bacteria, fungi and oomycetes affect microbial community composition and plant health. By inoculating mono and multi-kingdom bacterial, fungal and oommycetal communities on germ-free *A. thaliana*, Durán *et al.* demonstrated that a major physiological function of bacterial root commensals is to protect roots from extensive colonization by filamentous eukaryotes, which maintains optimal microbial inter-kingdom balance in roots and promotes host survival (**Durán et al., 2018**). Although many of the aforementioned examples indicate that direct microbe-microbe interactions the cause of microbial community shifts in rhizosphere or root compartments, it remains possible that at least part of these community shifts can occur indirectly via microbial interaction-induced change in the host metabolism.

1.2.2 Plant microbiota kingdoms

As discussed above, plant microbiota contains bacteria, fungi, oomycetes and protists and viruses. Bacteria is known as the highly abundant microbes in plant microbiota (**Hacquard et al., 2015**). Bulgarelli *et al.* found that Bacterial families *Comamonadaceae*, *Flavobacteriaceae*, and *Rhizobiaceae* were the dominated strains in the barley root-asscocated microbiota (**Bulgarelli et al., 2015**). Besides bacteria, fungi and oomycetes also colonize in plant and are related with plant development, fitness and immunity (**Hacquard et al., 2015**). Through characterizing tropical forests' fungal communities in the western Amazon basin, Peay *et al.* found that fungal diversities are strongly correlated with the diversities of trees suggesting that the diversity of fungal communities could regulate the diversity of tropical trees directly or indirectly (**Peay et al., 2013**). In contrast with the bacterial and fungal richness in plant microbiota, oomycetes are known as less enrichment and less diversity in plant microbiota (**Coince et al., 2013**; **Kamoun et al., 2015**). Notably, based on the current knowledge, most of oomycetes are pathogenic or neutral for plants (**Kamoun et al., 2015**). With the advance of next-generation sequencing technology and cultivation-independent technology, the single strains of bacteria, fungi and oomycetes could be isolated and independent cultivated under laboratory condition (**Coince et al., 2013**; **Bai et al., 2015**).

1.2.3 Plant microbiota and host health

The plant microbiota plays an important role on plant growth and health by promoting plant nutrients uptake, by enhancing plant defense towards various insects and pathogens, and by alleviating plant abiotic stresses (**Müller et al., 2016**).

1.2.3.1 Nutrient uptake

Plant microbiota is well known to improve nutrients uptake or availability for plants resulting in host growth promotion especially under nutrients deficient conditions (**Udvardi and Poole, 2013**; **Castrillo et al., 2017**; **Stringlis et al., 2018**; **Hiruma et al., 2016**). In symbiotic relationship, symbiotic microbes, for example arbuscular mycorrhizal fungi (AMF) and rhizobia, are long well studied functions of providing host phosphate and fixing nitrogen for hosts (**Smith et al., 2011**; **Udvardi and Poole, 2013**). Several lines of evidence indicate that response to microbial commensals and response to nutrients (i.e. P, N, iron) are tightly linked (**Castrillo et al., 2017**; **Stringlis et al., 2018**; **Voges et al., 2019**; **Zhang et al., 2019**; **Harbort et al., 2020**). For example, host genetic components involved in phosphate starvation response (i.e. PHR1, *A. thaliana*), nitrogen uptake (NRT1.1B, rice), or iron-mobilizing compounds (i.e. coumarins) shape root microbiota assembly. Conversely, signals from synthetic bacterial communities were found to interact with these same genetic components to promote plant growth under nutritional stresses. Stringlis et al. reported that rhizobacteria *P. simiae* WCS417 and *Pseudomonas capeferrum* WCS358 rescued *Arabidopsis* plants growth under iron deficiency conditions (**Stringlis et al., 2018**). Recently, the study from Harbort et al. proved that root bacterial commensals improved *Arabidopsis* plants iron nutrition through a coumarin-dependent mechanism (**Harbort et al., 2020**).

Interestingly it has been shown that a mechanistic link does exist between plant innate immunity and phosphate starvation responses in *A. thaliana*, suggesting that response to root microbiota members and nutrient starvation can be coordinated through modulation of defense responses (**Castrillo et al., 2017**; **Hacquard et al., 2016**). For example, Hacquard et al. showed that the beneficial fungal endophyte *Colletotrichum tofieldiae* activated plant defense responses in roots of *A. thaliana* facing phosphate sufficient conditions, whereas these responses were abolished under phosphate deficient conditions, to prioritize plant growth over defense (**Hacquard et al., 2016**). Consistent with this result, Castrillo et al. demonstrated that a synthetic bacterial community (SynCom)

can enhance response to phosphate limitation via the master regulator of phosphate starvation responses PHR1, which was also found to directly repress immunity, thereby exacerbating the phosphate starvation response (**Castrillo et al., 2017**). Taken together, these data suggest that phosphate starvation-induced trade-off between growth and defence in plants can be governed by signals from microbial root commensals.

1.2.3.2 Pathogen attack

Besides modulation of host nutrient status, the plant microbiota also protects plants from pathogens via direct microbe-microbe competition or microbiota-induced modulation of the host immune responses (**Vannier et al., 2019**). Plant beneficial microbes are well proved to improve plant defense against pathogens and insect herbivores via the mechanism of induced systemic resistance (ISR) (**Pieterse et al., 2014**). Santhanam et al. revealed that native bacterial isolates significantly improved tobacco *Nicotiana attenuate* resistance against fungal pathogens (**Santhanam et al., 2015**). Plant microbiota members act as a barrier in plant immune system to pathogen invasion. Ritpitakphong et al. demonstrated that the phyllosphere microbiome in *Arabidopsis* improved plants resistance to the fungal pathogen *Botrytis cinereal* (**Ritpitakphong et al., 2016**). Similarly, the study from Chen et al. proved that wheat microbiome bacteria reduced virulence and growth of a plant pathogenic fungus via manipulating fungal histone modification (**Chen et al., 2018**). Hu et al. reported that benzoxazinoids, a class of defensive secondary metabolites released by cereals roots, alter root-associated fungal and bacterial communities resulting in increasing jasmonate signaling and suppressing herbivore performance in the next plant generation suggesting that rhizosphere microbiota affect growth and defense of the next plant generation (**Hu et al., 2018**).

1.2.3.3 Other environmental stresses

Other environmental stresses

Plant microbiota is also well known as an important component alleviating plant abiotic stresses (**Castrillo et al. 2017; Fitzpatrick et al. 2018**). The study from Naylor et al. showed that root microbes improved plant drought tolerance and drought significantly drive Actinobacteria enriched in grass roots (**Naylor et al., 2017**). For example, Fitzpatrick et al. reported that root microbiota improved diverse lineages of plant species drought

tolerance and the abundance of one sequence variant strain from the genus *Streptomyces* was positively correlated with the ability of plants resistance to drought (**Fitzpatrick et al. 2018**). Berens et al. demonstrated that phyllosphere bacteria significantly improved *Arabidopsis* plants tolerance to salinity stress (**Berens et al., 2019**).

Taken together, plant microbiota plays multiple functions on host growth and health. Notably, the role of plant microbiota on host can be changed by different abiotic and biotic conditions. Gnotobiotic systems and plant microbiota reconstitution.

1.3 Gnotobiotic systems and plant microbiota reconstitution

The development of gnotobiotic plant systems (**Bai et al., 2015**; **Kremer et al., 2018**) and reference culture collections of root microbiota members (**Bai et al., 2015**; **Durán et al., 2018**) provide the possibility to reconstruct the plant microbiota under controlled laboratory conditions in order to study general ecological principles that would be otherwise impossible to address using field experiments only. Using this deconstruction-reconstruction approach, it becomes possible to test for causal relationships and study how microbe-microbe interactions and host-microbe interactions affect holobiont components under laboratory conditions (**Bai et al., 2015**; **Hacquard et al., 2016**; **Hiruma et al., 2016**; **Durán et al., 2018**; **Finkel et al., 2020**). Here, I summarize below three commonly used gnotobiotic systems that have been developed for plant microbiota research.

The Agar-plate system is the most commonly used system for gnotobiotic plant research in the laboratory. Agar-plate culture systems have been used for decades because they are cheap, it is easy to modulate nutritional status and plant growth conditions (**Xu et al., 2013**). Another advantage of agar-plate culture system is that it is possible to directly observe phenotypic traits since both shoot and root organs are directly visible and accessible. However, one major disadvantage is that it is highly artificial, especially in the context of root development. In order to mimic more natural soil conditions, calcined-clay or sand culture systems were developed by researchers working on the root microbiota. These culture systems use inert calcined-clay or sand as sterile soil matrices and plant growth is sustained by plant growth medium (i.e. MS medium). However, residual carbon

sources are extremely limited in these systems and microbial growth therefore exclusively rely on photo-assimilates from the host as sole carbon source. Recently, a third generation of gnotobiotic systems has been develop to sustain both plant and microbial growth (i.e. the FlowPot system **Kremer et al., 2018**). FlowPots contain a sterile peat substrate supplemented with vermiculite (i.e. complex carbon source) and are amenable to colonization by complex microbial communities (synthetic communities and soil slurries). The system supports growth of the model plant *A. thaliana* in the absence or presence of root commensals and allows for total-saturation of the sterile substrate by "flushing" with sterile water and/or nutrient solution via an irrigation port, which also prevents root anoxia. (**Kremer et al., 2018**).

The continuous development of more and more complex gnotobiotic plant systems, combined with the establishment of comprehensive plant-derived microbial culture collections that are largely representative of naturally occurring plant microbiomes represent key steps for the plant microbiota research field (**Daniel et al., 2016**; **Vorholt et al., 2017**). The major objective of these microbiota reconstitution experiments in gnotobiotic plant systems is to minimize environmental stochasticity through the design of experimentally tractable, yet representative synthetic communities, thereby allowing to test for causality.

1.4 Hypothesis and research questions (Chapter I)

One hypothesis is that complex microbial communities show self-organizational properties that are difficult to perturb and that modification of input ratios may not lead to dramatic change in microbial community structure and therefore host health. This hypothesis is consistent with the data obtained for the *A. thaliana* root and leaf microbiota (**Bai et al. 2015**). However, we cannot exclude the possibility that modification of input ratios will have a profound effect on host health. Another hypothesis is that root microbiota members might better promote plant growth when surrounding biotic and abiotic conditions are suboptimal.

In the first part of this chapter, experiments are therefore important to clarify whether 1) the assemblage of multi-kingdom microbial consortia is difficult to perturb and 2) whether the microbial ratio between bacteria, fungi and oomyceteshas a significant effect on *A. thaliana* health.

In the second part of this chapter, experiments are to select the adequate biotic or abiotic stresses in the

gnotobiotic systems that will be used for microbiota reconstitution experiments see (chapter II).

2. Experimental setup

In order to determine the most adequate input ratio between fungi, bacteria and oomycetes to use for microbiota reconstitution experiments, I chose two different gnotobiotic plant systems (FlowPot system and calcined-clay systems) in which the microbial communities can be manipulated as the only variable (**Figure 1**). As mentioned above, the FlowPot system has the advantage to mimic more closely natural soil texture and provides a suitable condition for both microbial and plant growth. Here, I used these two systems in order to take advantages of both systems and find adequate conditions in each system.

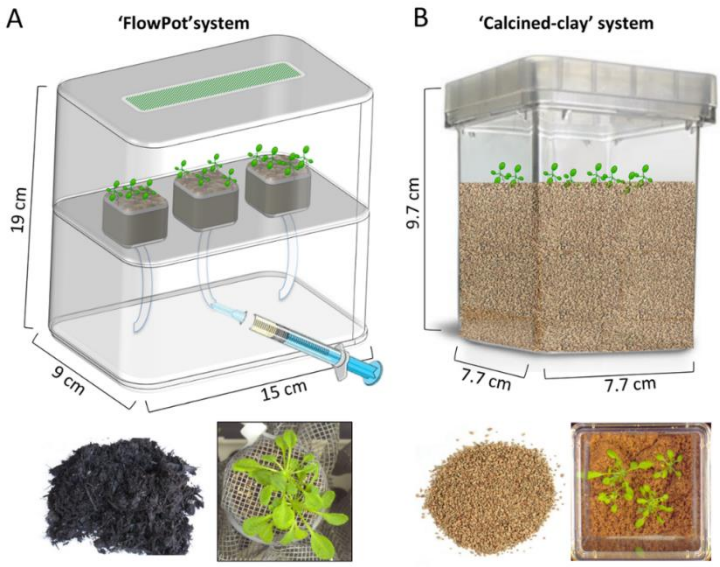

Figure 1. Illustration of the FlowPot (A) and calcined-clay (B)

For this experiment, I used taxonomically diverse microbes that were previously isolated from *A. thaliana* roots growing in the Cologne soil. I chose 183 bacterial strains, 24 fungal strains and 7 oomycetal strains (**Figure 2, Table 1**) that represent a diverse and representative set of root-associated microbes detected on *A. thaliana* roots in natural populations (Thiergart et al. 2020). In order to test whether the microbial input ratio influences host fitness, I have used two levels (high level and low level) of inoculum for each microbial group as described in the **Table 2**, leading to a total of eight different combinations of bacteria vs. fungi vs. oomycetes ratios (**Table 2**). Therefore, the sterile FlowPot and the Calcined-clay systems were repopulated with this synthetic microbial community having different inter-kingdom microbial input ratios (see below). Surface sterilized *A. thaliana* Col-0 seeds were disposed on the sterile matrices in the FlowPot and calcined-clay systems and plants were harvested five weeks (in FlowPot system) and six weeks (in calcined-clay system) post microbe inoculation. Root and matrix samples were harvest for DNA isolation and microbial community diversity and composition

was determined by amplicon sequencing. The V5V6 region of the bacterial 16S rRNA gene, the ITS1 region of the fungal Internal Transcribed Spacer (ITS) and the ITS1 region of the oomycetal ITS were amplified using barcoded primers, allowing multiplexing of all samples in a single MiSeq run.

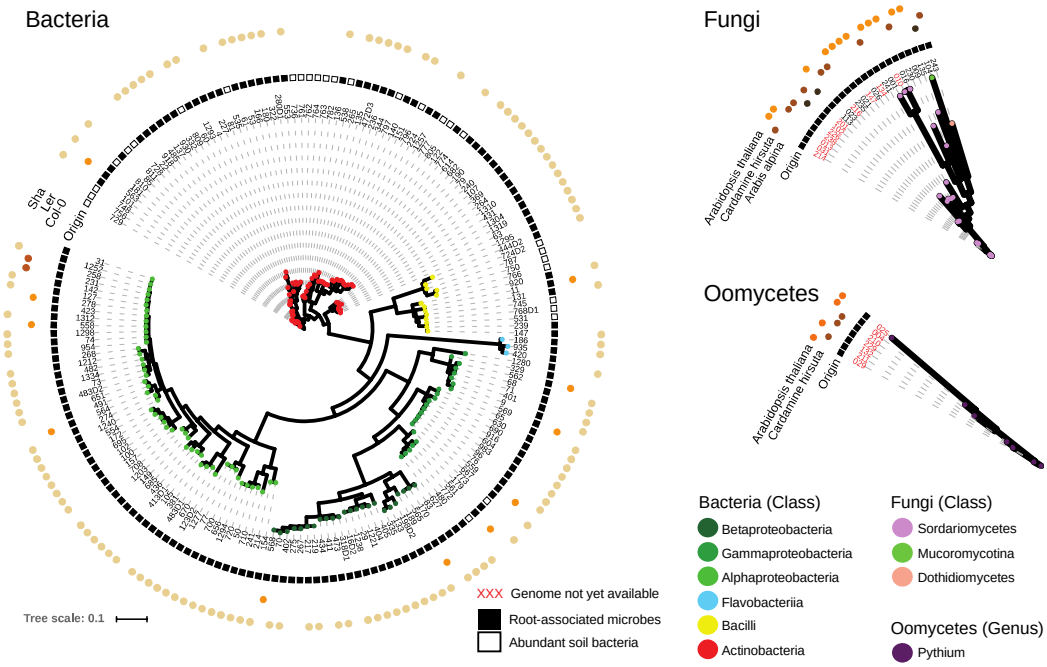

Figure 2. Phylogenetic trees of the bacterial, fungal and oomycetal strains used for microbiota reconstitution experiments. These microbes were isolated from the roots of *A. thaliana* or relative species grown in the Cologne Agricultural Soil (CAS). Different colours indicate different microbial classes. The strains labeled with red color name means genome is not available yet. For bacterial phylogenetic tree, black square next to the name of strains means this strain was isolated from plant root; white square means this strain was isolated from soil. In total, 183 strains of bacteria, 24 strains of fungi and 7 strains of oomycetes are showed here.

Table 1. The number of isolates used for the synthetic communities.

	Phyla covered	Family covered	Genera covered	Strains
Bacteria	4	25	34	183
Fungi	2	9	12	24
Oomycetes	-	-	1	7

Table 2. Different levels of inoculum in the FlowPot and calcined-clay systems (A) and experimental treatment (B).

A. Different levels of inoculum in the FlowPot and calcined-clay system.

	The FlowPot System		The Calcined-clay System	
	High Level	Low Level	High Level	Low Level
Bacteria	2 ml/50 ml (OD=0.5)	0.2 ml/50ml (OD=0.5)	2 ml/70 ml (OD=0.5)	0.2 ml/70ml (OD=0.5)
Fungi	100 mg/50 ml	10 mg/50 ml	100 mg/70 ml	10 mg/70 ml
Oomycetes	40 mg/50 ml	4 mg/50 ml	40 mg/70 ml	4 mg/70 ml

B. Experimental treatment.

	Bacteria	Fungi	Oomycetes
BFO_000	0	0	0
BFO_HHH	High Level	High Level	High Level
BFO_HHL	High Level	High Level	Low Level
BFO_HLH	High Level	Low Level	High Level
BFO_HLL	High Level	Low Level	Low Level
BFO_LHH	Low Level	High Level	High Level
BFO_LHL	Low Level	High Level	Low Level
BFO_LLH	Low Level	Low Level	High Level
BFO_LLL	Low Level	Low Level	Low Level

Given the fact that each system has pros and cons (FlowPot vs. calcined-clay, see above), I had to find adequate stress conditions that can be applied in these gnotobiotc plant systems in the absence of the root microbiota. Since the matrix used in the FlowPot system is a mixture of peat (2/3) and vermiculite (1/3), I anticipated that the levels of several plant nutritional elements remain present in high concentration. In contrast the calcined-clay and white sand represent more “inert” substrates, in which it might be easier to apply specific nutritional stresses. For the tested abiotic and biotic stresses (i.e. salt, drought, light and pathogen attack), I first had to define the degree of stresses needed to observe plant phenotypic growth variation in the FlowPot, calcined-clay and white sand systems. This part of my project required optimization since we have never tested how *A.*

thaliana respond to single and combined abiotic stresses in our gnotobiotic systems.

In order to select the adequate stress conditions that will be used for microbiota reconstitution experiments (chapter II), I tested *A. thaliana* Col-0 tolerance to various single abiotic or biotic stresses in the FlowPot, calcined-clay and white sand systems. In order to provide an abundance of nutrients for plant growth, I chose ½ MS medium (**Table 3**) as plant growth media. I tested *A. thaliana* Col-0 tolerance to salt (40 mM, 80 mM and 120 mM NaCl in ½ MS medium), drought (5%, 10% and 20% PEG 6000 in ½ MS in the FlowPot system, 1%, 2%, 3%, 5%, 10% and 20% PEG 6000 in ½ MS in the calcined-clay system and 5%, 7% and 10% PEG 6000 in ½ MS in the white sand system), shade stresses (**Figure 3**), nutrients deficient stresses (**Table 4**),and pathogen (*Golovinomyces orontii* and *Pseudomonas syringae* DC3000) stresses. *Golovinomyces orontii* is a powdery mildew fungus with an obligate biotrophic lifestyle that colonizes and infects *Arabidopsis* leaves under controlled laboratory conditions (**Micali et al., 2008**). *Pseudomonas syringae pv. tomato* DC3000 is a model bacterial pathogen largely used for probing disease susceptibility and hormone signalling in plant leaves.

Table 3. Composition of the ½ strength Murashige and Skoog medium (½ MS)

Nutrient	Mol. Wt. (Volume per liter)
$MgSO_4.7H_2O$	750 (25ml)
KH_2PO_4	625 (25ml)
NH_4NO_3	1000 (1ml)
KNO_3	9400 (10ml)
$CaCl_2.2H_2O$	1500 (10ml)
$CoCl_2.6H_2O$	0.055 (1ml)
$CuCl_2.2H_2O$	0.053 (1ml)
H_3BO_3	50 (1ml)
KI	2.5 (1ml)
$MnCl_2.4H_2O$	50 (1ml)
$Na_2MoO_4.2H_2O$	0.52 (1ml)
$ZnCl_2$	15 (1ml)
Na-Fe-EDTA	75 (0.75ml)

MES pH5.5	1000 (2ml)
KCl	0

Table 4. Nutrient deficient conditions of the ½ strength Murashige and Skoog medium (½ MS)

Nutrient	N1 stress	N2 stress	N3 stress	P1 stress	P2 stress	Fe stress
	Mol. Wt. (V/L)	Mol. Wt. (V/L)	Mol. Wt. (V/L)	Mol. Wt. (V/L)	Mol. Wt. (V/V)	Mol. Wt. (V/L)
$MgSO_4.7H_2O$	750 (25ml)	750 (25ml)	750 (25ml)	750 (25ml)	750 (25ml)	750 (25ml)
KH_2PO_4	625 (25ml)	625 (25ml)	625 (25ml)	**50 (2ml)**	**0 (0ml)**	625 (25ml)
NH_4NO_3	**25 (24.27ul)**	**10 (9.7ul)**	**0 (0ml)**	**10300 (10ml)**	1000 (1ml)	1000 (1ml)
KNO_3	**10 (9.7ul)**	**90 (96ul)**	**0 (0ml)**	9400 (10ml)	9400 (10ml)	9400 (10ml)
$CaCl_2.2H_2O$	1500 (10ml)	1500 (10ml)	1500 (10ml)	1500 (10ml)	1500 (10ml)	1500 (10ml)
$CoCl_2.6H_2O$	0.055 (1ml)	0.055 (1ml)	0.055 (1ml)	0.055 (1ml)	0.055 (1ml)	0.055 (1ml)
$CuCl_2.2H_2O$	0.053 (1ml)	0.053 (1ml)	0.053 (1ml)	0.053 (1ml)	0.053 (1ml)	0.053 (1ml)
H_3BO_3	50 (1ml)	50 (1ml)	50 (1ml)	50 (1ml)	50 (1ml)	50 (1ml)
KI	2.5 (1ml)	2.5 (1ml)	2.5 (1ml)	2.5 (1ml)	2.5 (1ml)	2.5 (1ml)
$MnCl_2.4H_2O$	50 (1ml)	50 (1ml)	50 (1ml)	50 (1ml)	50 (1ml)	50 (1ml)
$Na_2MoO_4.2H_2O$	0.52 (1ml)	0.52 (1ml)	0.52 (1ml)	0.52 (1ml)	0.52 (1ml)	0.52 (1ml)
$ZnCl_2$	15 (1ml)	15 (1ml)	15 (1ml)	15 (1ml)	15 (1ml)	15 (1ml)
Na-Fe-EDTA	75 (0.75ml)	75 (0.75ml)	75 (0.75ml)	75 (0.75ml)	75 (0.75ml)	**0 (0ml)**
MES pH5.5	1000 (2ml)	1000 (2ml)	1000 (2ml)	1000 (2ml)	1000 (2ml)	1000 (2ml)
KCl	**9175 (9.764ml)**	**9310 (9.907 ml)**	**9400 (10ml)**	**575 (0.612ml)**	**625 (0.665ml)**	0

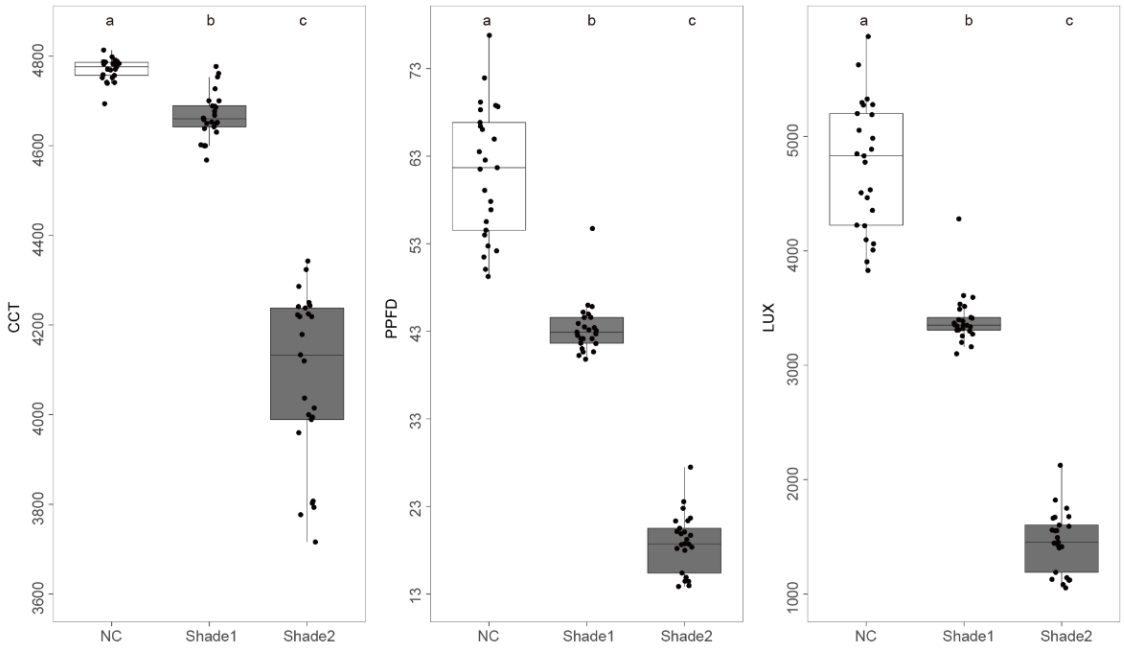

Figure 3. Light parameters measured in the FlowPot system at different positions in the plant growth chamber (λp = 545 nm). Light conditions (CCT: Correlated Color Temperature, PPFD: Photosynthetic Photon Flux Density, LUX: Luminous Flux per unit area) were determined in the gnotobiotic system when leaves were exposed to either direct (normal light condition, NC) or indirect light (shade1, shade2). Letters indicate statistical significance corresponding to ANOVA with post-hoc Tukey HSD test (α = 0.05).

3. Results

3.1 The assemblage of multi-kingdom microbial consortia

To gain insights into the microbial diversity detected in the matrix and root samples of both gnotobiotic plant systems, I compared the "observed OTUs" and "Shannon" diversity indices of the communities retrieved from matrix and root habitats (**Figure 4, Figure 5**). All the indices of bacterial community revealed a reduction of the bacterial richness and diversity in the calcined-clay system compared with the FlowPot system when the low bacterial inoculum was chosen. Notably, bacterial richness was similar in the FlowPot system regardless of the input level of bacteria. This result suggests that the low bacterial load affects bacterial diversity in the clay system, but not in the FlowPot system, likely because bacteria grow better in the carbon-rich peat substrate.

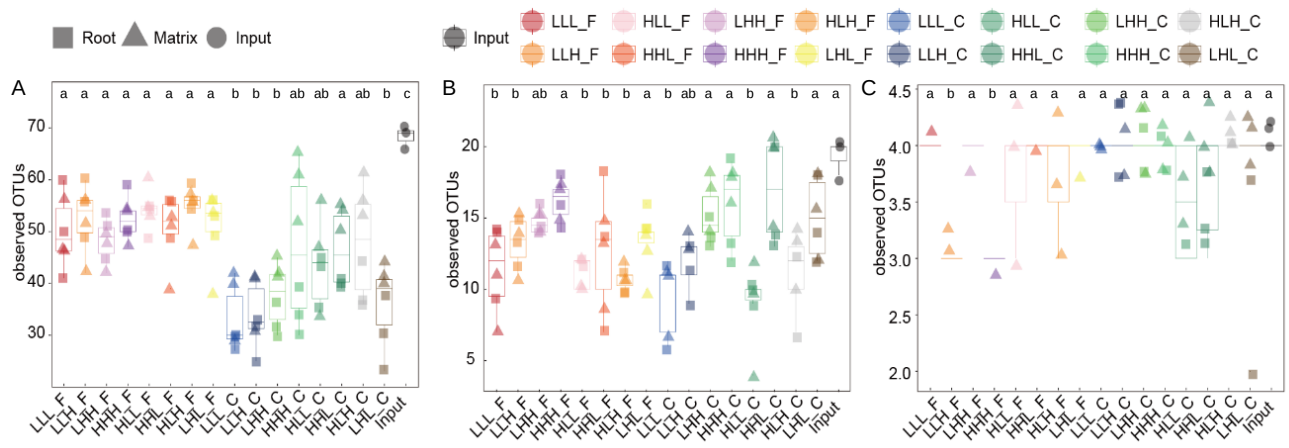

Figure 4. The observed OTUs diversity index of bacterial (A), fungal (B) and oomycetal (C) communities retrieved from matrix and root-associated compartments. F = FlowPot system. C = calcined-clay system. Root and matrix samples were harvested after 5 weeks of microbial inoculation in FlowPot system and 6 weeks of microbial inoculation in calcined-clay system. Three independent biological replicates (n = 99 samples). Letters indicate statistical significance corresponding to *Kruskal-Wallis* with *Dunn's* post hoc test (α = 0.05).

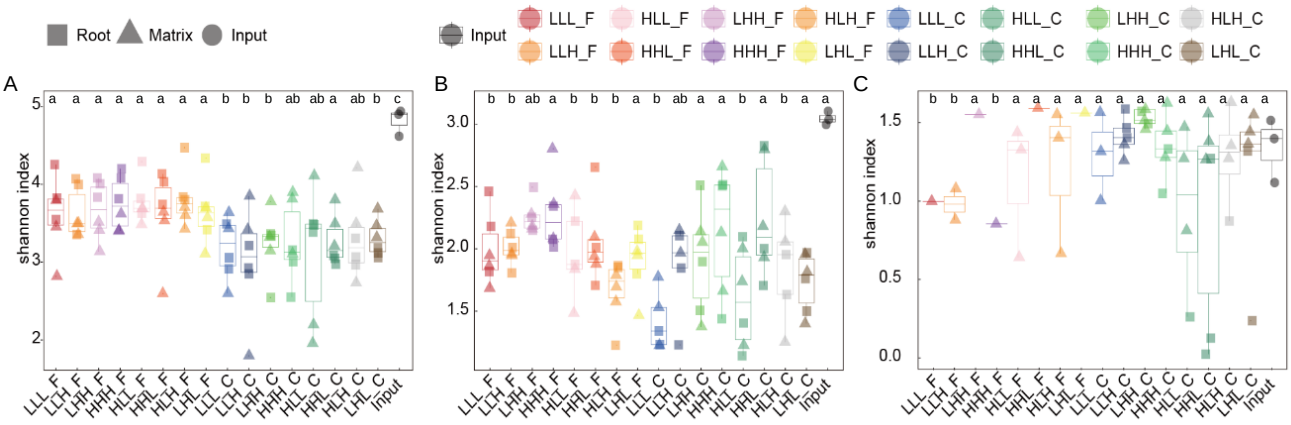

Figure 5. The Shannon diversity index of the bacterial (A), fungal (B) and oomycetal (C) communities retrieved from matrix and root-associated microhabitats. F means the FlowPot system. C represents the calcined-clay system. Root and matrix samples were harvested after 5 weeks of microbial inoculation in FlowPot system and 6 weeks of microbial inoculation in calcined-clay system. Three independent biological replicates (n = 99 samples). Letters indicate statistical significance corresponding to *Kruskal-Wallis* with *Dunn's* post hoc test (α = 0.05).

To elucidate whether the composition of the microbial communities correlated or was independent of the input ratio, the compartment and the system, I used the OTU count data to construct dissimilarity matrices with Bray-

Curtis distances. Along the firs Principal Coordinates Analysis of Bray-Curtis distances (PCoA) axis, the sample cluster according to the system explains most of the variation (52.92%) suggesting that difference between the two systems drive most of the differentiation in bacterial community composition (**Figure 6A**). For fungi, along the second PCoA axis, the sample cluster according to the system explains 18.62% variation (**Figure 6B**). That suggests that bacterial community is more strongly influenced by differences between the two gnotobiotic systems than fungi. This differentiation in community composition is probably explained by differences in carbon and nutrient content that could modulate the structure of bacterial and to a lesser extent fungal community.

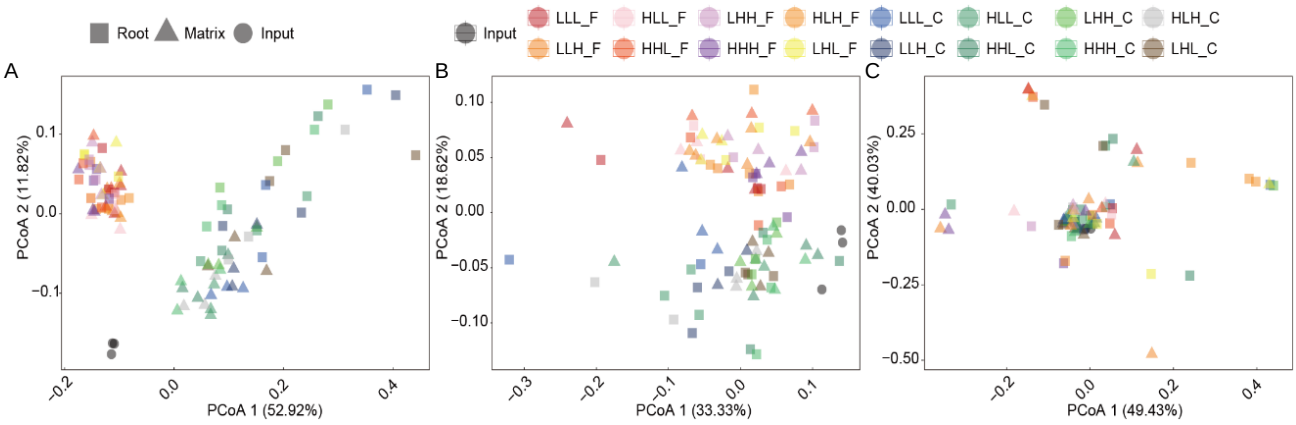

Figure 6. Principal coordinate analysis of Bray-Curtis dissimilarities on matrix- and root-associated bacterial (A), fungal (B) and oomycetal (C) communities in FlowPot and calcined-clay system. F = FlowPot system. C = calcined-clay system. Root and matrix samples were harvested 5 weeks post microbial inoculation in the FlowPot system and 6 weeks post microbial inoculation in the calcined-clay system. Three independent biological replicates (n = 99 samples).

To elucidate which factors explained compositional shifts in microbial communities in each system, I used the OTU count data to construct dissimilarity matrices with Bray-Curtis distances for FlowPot and calcined-clay systems separately. In the FlowPot system, the major factor driving differentiation in bacterial community composition was explained by the factor "experimental replicate" (see first PCoA axis, 30.04%, **Figure 7**). This result could be the consequence of slightly different bacterial input and/or bacterial growth rate among different experimental replicates. Along the second PCoA axis (explaining 15.3% of the variation, **Figure 7**), samples cluster according to the compartment, validating that the structure of root-associated bacterial community is

different from the structure observed in the matrix compartment, validating that growth of bacterial taxa is under the influence of the root niche. In contrast, no clear replicate or compartment effects were observed for fungal and oomycetal communities (**Figure 7**).

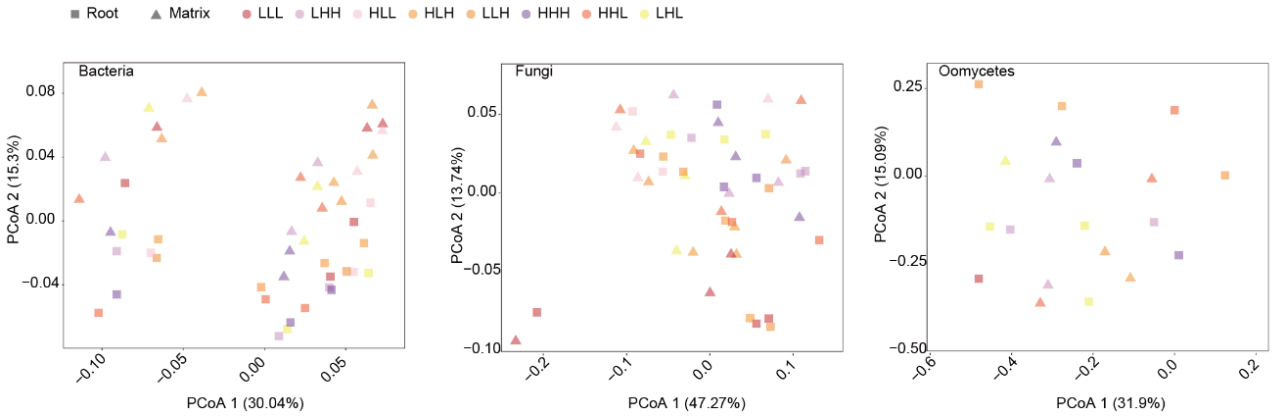

Figure 7. Principal coordinate analysis of Bray-Curtis dissimilarities on matrix- and root-associated bacterial, fungal and oomycetal communities in the FlowPot system. Root and matrix samples were harvested after 5 weeks of microbial inoculation in FlowPot system. Three independent biological replicates (n = 48 samples).

In the calcined-clay system, the major factor driving differentiation in bacterial community composition was explained by the factor "compartment" (see first PCoA axis, 52.92%, **Figure 8**) indicating strong influence of the root system on bacterial community assembly. In contrast, no clear compartment effect was observed for fungal and oomycetal communities (**Figure 8**), consistent with the results obtained for the FlowPot system.

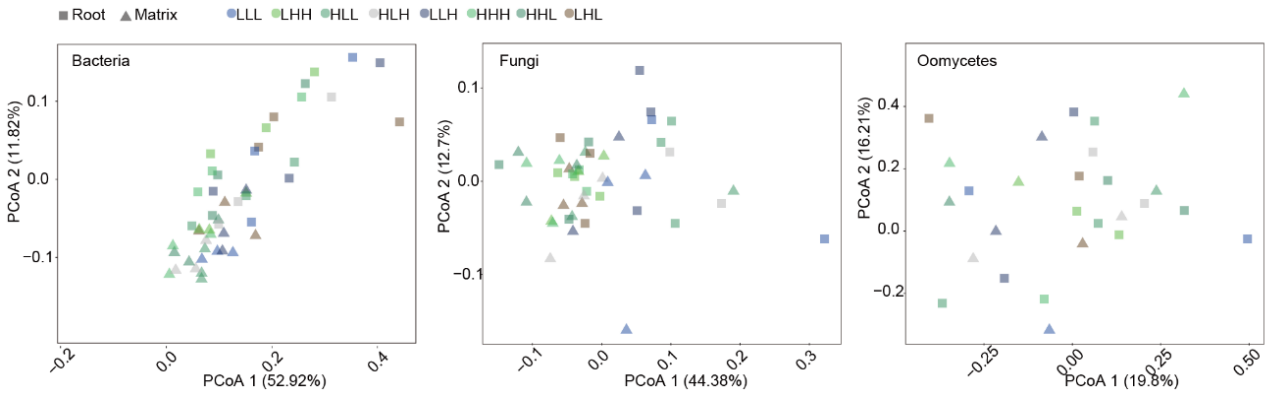

Figure 8. Principal coordinate analysis of Bray-Curtis dissimilarities on matrix- and root-associated bacterial, fungal and oomycetal communities in calcined-clay system. Root and matrix samples were harvested after 6 weeks of microbial inoculation in

calcined-clay system. Three independent biological replicates (n = 48 samples).

Further, in order to identify whether the different microbial inputs ratios significantly affect output microbial communities, I did a constrained principal coordinate analysis of Bray-Curtis dissimilarities on the matrix and root bacterial, fungal and oomycetal communities in the FlowPot system (**Figure 9**) and in the calcined-clay system (**Figure 10**) separately. The results showed that the different microbial input ratios do not statistically change microbial community structure in our gnotobiotic plant systems (both Flowpot system and calcined-clay system) (**Figure 9** and **Figure 10**). These results indicate that difference in initial abundance between bacterial, fungal and oomycetal communities did not influence the structure of microbial communities 5- and 6-weeks post microbe inoculation in the FlowPot and calcined-clay systems, respectively. I therefore conclude that the self-organizational properties of the microbial communities are difficult to perturb and that modification of microbial input ratios do not lead to dramatic change in microbial community structure.

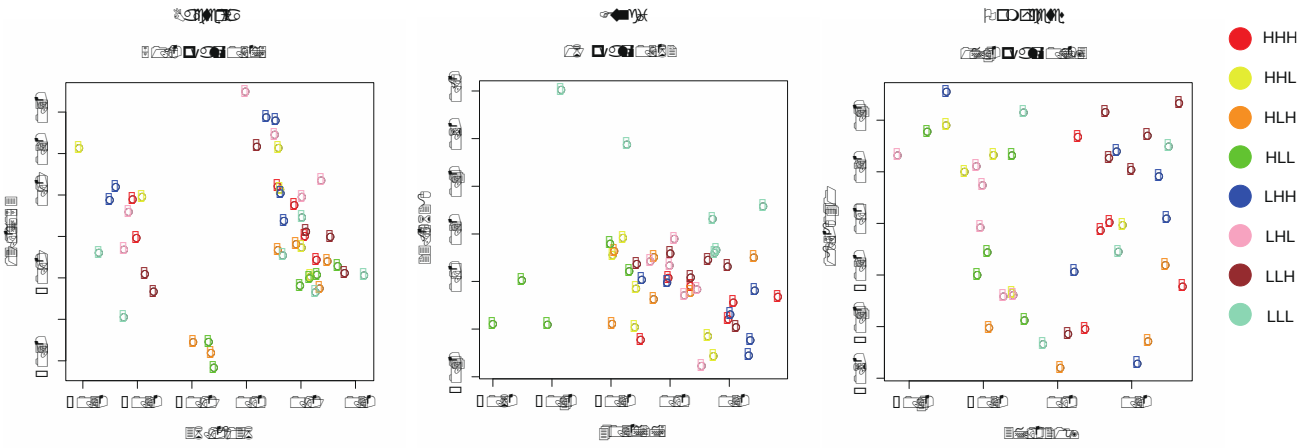

Figure 9. Constrained principal coordinate analysis of Bray-Curtis dissimilarities on matrix- and root-associated bacterial, fungal and oomycetal communities in FlowPot system. Root and matrix samples were harvested after 5 weeks of microbial inoculation in FlowPot system. Three independent biological replicates (n = 48 samples). Points labelled colour means the input ratio among bacteria, fungi and oomycetes.

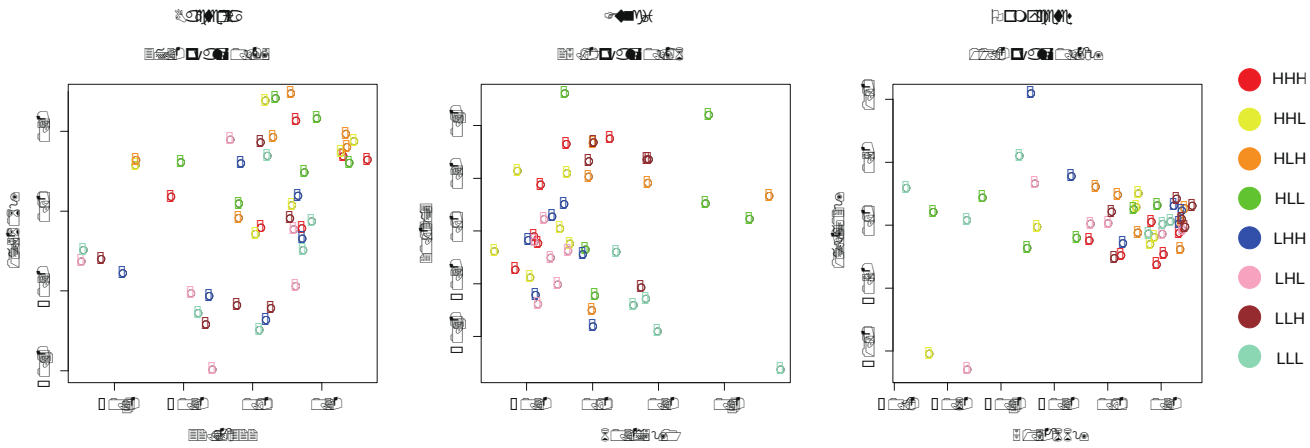

Figure 10. Constrained principal coordinate analysis of Bray-Curtis dissimilarities on matrix- and root-associated bacterial, fungal and oomycetal communities in calcined-clay system. Root and matrix samples were harvested after 6 weeks of microbial inoculation in calcined-clay system. Three independent biological replicates (n = 48 samples). Points labelled colour means the input ratio among bacteria, fungi and oomycetes.

3.2 The effect of inter-kingdom microbial input ratios on host fitness

To evaluate whether different original microbial input ratios affect plant growth in both FlowPot and calcined-clay systems, I harvested shoot samples and measured shoot fresh weight of 5-week old plants in the FlowPot system and 6-week old plants in the calcined-clay system.

In the calcined-clay system, eight combination of different microbial input ratio between bacteria, fungi and oomycetes did not significantly modulate shoot fresh weight (**Figure 12**). Similar results were observed in the FlowPot system (**Figure 11**). Based on shoot fresh weight measurements, our data suggested that in both gnotobiotic plant systems, the eight different combinatorial ratios between bacteria, fungi, and oomycetes impact similarly plant growth (**Figure 11 and Figure 12**).

Although the trend is not significant, it is interesting to note plants re-colonized by these multi-kingdom microbial consortia grow slightly better (according to the median) than non-colonized plants (**Figure 11** and **Figure 12**).

Taken together, we can conclude that modification of inter-kingdom microbial ratios does not significantly affect plant health, and this result is robust across two independent gnotobiotic systems.

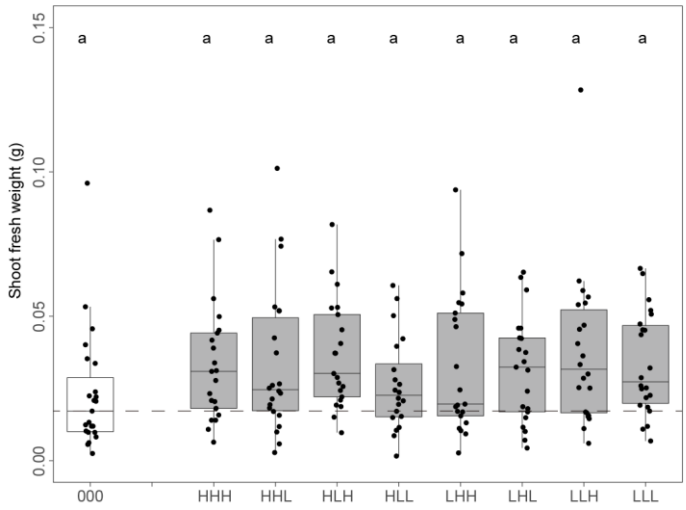

Figure 11. Effect of microbial input ratios on plant growth in the FlowPot system. B indicates plants inoculated with bacteria, F indicates plants inoculated with fungi, and O indicates plants inoculated with oomycetes. Each of bacteria, fungi and oomycetes have two inoculum concentration levels (High vs. Low, See Table 2). 000 indicates no microbes, H indicates high concentration level, and L indicates low concentration level. For example, BFO_HLH indicates the inputs including high level bacteria, low-level fungi and high-level oomycetes. The results are the combination of 3 independent biological replicates (n = 304). Letters indicate statistical significance corresponding to *Kruskal-Wallis* with *Dunn's* post hoc test (α = 0.05).

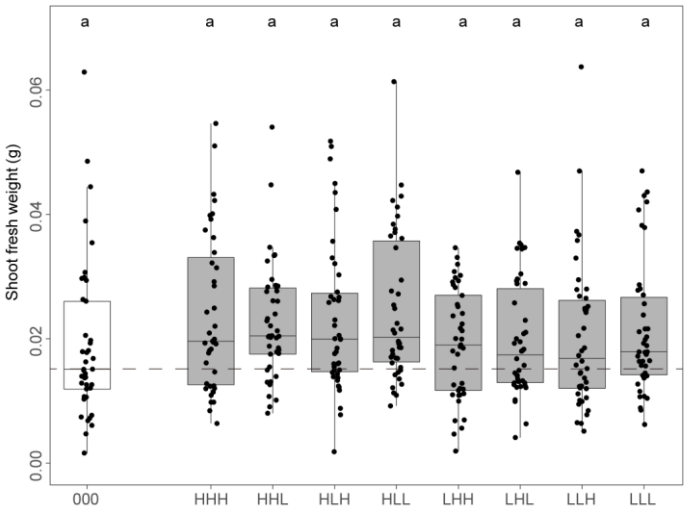

Figure 12. Effect of microbial input ratios on plant growth in the calcined-clay system. B indicates plants inoculated with bacteria, F

indicates plants inoculated with fungi, and O indicates plants inoculated with oomycetes. Each of bacteria, fungi and oomycetes have two inoculum concentration levels (High vs. Low, See Table 2). 000 indicates no microbes, H indicates high concentration level, and L indicates low concentration level. For example, BFO_HLH indicates the inputs including high level bacteria, low-level fungi and high-level oomycetes. The results are the combination of 3 independent biological replicates (n = 433). Letters indicate statistical significance corresponding to *Kruskal-Wallis* with *Dunn's* post hoc test (α = 0.05).

3.3 The effect of biotic and abiotic stresses on *Arabidopsis* growth in gnotobiotic systems

I tested *A. thaliana* Col-0 tolerance to various single abiotic or abiotic stresses in the FlowPot, calcined-clay, and white sand systems. In order to sustain plant but not microbial growth, I chose ½ MS liquid medium without sucrose (**Table 3**) as plant growth media for all three gnotobiotic systems. In these systems, I tested *A. thaliana* Col-0 tolerance to a series of salt stresses, PEG mimic drought stresses, shade stresses (**Figure 3**), nutrient (nitrogen, phosphate, and iron) stresses (**Table 4**) and leaf pathogens (*Golovinomyces orontii* and *Pseudomonas syringae* DC3000). Note that these experiments were performed in the absence of microbes in order to first define the range of stress-induced effects on plant growth in the context of germ-free plants.

To clarify the extent to which plant growth is affected by the different stress conditions, I harvested shoot and measured shoot fresh weight of five-week old plants grown in the FlowPot system, and six-week old plants growth in calcined-clay and white sand systems. Based on shoot fresh weight data, salt stress at 120 mM NaCl has a significant effect on plant growth in all three systems whereas 80 mM NaCl significantly restricts plant growth only in calcined-clay and white sand systems (**Figure 13, Figure 14, and Figure 15**). Drought stress, mimicked by the presence of Polyethylene glycol (10% and 20% PEG), and shade stress also strongly and significantly inhibit plant growth in all three systems (**Figure 13, Figure 14, and Figure 15**). In the FlowPot system, the shoot fresh weight under all nutritional stresses (-N, -P, -K) is not statistically different compared to control plants (**Figure 13**). However, N stress significantly inhibits plant growth in the calcined-clay and in white sand systems (**Figure 14 and Figure 15**) whereas P stress significantly inhibits plant growth in the white sand system only (**Figure 15**). In all systems, *G. orontii* and *P. syringae* DC3000 cause plant disease symptoms but had no significant impact on shoot fresh weight, which is explained by the fact that we inoculated the

pathogens on leaves of 4-week old plants only 5 days before harvesting the shoot compartment (**Figure 13, Figure 14, and Figure 15**).

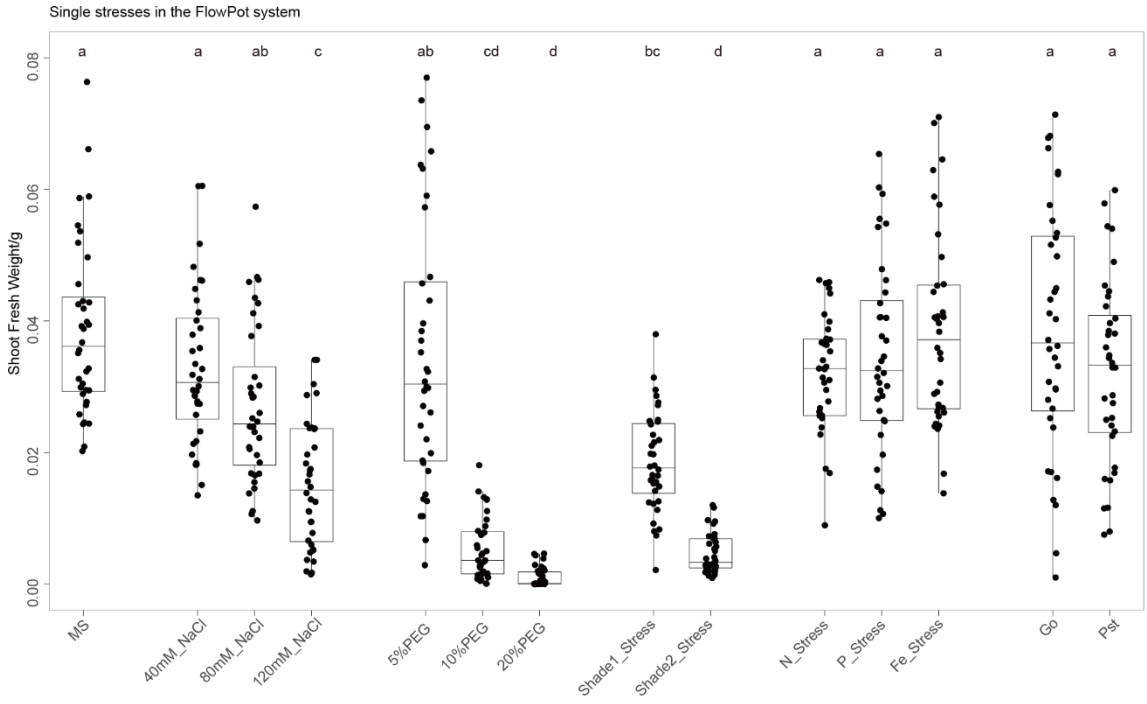

Figure 13. The effect of biotic and abiotic stresses on *Arabidopsis* growth in the FlowPot system. MS means plants growing in 1/2 MS medium without any stresses. 40 mM NaCl, 80 mM NaCl, and 120 mM NaCl mean adding 40 mM NaCl, 80 mM NaCl, and 120 mM NaCl in 1/2 MS medium separately. PEG means polyethylene glycol (PEG) 6000. 5% PEG, 10% PEG, and 20% PEG represent respectively adding 5% PEG, 10% PEG, and 20% PEG into 1/2 MS medium to mimic drought stresses. Shade1 stress and shade2 stress mean two different levels of low light intensity conditions (details in Figure 3). Go reflects four weeks plants inoculated with spaying the pathogen *Golovinomyces orontii* at a density of 4-6 conidia mm^{-2}. Pst means four weeks plants inoculated with spraying the pathogen *Pseudomonas syringae* DC3000 (OD = 0.2). The results are the combination of 3 independent biological replicates (n = 503). Letters indicate statistical significance corresponding to *Kruskal-Wallis* with *Dunn's* post hoc test (α = 0.05).

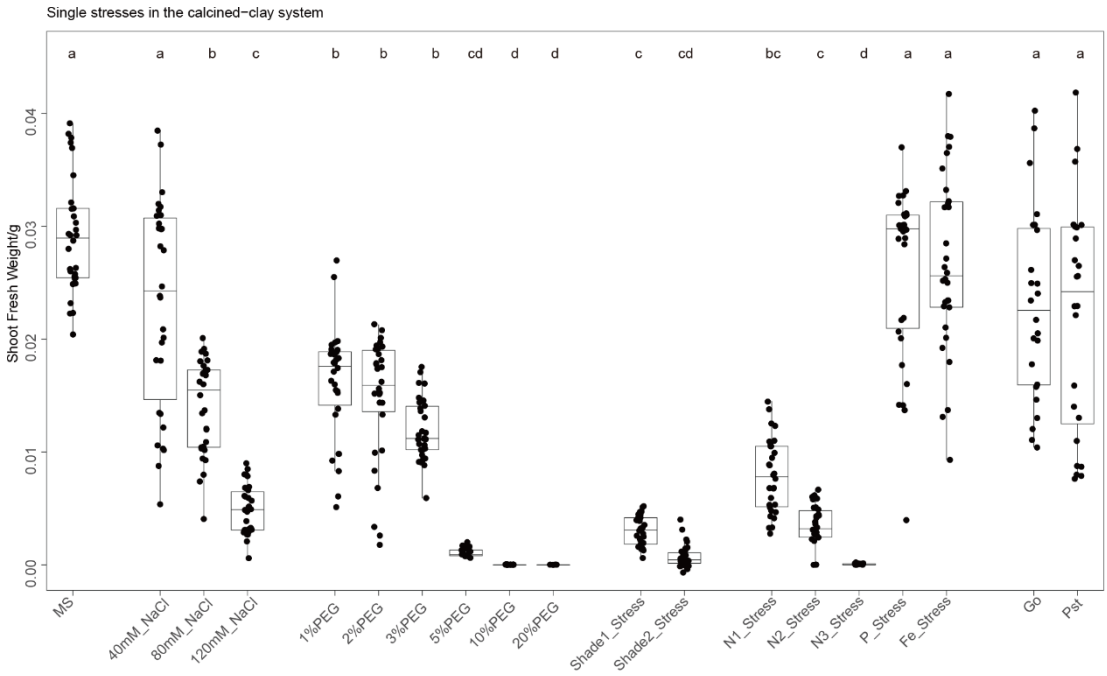

Figure 14. The effect of biotic and abiotic stresses on *Arabidopsis* growth in Calcined-clay system. MS means plants growing in 1/2 MS medium without any stresses. 40 mM NaCl, 80 mM NaCl, and 120 mM NaCl mean adding 40 mM NaCl, 80 mM NaCl, and 120 mM NaCl in 1/2 MS medium separately. PEG means polyethylene glycol (PEG) 6000. 1% PEG, 2% PEG, 3% PEG, 5% PEG, 10% PEG and 20% PEG respectively represent adding 1% PEG, 2% PEG, 3% PEG, 5% PEG, 10% PEG and 20% PEG into 1/2 MS medium to mimic drought stresses. Shade1 stress and shade2 stress mean two different levels of low light intensity conditions (details in Figure 3). N1 stress, N2 stress, and N3 stress mean three different levels of nitrogen deficient stresses (details in Table 4). P stress and Fe stress reflect respectively removing all phosphate and iron from 1/2 MS medium. Go reflects four weeks plants inoculated with spaying the pathogen *Golovinomyces orontii* at a density of 4-6 conidia mm^{-2}. Pst means four weeks plants inoculated with spraying the pathogen *Pseudomonas syringae* DC3000 (OD = 0.2). The results are the combination of 3 independent biological replicates (n = 530). Letters indicate statistical significance corresponding to *Kruskal-Wallis* with *Dunn's* post hoc test (α = 0.05).

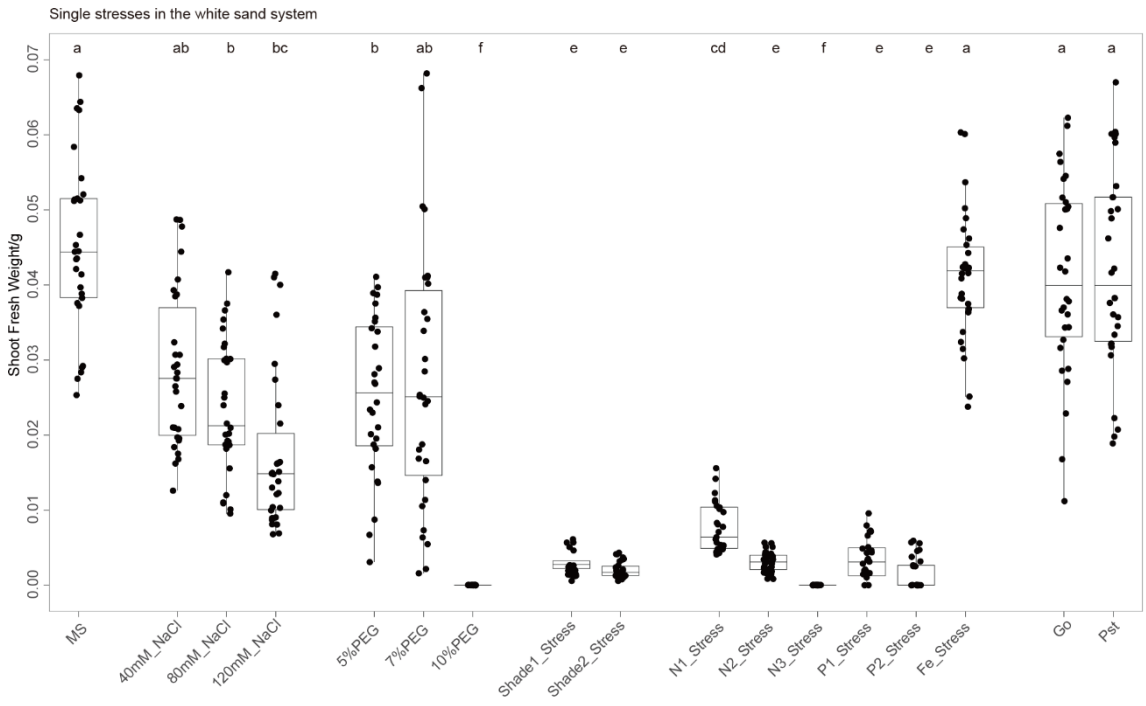

Figure 15. The effect of biotic and abiotic stresses on Arabidopsis growth in white sand system. MS means plants growing in 1/2 MS medium without any stresses. 40 mM NaCl, 80 mM NaCl, and 120 mM NaCl mean adding 40 mM NaCl, 80 mM NaCl, and 120 mM NaCl in 1/2 MS medium separately. PEG means polyethylene glycol (PEG) 6000. 5% PEG, 7% PEG, and 10% PEG respectively represent adding 5% PEG, 7% PEG, and 10% PEG into 1/2 MS medium to mimic drought stresses. Shade1 stress and shade2 stress mean two different levels of low light intensity conditions (details in Figure 3). N1 stress, N2 stress, and N3 stress mean three different levels of nitrogen deficient stresses (details in Table 4). P1 stress and P2 stress represent two different levels of phosphate deficient stresses (details in Table 4). Fe stress reflects removing all iron from 1/2 MS medium. Go reflects four weeks plants inoculated with spaying the pathogen *Golovinomyces orontii* at a density of 4-6 conidia mm^{-2}. Pst means four weeks plants inoculated with spraying the pathogen *Pseudomonas syringae* DC3000 (OD = 0.2). The results are the combination of 3 independent biological replicates (n = 504). Letters indicate statistical significance corresponding to *Kruskal-Wallis* with *Dunn's* post hoc test (α = 0.05).

Based on these experiments, I demonstrated that it is possible to apply different biotic and abiotic stresses in our three gnotobiotic plant systems. Particularly, salt, drought, and shade stresses can be recapitulated in all systems. In contrast, the nutritional stresses are highly system-dependant, likely due to the contrasted residual amount of iron, nitrogen and phosphate are present in the corresponding substrates (i.e. clay, sand, and peat). My results suggest that the white sand system is the most adequate for testing nutritional perturbations, contrasting with the FlowPot system that cannot be used for such kind of manipulation experiments.

3.4 The effect of microbiota on plant growth under single stress

Based on the microbial input ratio experiments (see above) and the stress tolerance experiments (see above), I chose the ratio low bacteria, low fungi and low oomycetes to decipher the plant growth-promoting effect of the root microbiota under single stress, as well as the effect of the stresses on the structure of the plant root microbiota.

Based on the shoot fresh weight measurements, I concluded that microbes have a significant positive effect on plant growth under drought stress (5% PEG) and shade stress in the FlowPot system (**Figure 16**) and under drought stress (5% and 7% PEG) in the white sand system (**Figure 18**). In contrast, no plant growth promoting activity was observed in the calcined clay system (**Figure 17**). Notably, the presence of the multi-kingdom microbial consortium in the FlowPot system under shade stress fully rescue plant growth to control levels (**Figure 16**), suggesting that the microbiota rescues plant growth under shade conditions.

To some extent, it supports our hypothesis that our synthetic multi-kingdom microbial consortium shows enhanced plant growth-promotion under some stresses compared to the effect observed under normal condition. Taken together, the FlowPot system, which mimic more closely natural soil structure and composition, appears to be the best system to study growth promotion and stress alleviation by the root microbiota. The results are consistent with other experiments conducted in the group suggesting that the carbon content in the substrate is critical for the beneficial activities of the microbiota.

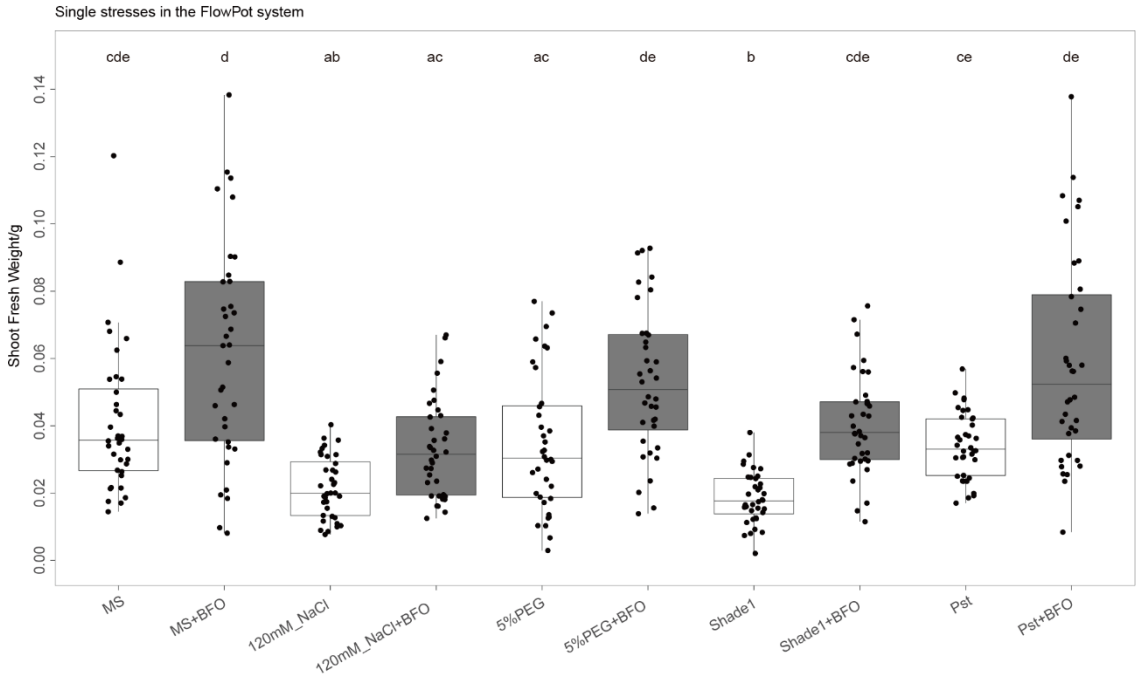

Figure 16. The effect of microbiota on plant growth under single stress in the FlowPot system. MS means plants growing in 1/2 MS medium without any stresses. 120 mM NaCl means adding 120 mM NaCl in 1/2 MS medium. PEG means polyethylene glycol (PEG) 6000. 5% PEG represents adding 5% PEG into 1/2 MS medium to mimic drought stresses. Shade1 stress means low light intensity condition (details in Figure 3). Pst means four weeks plants inoculated with spraying the pathogen *Pseudomonas syringae* DC3000 (OD = 0.2). The data is the combination of 3 independent biological replicates (n=360). Letters indicate statistical significance corresponding to Kruskal-Wallis with Dunn's post hoc test (α = 0.05).

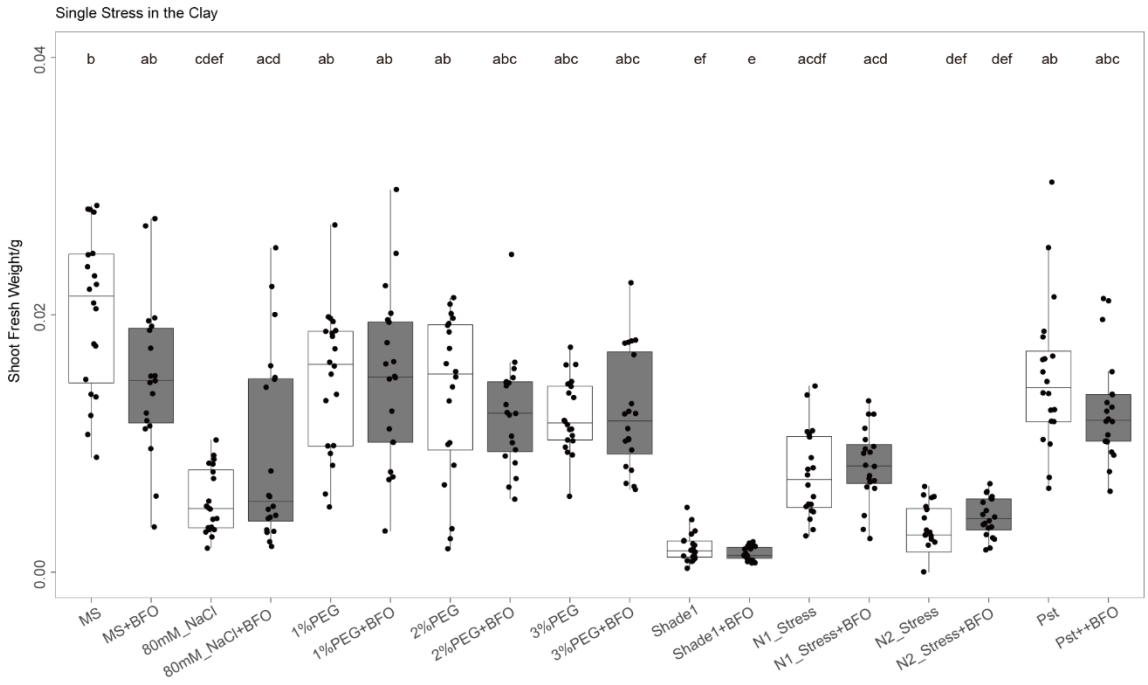

Figure 17. The effect of microbiota on plant growth under single stress in the Calcined-clay system. MS means plants growing in 1/2 MS medium without any stresses. 80 mM NaCl means adding 80 mM NaCl NaCl in 1/2 MS medium. PEG means polyethylene glycol (PEG) 6000. 1% PEG, 2% PEG, 3% PEG, 5% PEG, 10% PEG and 20% PEG respectively represent adding 1% PEG, 2% PEG, 3% PEG, 5% PEG, 10% PEG and 20% PEG into 1/2 MS medium to mimic drought stresses. Shade1 stress and shade2 stress mean two different levels of low light intensity conditions (details in Figure 3). N1 stress and N2 stress mean two different levels of nitrogen deficient stresses (details in Table 4). Pst means four weeks plants inoculated with spraying the pathogen *Pseudomonas syringae* DC3000 (OD = 0.2). The data is the combination of 3 independent biological replicates (n=360). Letters indicate statistical significance corresponding to Kruskal-Wallis with Dunn's post hoc test (α = 0.05).

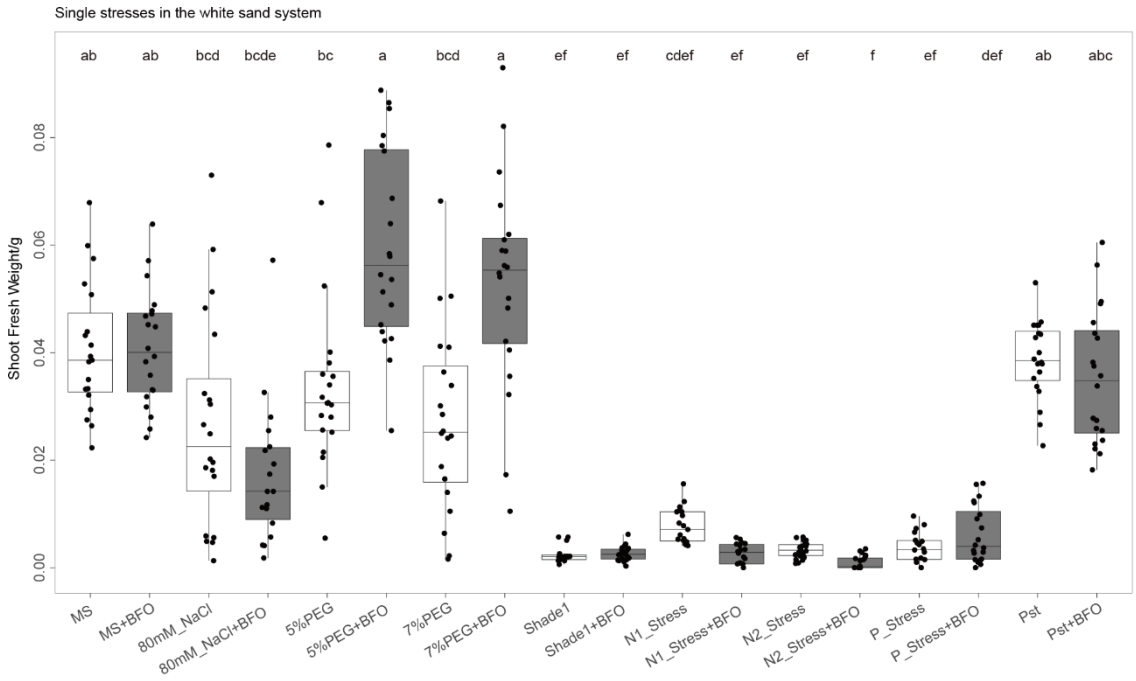

Figure 18. The effect of microbiota on plant growth under single stress in the white sand system. MS means plants growing in 1/2 MS medium without any stresses. 80 mM NaCl means adding 80 mM NaCl in 1/2 MS medium. PEG means polyethylene glycol (PEG) 6000. 5% PEG and 7% PEG respectively represent adding 5% PEG and 7% PEG into 1/2 MS medium to mimic drought stresses. Shade1 stress and shade2 stress mean two different levels of low light intensity conditions (details in Figure 3). N1 stress and N2 stress mean two different levels of nitrogen deficient stresses (details in Table 4). P stress represents removing all phosphate from 1/2 MS medium. Pst means four weeks plants inoculated with spraying the pathogen *Pseudomonas syringae* DC3000 (OD = 0.2). The data is the combination of 3 independent biological replicates (n=352). Letters indicate statistical significance corresponding to Kruskal-Wallis with Dunn's post hoc test (α = 0.05).

3.5 The effect of single stress on microbial communities in FlowPot system

To gain insights into microbial diversity detected in matrix and root samples, I compared the total number of observed OTUs and the Shannon diversity indices of the communities retrieved from matrix and root compartments using a direct mapping approach (**Figure 19 and Figure 20**). 183 bacteria, 24 fungi and 7 oomycetes, respectively, could be discriminated into 115, 17, and 7 strain variants at single nucleotide resolution against reference 16S rRNA and ITS sequences. Based on the observed OTUs and Shannon index, the different stresses did not significantly affect the alpha diversity of bacterial, fungal, and oomycetal communities (**Figure**

19 and Figure 20).

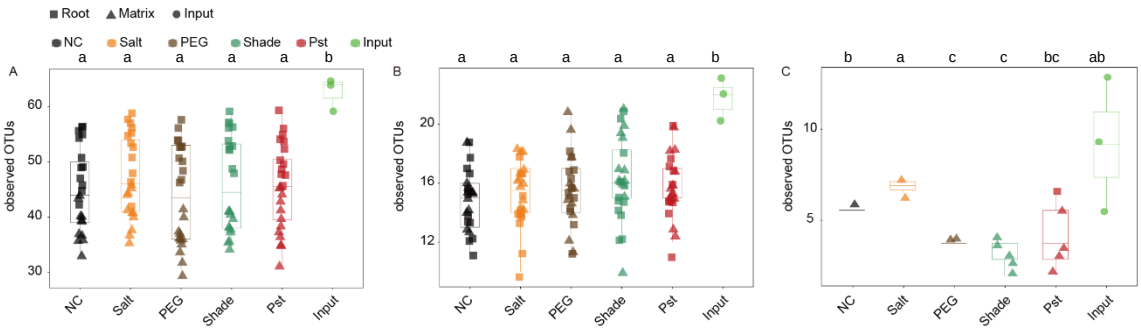

Figure 19. The observed OTUs diversity index of the bacterial (A), fungal (B) and oomycetal (C) communities retrieved from matrix and root compartments. Root and matrix samples were harvested 5 weeks post microbial inoculation in the FlowPot system. Three independent biological replicates (n = 63 samples). Letters indicate statistical significance corresponding to Kruskal-Wallis with Dunn's post hoc test (α = 0.05).

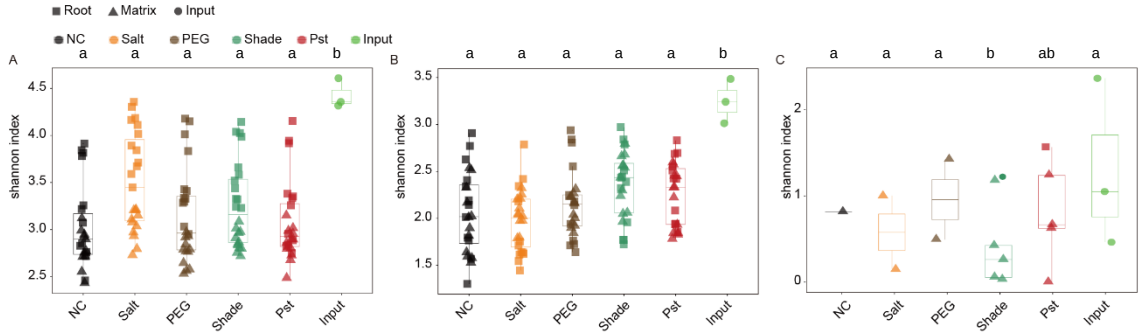

Figure 20. The Shannon diversity index of the bacterial (A), fungal (B) and oomycetal (C) communities retrieved from matrix and root compartments. Root and matrix samples were harvested 5 weeks post microbial inoculation in the FlowPot system. Three independent biological replicates (n = 63 samples). Letters indicate statistical significance corresponding to Kruskal-Wallis with Dunn's post hoc test (α = 0.05).

To elucidate whether these four environmental stresses modulate microbial community composition, I used OTU count data to construct dissimilarity matrices with Bray-Curtis distances. Principal coordinates analysis of Bray-Curtis distances (PCoA, **Figure 21**) validated the prominent effect of the compartment on bacterial, but not fungal and oomycetal community composition in the FlowPot system.

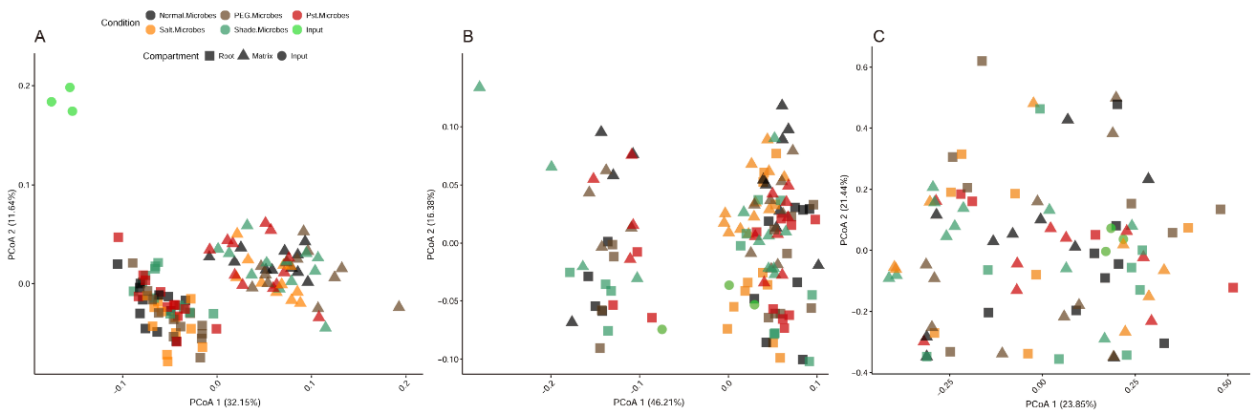

Figure 21. Principal coordinate analysis of Bray-Curtis dissimilarities on the matrix and root bacterial (A), fungal (B) and oomycetal (C) communities in the FlowPot system. Root and matrix samples were harvested after 5 weeks of microbial inoculation in the FlowPot system. Three independent biological replicates (n = 63 samples).

In order to identify whether the stress condition affects the structure of bacterial, fungal and oomycetal communities, I did a constrained principal coordinate analysis of Bray-Curtis dissimilarities on the matrix (**Figure 22**) and root samples (**Figure 23**) separately. The different stress conditions significantly explain 17.9% of the variance (p = 0.001) observed for bacterial community from matrix samples (**Figure 22A**) and 23% of the variance (p = 0.001) from root samples (**Figure 23A**), with salt stresses having the strongest effect on bacterial community structure in both matrix and root samples. The second strongest factor is PEG mimic drought stress since PEG mimic drought stress shifted bacterial communities clearly separated with samples under normal condition both matrix (**Figure 22A**) and root samples (**Figure 23A**). Notably, the factor shade appeared to affect more strongly bacterial community composition in the root than in the matrix compartment, suggesting a potential host-dependent modulation of bacterial assembly under suboptimal light conditions. Given the fact that the multi-kingdom microbial community promotes plant growth under shade and that reciprocally shading altered root but not soil bacterial assemblages, I will focus on the interplay between aboveground light and belowground microbial commensal in the next chapter.

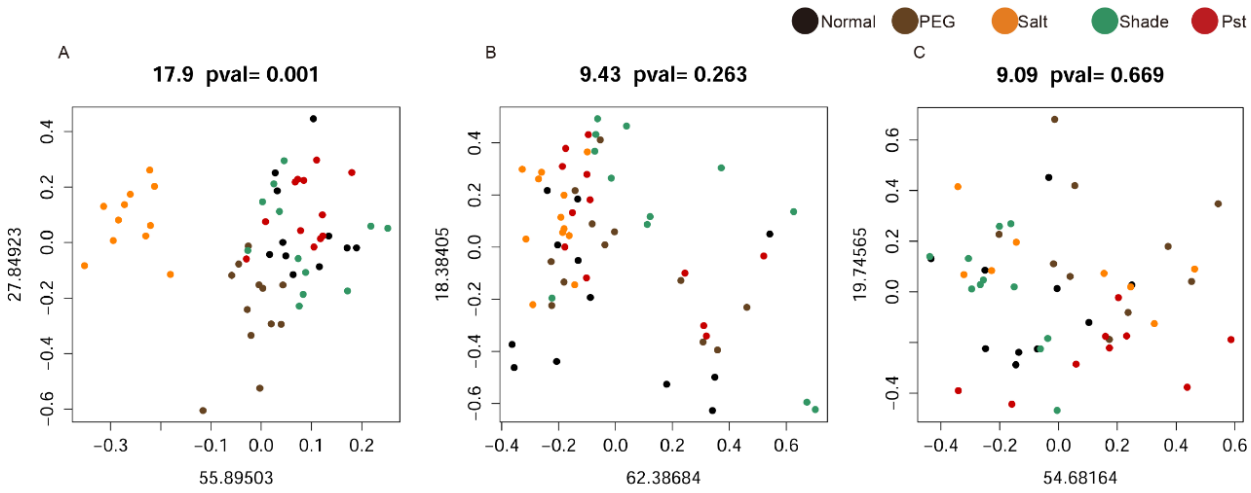

Figure 22. Constrained principal coordinate analysis of Bray-Curtis dissimilarities on bacterial (A), fungal (B) and oomycetal (C) communities from matrix samples in the FlowPot system. Matrix samples were harvested after 5 weeks of microbial inoculation in the FlowPot system. Points colour means different conditions as mentioned before. Three independent biological replicates (n = 63 samples).

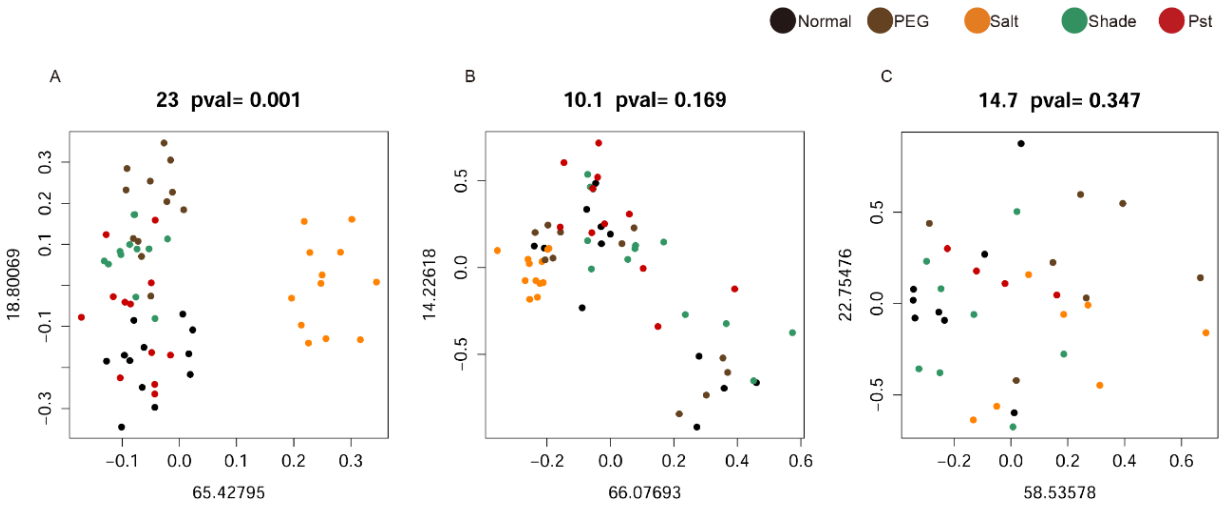

Figure 23. Constrained principal coordinate analysis of Bray-Curtis dissimilarities on bacterial (A), fungal (B) and oomycetal (C) communities from root samples in the FlowPot system. Root samples were harvested after 5 weeks of microbial inoculation in the FlowPot system. Points colour means different conditions as mentioned before. Three independent biological replicates (n = 63 samples).

4. DISCUSSION AND CONCLUSIONS

Previous studies showed that microbial growth is rate limiting in soil but nonetheless that high microbial life can be sustained by highly complex soil-derived carbon sources (**Apple et al., 2007**; **Taylor et al., 2010**). Based

on alpha diversity indices (**Figure 4 and Figure 5**), I observed that bacterial diversity is lower in the calcined-clay system compared with the FlowPot system. The complex carbon sources provided by the peat substrate in the FlowPot system might account for this difference and also likely explains the fact that the factor "system" is the major factor driving microbial community differentiation based on PCoA (**Figure 6**). Moreover, I observed that our synthetic microbial community did not promote plant growth in the calcined clay system (**Figure 17**) but did positively stimulate plant growth under drought stress (5% PEG) and shade stress in the FlowPot system (**Figure 16**), indirectly suggesting that at least some beneficial functions conferred by microbial commensals are dependent on the composition of the soil matrix.

It is well known that the host is one of the factors of driving the establishment of root-associated microbial assemblages (**Bulgarelli et al., 2013**). Using Principal coordinates analysis of Bray-Curtis distances (PCoA), I showed that the root-associated bacterial community is different from the surrounding soil microbial community in both FlowPot and calcined-clay systems (**Figure 7 and Figure 8**, **Figure 21**). These results validate that the composition of the bacterial – and to a lesser extent the fungal – root microbiota is directly or indirectly influenced by the host, consistent with previous studies (**Bulgarelli et al., 2013**; **Müller et al., 2016**; **Durán et al., 2018**).

Microbe-microbe interactions are also important forces driving the composition of plant-associated microbial communities (**Erlacher et al., 2014**) and having cascading consequences on plant health (**Hassani et al., 2018**). By taking advantage of comprehensive microbial culture collections and gnotobiotic plant systems, we performed microbiota manipulation experiments to determine whether initial differences in abundance between bacterial, fungal and oomycetal communities can influence output microbial community composition and outcome on plant growth. Durán *et al.* demonstrated that a primary physiological function of bacterial root commensals is to protect plant from extensive colonization by filamentous eukaryotes, which maintains microbial interkingdom balance for plant health (**Durán et al., 2018**). However, the extent to which the bacterial-to-fungal-to-oomycetal abundance ratio can affect root microbiota assembly and host health remained unknown. Here, I demonstrated that modification of inter-kingdom microbial ratios does not significantly affect plant health and do not influence output microbial community composition in both root and soil compartment. Given the fact that the microbial input ratio does not impact microbial community structure, I selected the

combination of low-level bacteria, low-level fungi and low-level oomycetes (BFO_LLL) as microbial inputs for the following experiments (see chapter II). The rationale behind the selection of the BFO_LLL ratio has the following: 1) we do not force the system and inoculate below the carrying capacity of the roots 2) we let the community establish and self-organize 3) we can perform more experiments/conditions using the same input microbes.

Previous studies demonstrated the advantages of using gnotobiotic systems to dissect microbe-microbe interactions, host-microbe interactions and beneficial functions of plant-associated microbiota members under the strictly controlled laboratory conditions (**Bai et al., 2015**; **Xu et al., 2013**; **Vaughan et al., 2011**; **Kremer et al., 2018**; **Durán et al., 2018**). I tested and compared three different gnotobiotic systems (the calcined-clay system, the white sand system and the FlowPot system) in this chapter. Based on shoot fresh weight data, I observed that the FlowPot system provides the best conditions for plant growth among these three gnotobiotic systems (**Figure 13, Figure 14, and Figure 15**), which is consistent with the fact that this system is the one that resemble more natural soil matrices. Moreover, in the FlowPot system, the outside microbox contains an air filter on the top which likely contributes to better regulate oxygen, carbon dioxide, and humidity levels inside the gnotobiotic system. However, it appears more difficult to impose a nutrient stress in the FlowPot system, suggesting that peat particles contain high residual amounts of phosphorous, nitrogen and iron, thereby preventing the use of this matrix for these specific research questions. In contrast, the calcined clay and white sands appears to contain fewer residual amounts of these same nutrients and therefore must be prioritize to test the interplay between soil nutrients, root microbiota and plant health. All three tested gnotobiotic systems (the FlowPot system, the calcined-clay system, and the white sand system) are possible to construct salt stresses, PEG mimic drought stresses and shade stresses. However, the nitrogen deficient stress is possible in the calcined clay system and the white sand system and the phosphate and iron stresses are only possible in the while sand system.

It is well proved that plant microbiota provides benefit for plant growth and plant health (**Müller et al., 2016**; **Hacquard et al., 2017**; **Durán et al., 2018**). In the experiments testing the effect of root microbiota on plant growth under different stresses in three gnotobiotic systems, I found that the root microbiota significantly rescued plant growth under drought stress (5% PEG) and shade stress in the FlowPot system (**Figure 16**) and

under drought stress (5% and 7% PEG) in the white sand system (**Figure 18**) which are consistent with previous study from previous studies (**Fitzpatrick et al., 2018; de Zélicourt et al., 2018**). Fitzpatrick et al. found that root microbiota improved plants drought tolerance and the abundance of one sequence variant strain from the genus *Streptomyces* was positively correlated with the ability of plants resistance to drought (**Fitzpatrick et al., 2018**). Notably, a novel finding is that a potential link might exist between aboveground light conditions and belowground root microbiota composition and function (**Figure 16**), which will be further dissected in the chapter II. Although the mechanism by which the root microbiota can confer host tolerance to abiotic stresses remains unclear, I suggest two potential mechanisms that are not necessarily mutually exclusive: 1) plant can take advantage of beneficial microbes and selectively recruit specific microbes to modulate resistance to stresses (i.e. cry for help hypothesis, **Dicke and Baldwin 2010**; **Rolfe et al., 2019**); 2) response to root microbiota members and response to abiotic stresses are interconnected in plants to prioritize microbiota-induced growth when environmental conditions are suboptimal.

Given the fact that the blank space of study in the interaction between aboveground abiotic stresses and belowground root microbiota, I further focused on how response to light and response to microbes are interconnected along the shoot-root axis, thereby promoting tolerance to light limitation stress (Chapter II).

5. MATERIALS AND METHODS

5.1 Microbial culture collection

Microbial strains utilized are showed in the **Figure 2**. In total, 184 strains of bacteria were selected from the bacterial culture collection isolated by Bai et al. (**Bai et al., 2015**). 24 strains of fungi and 7 strains of oomycetes were selected from the culture collection isolated by Durán et al. (**Durán et al., 2018**).

Microbes used that were previously isolated from *A. thaliana* roots growing in the Cologne soil. Bacterial strains and fungal strains were stored in a 25% glycerol solution at -80 ºC. Oomycetal stains were stored in PGA plates at 4 ºC.

For bacterial strains, I took the original bacterial stock (one stain was in one tube with 25% glycerol solution).

Each strain was plating on TSA plate separately and incubated for 7 days at 22 ºC. For each strain, one colony was picked and transferred to a well with 400 µL 50 %TSB in 96 deep well plate (Eppendorf, Hamburg, Germany). Two deep well plates were incubated with 180 rpm shaking speed for 7 days at 22 ºC. Then two 96 deep well plates were centrifuged for 10 min at 4000 xg (5810R, Eppendorf, Hamburg, Germany). 300 µL of the supernatant were trashed and the residue 100 µL were resuspended. Each well was added 100 µL 50% glycerol (Glycerin, 98 %, Carl Roth, Karlsruhe, Germany). Then each well was resuspended. For each well, 10 µL mixed liquid was transferred to a 96 microwell plate (96 Microwell Plates, Thermo Scientific Nunc, USA) (three replicates in three separate plates). Two 96 microwell plate were covered with aluminum film (Plate sealer, Silver Seal, Aluminums, 80x140mm, Greiner Bio-One, Austria) with a sterile lid on the top. Two 96 microwell plates were stored at -80 ºC.

For fungal strains, I took the original fungal stock (for each stain, the piece of fungal mycelium was in one tube with 25% glycerol solution). One piece of fungal mycelium was transferred to a PGA plate (Potato Glucose Agar, Sigma-Aldrich, USA) separately. The plates were incubated for 14 days at 22 ºC. Fungal mycelium of each strain was cutting into small pieces approximately 3x3 mm. The pieces of fungal mycelium were put into a 2 ml sterile tube (Eppendorf, Hamburg, Germany) with 1 ml 25% glycerol (Glycerin, 98 %, Carl Roth, Karlsruhe, Germany). The tubes were frozen with liquid nitrogen and stored at -80 ºC.

For ommycetal strains, I took the original ommycetal stock from PGA plate. For each strain, a piece of ommycetal mycelium around 3x3 mm was cut and transferred to a new PGA plate. The new plates were incubated for 7 days at 22 ºC then were stocked at -4 ºC. The oomycetal stock was renewed each month.

5.2 FlowPot experimental setup

The plant growth substrate in FlowPot system is the mixture of peat (Einheits Erde Special, Sinntal-Altengronau, Germany) and vermiculite (Agra-vermiculite M3, RHP, Netherlands) (volume ratio of peat/vermiculite=2:1). The moisten mixture was autoclaved twice using the liquid autoclaved system at 121 °C for 20 min. The internal time between two autoclaves was one day. Meanwhile, other stuffs for FlowPot, glass beads (2.85-3.45 mm, Carl Roth, Karlsruhe, Germany), mesh (Mesh fiberglass “Phiferglass”, 18 X 14 standard

charcoal mesh, Phifer Incorporated, USA), cable binder, truncated 25 ml syringe (Omnifix, 50 mL, Braun, USA), microboxs fixed with the stand of 10 µL pipette tip on the bottom (model TP1600+TPD1600 or OV80+OVD80, with L filter, Combiness, Nevele, Belgium), were autoclaved with the solid system at 121 °C for 20 min. For building up FlowPot system, each 25 truncated syringe called pot was put one layer of glass beads, then filled with the sterile substrate. Each pot was coved with sterile mesh fixed with the cable binder. The build-up pots were put on the stand of the microbox. Then microboxes were put into the Sun bag and autoclaved using the liquid system at 121 °C for 45 min. After autoclaving, each pot was flushing with 50 ml sterile Milli-Q water.

5.3 Calcined-clay experimental setup

Calcined-clay firstly was washed with Milli-Q water 5 times. The washed calcined-clay was transfer to a plastic box and covered with aluminium foil. Then the box was autoclaved using the liquid system at 121 °C for 20 min. After autoclaving, the box was put into the oven at 65 °C until the calcined-clay was totally dry (around 10 days). Meanwhile, the magenta boxes were autoclaved using the solid system at 121 °C for 20 min. Under clean bench, each magenta box was filled with 100 g sterile calcined-clay. The filled magenta boxes were autoclaved using solid system at 121 °C for 45 min.

5.4 Microbial inoculation

Bacterial glycerol 96 well plate stocks were taken and re-culture in 96 deep well plate with 400 µL 50 % TSB per each well using the sterile plastic 96 well replicator. The 96 deep well plates were incubated with 180 rpm shaking speed for 7 days at 22 ºC. On the day of inoculation, the liquid in 96 deep well plates were transferred to 50 ml falcon tubes. Falcon tubes were centrifuged for 10 min at 4000 xg (5810R, Eppendorf, Hamburg, Germany). All of the supernatant was trashed and 10 mM $MgCl_2$ was used to resuspend the residues. A mixture of 1:10 dillution of the resuspended liquid was measured OD value (absorbance at 600nm, BioPhotometer Plus, Eppendorf, Hamburg, Germany). 10 mM $MgCl_2$ was used to adjust OD600 to 0.5. Then bacterial input was ready.

Fungal mycelium pieces were taken from the glycerol stocks and re-culture on new fresh PGA plates. PGA plates were incubated at 22 ºC for 2 weeks. On the day of inoculation, each fungal mycelium was harvested and

put into a 2 ml sterile tube with a sterile metal bead (3.2 mm of diameter, Next Advance, USA) and 10 mM $MgCl_2$ (100 mg/ 1ml 10 mM $MgCl_2$). Then tubes were put into a paint shaker (SK450, Fast & Fluid Management, Sassenheim, Netherlands) and used grinding system for 10 min. 900 µL liquid from each tube was transferred to a sterile 50 ml falcon tube and mixed. Then fungal input was ready.

Oomycetal mycelium pieces were taken from the PGA plate stocked and re-culture on new fresh PGA plates. PGA plates were incubated at 22 ºC for 2 weeks. On the day of inoculation, each oomycetal mycelium was harvested and put into a 2 ml sterile tube with a sterile metal bead (3.2 mm of diameter, Next Advance, USA) and 10 mM $MgCl_2$ (100 mg/ 1ml 10 mM $MgCl_2$). Then tubes were put into a paint shaker (SK450, Fast & Fluid Management, Sassenheim, Netherlands) and used grinding system for 15 min. 900 µL liquid from each tube was transferred to a sterile 50 ml falcon tube and mixed. Then oomycetal input was ready.

For FlowPot system, each small pot was flushing with 50 ml sterile Milli-Q water. Then for the microbe condition, a mixture of bacteria, fungi and oomycetes was prepared as **Table 2**. For the microbe-free condition, same volume of pure sterile 10 mM $MgCl_2$ was prepared as the control. Then each small pot was flushing with 50 ml prepared liquid with 1/2 MS medium. Meanwhile, a mixture of bacteria, fungi and oomycetes was taken into a 2 ml tube with screw lid and centrifuged for 15 min at 40000 rpm (5810R, Eppendorf, Hamburg, Germany). The supernatant was trashed. The tube with the residue was frozen with the liquid nitrogen as the input sample.

For calcined-clay system, each magenta box was added 70 ml 1/2 MS medium. For the microbe condition, a mixture of bacteria, fungi and oomycetes was prepared as **Table 2** and was mixed with 1/2 MS medium. For the microbe-free condition, same volume of pure sterile 10 mM $MgCl_2$ was prepared as the control and mixed with 1/2 MS medium. Meanwhile, a mixture of bacteria, fungi and oomycetes was taken into a 2 ml tube with screw lid and centrifuged for 15 min at 40000 rpm (5810R, Eppendorf, Hamburg, Germany). The supernatant was trashed. The tube with the residue was frozen with the liquid nitrogen as the input sample.

5.5 Seeds sterilization and plant growth condition

A. thaliana Col-0 seeds were sterilized before using. First step, *A. thaliana* Col-0 seeds were put into a 2 ml

Eppendorf tube with1 ml 70 % ethanol (Ethanol absolute, VWR Chemicals, USA). Then the tube was incubated in a rotator (Rotator SB3, Stuart, UK) and shaken for 18 min. The tube was centrifuged for 1 min at 1000 rpm (5810R, Eppendorf, Hamburg, Germany). The second step, under clean bench, the supernatant was trashed and 1 ml 100 % ethanol added into the tube. Then the tube was centrifuged for 1 min at 1000 rpm (5810R, Eppendorf, Hamburg, Germany). The supernatant was trashed. The tube was opened the lip and dry under the clean bench. The dried seeds were incubated at 4 ºC for 2 days under dark condition.

On the sowing seeds day, the seeds were put on the surface of the matrix. For both FlowPot system and calcined-clay system, 10 seeds were put on each pot. Then FlowPot microboxes and magenta boxes were put into the chamber (Panasonic; Day conditions: light intensity 4, 21ºC, 10 hours light; Night conditions: light intensity 0, 19ºC, 14 hours dark). For FlowPot system, plants were grown 5 weeks. For calcined-clay system, plants were cultured for 6 weeks.

5.6 Sample harvesting

After 5 weeks of plant growth in FlowPot system and 6 weeks of plant growth in calcined-clay system, plant shoots were harvested and measured the shoot fresh weight using a precision balance (ABS-N/ABJ-NM, Kern & Sohn, Balingen, Germany). Meanwhile, plant roots were washed with sterile Milli-Q water and dried with sterile Whatman paper (Whatman® glass microfiber filters, Grade GF/B, Sigma-Aldrich, Hamburg, Germany). The root samples were put into a 2 ml tube with screw lid and frozen with liquid nitrogen. In FlowPot system, the matrix samples were taken from the mixture of peat and vermiculite without roots and placed into 2 ml tube with screw lid and frozen with liquid nitrogen. In calcined-clay system, the matrix samples were taken from the calcined-clay without roots. Fist, 35 ml calcined-clay were transferred to a 50 ml falcon tube. 1×TE buffer was added to the falcon tube to 50 ml. The falcon tubes were shacked for 1 min by hand. The supernatant was transferred to a new falcon tube and centrifuged for 15 min at 4000 xg (5810R, Eppendorf, Hamburg, Germany). Each falcon tube was added 1 ml 1×TE to resuspend. Then the resuspended liquid was transferred to 2 ml tube with screw lid and frozen with liquid nitrogen.

5.7 Amplicon based microbial community profiling

5.7.1 DNA isolation and DNA concentration measurement

All samples of roots and matrixes placed in a 2 ml tube with screw lip separately were crashed using the Precellys®24 tissue lyzer (Bertin Technologies, Montigny-le-Bretonneux, France). For soil, calcined-clay and input samples, 978 µl SPB (Sodium Phosphate Buffer) with 122 µl MT-Buffer were added to each tube. The tubes were crashed (Nr. 5) 1×30 sec. For root samples, the tubes were crashed (Nr. 5) 1×30 sec fist and then added 978 µl SPB (Sodium Phosphate Buffer) with 122 µl MT-Buffer. The tubes with buffer were crashed again (Nr. 5) 1×30 sec. All the tubes were centrifuge 15 minutes at 14000×g (rcf). Then all samples of roots and matrixes were performed DNA isolation using he FastDNA ® SPIN for soil kit (MP Biomedicals, Solon, USA). After DNA isolation, the concentration of sample DNA was measured by PicoGreen method. First 1×TE Buffer was prepared. Then the dye of PicoGreen was added into 1×TE Buffer (PicoGreen: Pico Working Solution=1:200), mixed, this was the working Pico solution. 40 µl working Pico solution was added into QPCR plate wells. 4 µl DNA sample was added to the well. The fluorescence of samples was measured by QPCR machine (IQ5 real-time PCR Thermocycler, Biorad, Munich, Germany). The procedure of QPCR was 30 sec at 25 °C, 3x30 seconds at 25 °C for measuring fluorescence, 30 seconds at 15 °C. Finally, all of samples DNA were adjusted to 3.5 ng/µl.

5.7.2 Sample library preparation and sequencing

Sample library preparation started with two steps of PCR for bacteria, fungi and oomycetes separately. For bacteria, the first step PCR used 25 cycles with primer V5-V6 (799F/1192R). For fungi, the first step PCR used 25 cycles with primer ITS1 (ITS1F/ITS2). For oomycetes, the first step PCR used 25 cycles with primer ITS1 (ITS1-O/5.8s-O-Rev). The first step PCR in total contains 25 µL containing 3 µL sample DNA, 1x incomplete reaction buffer, 1.25 U DFS-Taq DNA Polymerase, 2 mM of MgCl2, 0.3 % BSA, 200 µM of dNTPs and 400 nM of each primer. The procedure of PCR was 94 °C for 2 minutes, 94 °C for 30 seconds, 55 °C for 30 seconds, 72 °C for 30 seconds and 72 °C for 10 minutes in total 25 cycles. After the first step PCR, digestion was conducted to remove the enzyme and primers in the first step PCR. For digestion step, a mixture of 1 µl Antarctic

phosphatase, 1 µl Exonuclease I and 2.44 µl Antarctic phosphatase buffer was added to 20 µl of the pooled first step PCR product. The procedure of digestion was 37 °C for 30 minutes and 85 °C for 15 minutes. After the digestion, 3 µl liquid was taken as the sample for the second step PCR. The second step PCR was used the same PCR mixture solution except primers that barcode primes including barcodes and Illumina adaptors (B5-barcodes for bacteria, Ft-barcodes for fungi, Ot-barcodes for oomycetes). The procedure of second step PCR was 94 °C for 2 minutes, 94 °C for 30 seconds, 55 °C for 30 seconds, 72 °C for 30 seconds and 72 °C for 10 minutes in total 10 cycles.

After two steps PCR, 5 µl PCR product was mixed with 5 µl 6×Orange G DNA Loading Dye for each sample. Then the mixture mixed with 5 µL of Gel Loading Dye (Orange G, 6X, Sigma, Hamburg, Germany) was run on the 1 % agarose gel with TAE to check the DNA bind. After control gel checking, for bacteria, all PCR product (around 70 µL) was mixted with 20 µL Gel Loading Dye (Orange G) and run on a 1.5 % agarose gel for 2 hours at 80 V. Bands with the 500 bp size were cut and purified using the QIAquick gel extraction kit (Qiagen, Hilden, Germany). After gel extraction, DNA concentration was measured using the PicoGreen method as described already. For fungi and oomycetes, the purification was used Agencourt AMPure XP-PCR Purification (AMPure XP-PCR Purification, Beckman Coulter, Krefeld, Germany). The pure DNA samples concentration was measure by the PicoGreen method described before. For each kingdom (bacteria, fungi and oomycetes), the same amount DNA of each sample was mixed. Then for each kingdom, the mixture was purified with Agencourt AMPure XP-PCR Purification (AMPure XP-PCR Purification, Beckman Coulter, Krefeld, Germany) twice. The DNA concentration was measured by the Quantus™ Fluorometer (Promega, Manheim, Germany). The same amount of DNA from bacteria, fungi and oomycetes was mixed. The mixture DNA concentration was measure by the Quantus™ Fluorometer (Promega, Manheim, Germany).

Finally, paired-end Illumina DNA sequencing was performed using the Illumina MiSeq system at the Department of Plant-Microbe Interactions, Max Planck Institute for Plant Breeding Research, following manufacturer instructions. Sequencing data analysis was conducted with bioinformatic pipelines developed by Dr. Rubén Garrido-Oter and Dr. Thorsten Thiergart.

5.8 Data analysis and figure generation

Data analysis and figure generation were performed in R (R version 3.6.3). For the alpha-diversity (**Figure 3 and Figure 4**), observed OTUs were calculated using QIIME (alpha-diversity function in R). For the beta-diversity (**Figure 5, Figure 6 and Figure 7**), OUT data were normalized based on the method of the cumulative sum scaling (CSS), then Bray-Curtis distances among samples were calculated using the method of principal coordinate analysis (PCoA, Function "cmdscale" in R). For constrained PCoA (**Figure 8 and Figure 9**), different factors were calculated the effect on the estimated explained variance using PERMANOVA analysis (Function "capscale", "vegan" package in R). Figure 10 was generated with the P package of "ggplot2". The statistics were performed using Kruskal-Wallis post with Dunn test in R.

References

Agler MT, **Ruhe J**, **Kroll S**, **Morhenn C**, **Kim ST**, *et al.* (**2016)**. Microbial hub taxa link host and abiotic factors to plant microbiome variation. *PLOS Biol*. 14: e1002352

Apple, J. K. & del Giorgio, P. A. (2007). Organic substrate quality as the link between bacterioplankton carbon demand and growth efficiency in a temperate salt-marsh estuary. *Multidisc. J. Microb. Ecol.* 1, 729–742.

Augé, R. M. (2001). Water relations , drought and vesicular-arbuscular mycorrhizal symbiosis. *Mycorrhiza*. 3–42.

Bahram M, Hildebrand F, Forslund SK, Anderson JL, Soudzilovskaia NA, *et al.* (2018). Structure and function of the global topsoil microbiome. *Nature* 560:233–37.

Bai Y, Mu¨ller DB, Srinivas G, Garrido-Oter R, Potthoff E, *et al.* (2015). Functional overlap of the Arabidopsis leaf and root microbiota. *Nature* 528:364–69.

Berendsen R L, Vismans G, Yu K, Song Y, De Jonge R, *et al.* (2018). Disease-induced assemblage of a plant-beneficial bacterial consortium. *ISME J*. 12:1496–507.

Berendsen, R. L. (2012). The rhizosphere microbiome and plant health. Trends in Plant *Science* **17**.

Berer, K. *et al.* (2011). Commensal microbiota and myelin autoantigen cooperate to trigger autoimmune demyelination. *Nature* **479**, 538–541.

Berg G, Smalla K. (2009). Plant species and soil type cooperatively shape the structure and function of microbial communities in the rhizosphere. *FEMS Microbiol. Ecol*. 68:1–13.

Bodenhausen N, Horton MW, Bergelson J. (2013). Bacterial communities associated with the leaves and the roots of Arabidopsis thaliana. *PLOS ONE* 8: e56329.

Bogino P, Abod A, Nievas F, Giordano W. (2013). Water-limiting conditions alter the structure and biofilm-forming ability of bacterial multispecies communities in the alfalfa rhizosphere. *PLOS ONE* 8: e79614.

Bouasria A, Mustafa T, De Bello F, Zinger L, Lemperiere G, et al. (2012). Changes in root-associated microbial communities are determined by species-specific plant growth responses to stress and disturbance. *Eur. J. Soil Biol*. 52:59–66.

Bowsher AW, Kearns PJ, Popovic D, Lowry DB, Shade A. (2020). Locally adapted Mimulus ecotypes differentially impact rhizosphere bacterial and archaeal communities in an environment-dependent manner. *Phytobiomes J*. 4:53–63.

Buffie, C. G. & Pamer, E. G. (2013). Microbiota-mediated colonization resistance against intestinal pathogens. *Nat. Publ. Gr.* **13**, 790–801.

Bulgarelli D, Garrido-Oter R, Muench PC, Weiman A, Droege J, *et al.* (2015). Structure and function of the bacterial root microbiota in wild and domesticated barley. *Cell Host Microbe* 17:392–403.

Bulgarelli, D., Rott, M., Schlaeppi, K., *et al*. (2012). Revealing structure and assembly cues for Arabidopsis root-inhabiting bacterial microbiota. *Nature*, 488, 91–95.

Bulgarelli, D., Schlaeppi, K., Spaepen, S., *et al*. (2013). Structure and Functions of the Bacterial Microbiota of Plants. *Annual Review of Plant Biology*, 64, 807–838.

Burch AY, Zeisler V, Yokota K, Schreiber L, Lindow SE. (2014). The hygroscopic biosurfactant syringafactin produced by Pseudomonas syringae enhances fitness on leaf surfaces during fluctuating humidity. *Environ. Microbiol*. 16:2086–98.

Carlström, C.I., Field, C.M., Bortfeld-Miller, M. *et al*. (2019). Synthetic microbiota reveal priority effects and keystone strains in the Arabidopsis phyllosphere. *Nat Ecol Evol* 3, 1445–1454. https://doi.org/10.1038/s41559-019-0994-z

Castrillo, G. *et al.* (2017). Root microbiota drive direct integration of phosphate stress and immunity. *Nature.* **543**, 513–518.

Chapelle E, **Mendes R**, **Bakker PA**, **Raaijmakers JM**. **(2016)**. Fungal invasion of the rhizosphere microbiome. *ISME J*. 10:265–68.

Chen Y, Wang J, Yang N, Wen Z, Sun X, Chai Y, Ma Z. (2018). Wheat microbiome bacteria can reduce virulence of a plant pathogenic fungus by altering histone acetylation. *Nat Commun.* 9(1):3429. doi: 10.1038/s41467-018-05683-7. PMID: 30143616; PMCID: PMC6109063.

Coince, A., Caël, O., Bach, C., *et al.* (2013) Below-ground fine-scale distribution and soil versus fine root detection of fungal and soil oomycete communities in a French beech forest. *Fungal Ecology*, **6**, 223–235.

Copeland JK, Yuan L, Layeghifard M, Wang PW, Guttman DS. (2015). Seasonal community succession of the phyllosphere microbiome. Mol. *Plant-Microbe Interact*. 28:274–85.

Daniel B. Müller, Christine Vogel, Yang Bai, Julia A. (2016). The Plant Microbiota: Systems-Level Insights and Perspectives. *Annual Review of Genetics.* 50:1, 211-234.

Delmotte N, Knief C, *et al*. (2009). Community proteogenomics reveals insights into the physiology of phyllosphere bacteria. *PNAS* 106:16428–33.

Dicke M., Baldwin I. T. (2010). The evolutionary context for herbivore-induced plant volatiles: beyond the 'cry for help'. *Trends in Plant Science*, Volume 15, Issue 3, Pages 167-175, ISSN 1360-1385, https://doi.org/10.1016/j.tplants.2009.12.002.

Durán, P. Thiergart T. *et al.* (2018). Microbial Interkingdom Interactions in Roots Promote Arabidopsis Survival. *Cell* **175**, 973-983.e14.

Edwards J, Johnson C, Santos-Medellin C, Lurie E, Podishetty NK, *et al*. (2015). Structure, variation, and assembly of the root-associated microbiomes of rice. *PNAS* 112: E911–20.

Erlacher A, Cardinale M, Grosch R, Grube M, Berg G. (2014). The impact of the pathogen Rhizoctonia

solani and its beneficial counterpart Bacillus amyloliquefaciens on the indigenous lettuce microbiome. *Front. Microbiol*. 5:175

Eugene Rosenberg, Ilana Zilber-Rosenberg. (2016).Microbes Drive Evolution of Animals and Plants: the Hologenome Concept. *mBio.* e01395-15.

Finkel OM, Burch AY, Lindow SE, Post AF, Belkin S. (2011). Geographical location determines the population structure in phyllosphere microbial communities of a salt-excreting desert tree. Appl. Environ. *Microbiol*. 77:7647–55.

Finkel, O.M., Salas-González, I., Castrillo, G. et al. (2020). A single bacterial genus maintains root growth in a complex microbiome. *Nature*. https://doi.org/10.1038/s41586-020-2778-7

Frey B, Bühler L, Schmutz S, Zumsteg A, Furrer G (2013). Molecular characterization of phototrophic microorganisms in the forefield of a receding glacier in the Swiss Alps. Environmental Research Letters, 8, 015033.

Garcia-Pichel, F., Loza, V., Marusenko, Y., Mateo, P. & Potrafka, R. M. (2013). Temperature Drives the Continental-Scale Distribution of Key Microbes in Topsoil Communities. *Science (80-.).* 340, 1574 LP – 1577.

Hacquard S, Garrido-Oter R, Gonzalez A, Spaepen S, Ackermann G, *et al.* (2015). Microbiota and host nutrition across plant and animal kingdoms. *Cell Host Microbe* 17:603–16.

Hacquard, S., Kracher, B., Hiruma, K. *et al.* (2016). Survival trade-offs in plant roots during colonization by closely related beneficial and pathogenic fungi. *Nat Commun* **7,** 11362. https://doi.org/10.1038/ncomms11362

Harbort C. J., Hashimoto M., Inoue H., *et al.* (2020). Root-Secreted Coumarins and the Microbiota Interact to Improve Iron Nutrition in Arabidopsis. Cell Host & Microbes, 28, 1–13. https://doi.org/10.1016/j.chom.2020.09.006

Hassani, M. A., Durán, P. & Hacquard, S. (2018). Microbial interactions within the plant holobiont. *Microbiome* **6**, 58.

Hassani, M.A., Durán, P. & Hacquard, S. (2018). Microbial interactions within the plant holobiont. *Microbiome* **6,** 58. https://doi.org/10.1186/s40168-018-0445-0

Horton M W, Bodenhausen N, Beilsmith K *et al.* (2014). Genome-wideassociation study of Arabidopsis thaliana leaf microbial community. *Nat. Commun*. 5:5320.

Horton MW, **Bodenhausen N**, **Beilsmith K**, **Meng D**, **Muegge BD**, *et al.* (**2014**). Genome-wide association study of *Arabidopsis thaliana* leaf microbial community. *Nat. Commun.* 5:5320

Hu, L., Robert, C.A.M., Cadot, S. et al. (2018). Root exudate metabolites drive plant-soil feedbacks on growth and defense by shaping the rhizosphere microbiota. *Nat Commun* 9, 2738. https://doi.org/10.1038/s41467-018-05122-7

Ivanov, I. I. (2013). Intestinal commensal microbes as immune modulators. *NIH Public Access*. **12**, 496–508.

Kamoun, S., Furzer, O., Jones, J.D.G., *et al.* (2015) The Top 10 oomycete pathogens in molecular plant pathology. *Molecular Plant Pathology*, **16**, 413–434.

Kembel S W, O'Connor T K, Arnold H K, *et al.* (2014). Relationships between phyllosphere bacterial communities and plant functional traits in a neotropical forest. *PNAS* 111:13715–20.

Kemen E. (2014). Microbe–microbe interactions determine oomycete and fungal host colonization. Current Opinion in Plant Biology, 20, 75-81, https://doi.org/10.1016/j.pbi.2014.04.005.

Knief C, Ramette A, Frances L, Alonso-Blanco C, Vorholt JA. (2010). Site and plant species are important

determinants of the Methylobacterium community composition in the plant phyllosphere. *ISME J*. 4:719–28.

Kong, H. G., Kim, B. K., Song, G. C., Lee, S. & Ryu, C.-M. (2016). Aboveground Whitefly Infestation-Mediated Reshaping of the Root Microbiota. *Frontiers in Microbiology* **7**, 1314.

Kremer, J. M. *et al.* (2018). FlowPot axenic plant growth system for microbiota research. *bioRxiv* 254953. doi:10.1101/254953.

Lundberg D S, Lebeis S L *et al.* (2012). Defining the core Arabidopsis thaliana root microbiome. *Nature* 488:86–90.

Margulis L. (1991). Symbiogenesis and symbionticism, p 1–14. In Margulis L, Fester R (ed), Symbiosis as a source of evolutionary innovation: speciation and morphogenesis. MIT Press, Cambridge, MA.

Mariat, D. *et al.* (2009). The Firmicutes/Bacteroidetes ratio of the human microbiota changes with age. *BMC Microbiology*. **6**, 1–6.

Matsuoka, M. & Jeang, K. (2007). Human T-cell leukaemia virus type 1 (HTLV-1) infectivity and cellular transformation. *Nature*. **7**, 270–280.

Matthew T. Agler, Jonas Ruhe,Samuel Kroll, *et al.* (2016). Microbial Hub Taxa Link Host and Abiotic Factors to Plant Microbiome Variation. *Plos Biology*. 14(1): e1002352.

Melnyk, R.A., Hossain, S.S. & Haney, C.H. (2019). Convergent gain and loss of genomic islands drive lifestyle changes in plant-associated Pseudomonas. *ISME J* 13, 1575–1588.

Mendes LW, Kuramae EE, Navarrete AA, van Veen JA, Tsai SM. (2014). Taxonomical and functional microbial community selection in soybean rhizosphere. *ISME J*. 8:1577–87.

Müller D. B., Vogel C., Bai Y., Vorholt J. A. (2016). The Plant Microbiota: Systems-Level Insights and Perspectives. *Annual Review of Genetics*, 50:1, 211-234

Naylor, D., DeGraaf, S., Purdom, E. et al. (2017). Drought and host selection influence bacterial community dynamics in the grass root microbiome. *ISME J* 11, 2691–2704. https://doi.org/10.1038/ismej.2017.118

NIH HMP Working Group; Peterson, J; Garges, S; *et al.* (2009). "The NIH Human Microbiome Project". *Genome Res*. 19 (12): 2317–2323. doi:10.1101/gr.096651.109. PMC 2792171. PMID 19819907.

Oldroyd GED, Murray JD, Poole PS, Downie JA. (2011). The rules of engagement in the legume-rhizobial symbiosis. Annu. Rev. Genet. 45:119–44.

Parniske M. (2008). Arbuscular mycorrhiza: the mother of plant root endosymbioses. *Nat. Rev. Microbiol.* 6:763–75.

Peay, K., Baraloto, C. & Fine, P. (2013). Strong coupling of plant and fungal community structure across western Amazonian rainforests. *ISME J* **7,** 1852–1861.

Peiffer JA, Spor A, Koren O, Jin Z, Tringe SG, *et al*. (2013). Diversity and heritability of the maize rhizosphere microbiome under field conditions. *PNAS* 110:6548–53.

Pieterse C. M.J., Zamioudis C., Berendsen R. L., et al. (2014). Induced Systemic Resistance by Beneficial Microbes. *Annual Review of Phytopathology*. 52:1, 347-375

Rastogi, G., Coaker, G.L. and Leveau, J.H.J. (2013). New insights into the structure and function of phyllosphere microbiota through high-throughput molecular approaches. *FEMS Microbiol Lett*, 348, 1–10.

Road, A. (2002). Pathogen profile Bipolaris sorokiniana , a cereal pathogen of global concern : cytological and molecular approaches towards better control. *Molecular Plant Pathology*. **3**, 185–195.

Rolfe S. A., Griffiths J., Ton J. (2019). Crying out for help with root exudates: adaptive mechanisms by which

stressed plants assemble health-promoting soil microbiomes. *Current Opinion in Microbiology*, Volume 49, Pages 73-82, ISSN 1369-5274, https://doi.org/10.1016/j.mib.2019.10.003.

Santhanam R., Luu V. T., Weinhold A., et al. (2015). Native root bacteria rescue a native plant. *Proceedings of the National Academy of Sciences*, 112 (36) E5013-E5020; DOI: 10.1073/pnas.1505765112

Schlaeppi K, Dombrowski N, Oter RG, *et al.* (2014). Quantitative di-vergence of the bacterial root microbiota in Arabidopsis thaliana relatives. *PNAS* 111:585–92.

Stringlis, I. A. *et al.* (2018). MYB72-dependent coumarin exudation shapes root microbiome assembly to promote plant health. *Proc. Natl. Acad. Sci.* **115**, E5213 LP-E5222.

Taylor, P., Townsend, A. (2010). Stoichiometric control of organic carbon–nitrate relationships from soils to the sea. *Nature* **464,** 1178–1181.

Thiergart, T., Durán, P., Ellis, T. *et al.* (2020). Root microbiota assembly and adaptive differentiation among European *Arabidopsis* populations. *Nat Ecol Evol* **4,** 122–131.

Vannier, N. & Agler, M. (2019). Microbiota-mediated disease resistance in plants. *Plos Pathogens*. 1–7. doi:10.1371/journal.ppat.1007740

Vaughan, M.M., Tholl, D. & Tokuhisa, J.G. (2011). An aeroponic culture system for the study of root herbivory on *Arabidopsis thaliana*. *Plant Methods* **7,** 5.

Vorholt J. A., Vogel C., Carlström C. I., et al. (2017). Establishing Causality: Opportunities of Synthetic Communities for Plant Microbiome Research. *Cell Host & Microbe*, Volume 22, Issue 2, https://doi.org/10.1016/j.chom.2017.07.004

Wagner, M., Lundberg, D., del Rio, T. *et al*. (2016). Host genotype and age shape the leaf and root microbiomes of a wild perennial plant. *Nat Commun* **7,** 12151. https://doi.org/10.1038/ncomms1215

Walitang, D. I. C., Kim, K., Kim, Y., Kang, Y. K. Kim., & Sa, T. (2018). The influence of host genotype and salt stress on the seed endophytic community of salt-sensitive and salt-tolerant rice cultivars. *BMC Plant Biology*, **18**(1), 51. https://doi.org/10.1186/s12870-018-1261-1

Walitang, D.I., Kim, C., Kim, K. *et al*. (2018). The influence of host genotype and salt stress on the seed endophytic community of salt-sensitive and salt-tolerant rice cultivars. BMC *Plant Biol* 18, 51.

Xiong, C., Zhu, Y.-G., Wang, J.-T., Singh, B., *et al*. (2020). Host selection shapes crop microbiome assembly and network complexity. *New Phytol.* doi:10.1111/nph.16890

Xu, W., Ding, G., Yokawa, K. *et al.* (2013). An improved agar-plate method for studying root growth and response of *Arabidopsis thaliana*. *Sci Rep* **3,** 1273.

Hiruma, K. et al. (2016). Root endophyte *Colletotrichum tofieldiae* confers plant fitness benefits that are phosphate status dependent. *Cell* **165**, 464–474.

Udvardi M. and Poole P. S. (2013). Transport and Metabolism in Legume-Rhizobia Symbioses. *Annual Review of Plant Biology* 64:1, 781-805

Smith SE, Smith FA (2011). Roles of arbuscular mycorrhizas in plant nutrition and growth: new paradigms from cellular to ecosystem scales. *Ann Rev Plant Biol* 62:227–250

Voges, M. J. E. E. E., Bai, Y., Schulze-lefert, P., & Sattely, E. S. (2019). Plant-derived coumarins shape the composition of an Arabidopsis synthetic root microbiome, *PNAS 116*(25). https://doi.org/10.1073/pnas.1820691116

Ritpitakphong, U., Falquet, L., Vimoltust, A., Berger, A., Métraux, J.-P. and L'Haridon, F. (2016), The microbiome of the leaf surface of Arabidopsis protects against a fungal pathogen. *New Phytol*, 210: 1033-1043. doi:10.1111/nph.13808

Fitzpatrick CR, et al. (2018) Assembly and ecological function of the root microbiome across angiosperm plant species. *Proc Natl Acad Sci*, **115**:E1157–E1165.

Berens M, Wolinska K, Spaepen S, Ziegler J, Nobori T, Nair A, Krüler V, Winkelmüller T, Wang Y, Mine A *et al.* (2019). Balancing trade-offs between biotic and abiotic stress responses through leaf age-dependent variation in stress hormone cross-talk. *Proceedings of the National Academy of Sciences, USA* **116**: 2364– 2373.

de Zélicourt A, Synek L, Saad MM, Alzubaidy H, Jalal R, et al. (2018). Ethylene induced plant stress tolerance by *Enterobacter* sp. SA187 is mediated by 2-keto-4-methylthiobutyric acid production. *PLOS Genetics* 14(3): e1007273.

Chapter II

Microbiota-root-shoot axis modulation by MYC2 alleviates light limitation stress in *Arabidopsis*

1. INTRODUCTION

1.1 Plant development in response to aboveground stresses

Unlike animals, plants are sessile organisms that must simultaneously integrate various responses to biotic and abiotic stresses to prioritize either growth or defense depending on rapidly changing surrounding conditions (**Huot et al., 2014**). The amplitude and dynamics of variation observed for aboveground stresses (i.e., light, temperature, pathogens, insects) is known to be greater than that observed in soil, suggesting that plants must respond to aboveground stresses rapidly and dynamically to ensure survival. In this part, I summarized the effect of the aboveground stresses including temperature, light, herbivores, and leaf pathogens on plant growth and defense based on previous reports.

1.1.1 Impact of temperature on plant growth and defense

Temperature is one of the most important environmental factors influencing plant growth and defense responses (**Hatfield et al., 2015**). Along with the problem of the global warming, heat waves or extreme temperature events are becoming more and more frequent (**Intergovernmental Panel Climate Change (IPCC) - AR6 Synthesis Report: Climate Change 2022**). According to IPCC AR6 report, human activities are estimated to have caused approximately 1.0°C of global warming above pre-industrial levels, with a likely range of 0.8°C to 1.2°C. That will result in the enhanced effect of temperature on plant development, growth and defense.

Plants response to temperature differs among species throughout their life cycle and their development stages (**Hatfield et al., 2015**). Different Plants have evolved mechanisms to adapt to specific ranges of maximum

and minimum temperatures for their development and growth (**Schlenker et al., 2009**; **Hatfield et al., 2015**). For example, the growth response range of temperature for *Zea mays L.* is 12 °C to 38 °C while for broccoli, *Brassica oleracea L.* plants from cool season is 7 °C to 23 °C (**Hatfield et al., 2015**). For example, Schlenker and Roberts (2009) found that the yield of corn, soybean, and cotton sharply decreased when temperatures exceeded their growth maximum threshold of 32°C (**Schlenker et al., 2009**). Recently, the study from Hinojosa et al. showed that heat stress reduced the pollen viability in *Chenopodium quinoa* Willd between 30% and 70% (**Hinojosa et al., 2019**). Oppositely, previous studies show that low temperature also restricts plant growth via affecting meristematic growth processes at the level of cell and resulting in sink limitation (**Hoch et al., 2003**; **Hoch et al., 2009**; **Shi et al., 2008**; **Molina-Montenegro et al., 2012**; **Zuther et al., 2018**; **Wang et al., 2019**). For instance, Zheng et al. found that fiber elongation in cotton is largely reduced under low temperature (**Zheng et al., 2012**). To cope with the low temperature, plants evolved some signaling pathways to adjust growth in response to low temperature. In *Arabidopsis thaliana*, the well-known pathway is the gibberellins pathway via the repressor of DELLA protein for plants to control growth under low temperature stress (**Achard and Genschik, 2009**; **Colebrook et al., 2014**; **Xu et al., 2014**). Under low temperature stress, the content of gibberellins (GAs) is decreased. Since DELLA proteins are repressors of the GA signaling pathway, DELLA proteins will accumulate when the content of GAs decreases, thereby resulting in the inhibition of plant growth (**Achard et al., 2008**). Exogenous application of salicylic acid (SA) could improve wheat and maize tolerance to low-temperature since SA could regulate cell growth and protect the cell structure by modulating cell enlargement and division (**Wang et al., 2018**; **Wang et al., 2020**).

Besides plant development and growth, the temperature could also modulate plant innate immunity (**Penfield 2008**; **Huot et al., 2017**; **Hammoudi et al., 2018**). The elevated temperature inhibits plant resistance (R) gene expression, thereby resulting in low defense under high temperature stress (**Wang et al., 2009**). Yang and Hua found that the elevated temperature could suppress the accumulation of some immune regulators, for example Enhanced Disease Susceptibility1 (EDS1) and Phytoalexin Deficient 4 (PAD4), which have function in plant basal resistance towards leaf pathogens (**Yang and Hua, 2004**). Similarly, Huot et al. showed that the elevated temperature significantly increases *Arabidopsis thaliana* plants' susceptibility to *Pseudomonas syringae pv. tomato* (*Pst*) DC3000 which was independent of the phyB and PIF thermosensing pathway (**Huot et al., 2017**). Conversely, low temperature was shown to enhance plant immunity via salicylic acid pathway genes (**Li et al.,**

2020). The study from Li et al. found that low temperature reduced propagation of *Pst* DC3000 due to an increase of NLR-triggered immunity and basal resistance under low temperature conditions (**Li et al., 2020**). Li et al. further demonstrated that low temperature increased plant immunity depended on SA pathway through using mutants defective in SA biosynthesis and signaling (**Li et al., 2020**).

1.1.2 Effect of circadian clock on plant growth and defense

The circadian clock or the circadian rhythm in plants is a molecular timing mechanism that regulates numerous developmental and defense processes with a cyclic period of 24 hours (**Zhang et al., 2019**). In recent decades, great process has been made in understanding the network of regulators in the circadian clock in *Arabidopsis thaliana*. Previous studies found that the plant circadian clock system contains multiple negative feedback loops which depend on genes of *CCA1* (circadian clock-associated 1), *PRR* (pseudo-response response regulator), *LHY* (late elongated hypocotyl), *TOC1* (timing of cab expression 1), *GI* (gigantea), *LUX* (lux arrhythmo), *ELF* (early flowering), *HSP90* (heat shock protein 90), *ZTL* (zeitlupe), strigolactone signaling, and sugar sensing (**Nakamichi et al ., 2010**; **Pruneda-Paz and Kay, 2010**; **Nusinow et al ., 2011**; **Gendron et al ., 2012**; **Huang et al ., 2012**; **Nagel and Kay, 2013**; **Fung-Uceda et al., 2018**; **Zhang et al., 2019**; **Wang et al., 2020**). The circadian clock controls plant growth via affecting the cell cycle. One key component of the circadian system in *Arabidopsis* is *TOC1* (TIMING OF CAB EXPRESSION 1). Fung-Uceda et al. found that *TOC1* regulates the timing of cell division in developing leaves via regulating the expression of the DNA replication licensing gene *CDC6* (**Fung-Uceda et al., 2018**).

Besides the effect of the circadian clock on plant growth, the circadian clock also has a profound influence on plant immunity building on the observation that the circadian rhythm modulates the expression of some defense related genes (i.e., *EDS1*, *JAZ5*, *PAD4*) and/or the closure/opening of the stomata (**Roden and Ingle 2009**; **Zhang et al., 2019**). For example, Wang et al. found that the CIRCADIAN CLOCK-ASSOCIATED 1 (*CCA1*), one of the circadian regulators, is involved in *R*-gene-mediated defense towards downy mildew in *Arabidopsis* (**Wang et al., 2011**). Moreover, the circadian clock plays a critical role in plant defense towards herbivory via the regulation with jasmonate signaling in *Arabidopsis* (**Goodspeed et al., 2012**; **Joo et al., 2019**).

1.1.3 Effect of light on plant growth and defense

Light is a fundamental source of energy that plants can convert into chemical energy through photosynthesis (**Bailey-Serres et al., 2018**). Plants sense and capture a variety of light colors and intensities via photoreceptors (**Kobayashi and Weigel, 2007**; **Turck et al.,2008**; **Tilbrook et al., 2013**; **Christie et al., 2015**; **Viczian et al., 2017**). It has been determined that the photoreceptors in *Arabidopsis* contain four main gene families: phytochrome (PHY), cryptochrome (CRY), phototropin (PHOT), and zeitlupe (ZTL) (**Chen et al., 2004**; **Somers and Fujiwara, 2009**). The PHY family encompass five genes (*PHYA* to *PHYE*), the CRY family contains three genes (*CRY1* to *CRY3*), the PHOT family has two phototropin genes – (*PHO1*and *PHO2*), whereas the ZTL family contains three Zeitlupe genes (*ZTL*, *FKF1* and *LKP2*) (**Chen et al., 2004**; **Somers and Fujiwara, 2009**). Downstream light perception by photoreceptors, numerous light signaling components exist and transfer the light signals. For example, COP1 (CONSTITUTIVE PHOTOMORPHOGENIC 1), the ubiquitin E3 ligase, is light-regulated protein via conjunction with PHYA and the COP1/SPA (CONSTITUTIVE PHOTOMORPHOGENIC 1/SUPPRESSOR OF PHYTOCHROME A-105) complex is a central repressor of light signaling (**Höcker 2017**). Meanwhile COP1 is also connected with other downstream components in the light signaling, for example *HY5* (ELONGATED HYPOCOTYL 5) and *LAF1* (LONG AFTER FR LIGHT 1), to regulate plant physiological responses (**Zhu et al., 2008**; **Jenkins, 2009**). Moreover, COP1 can be suppressed by photoactivated cryptochromes in blue light (**Ponnu et al., 2019**). Interplay between photochrome signaling and phytohormone signaling also regulate plant response to light (**Shin et al., 2012**), such as the crosstalk between photochrome signaling and JA signaling (**Robson et al., 2010**). PHYA involves in the degradation of JAZ1 (the repressor in JA signaling) regulated by MYC2 (the transcription factor in JA signaling) (**Wang et al., 2020**). Meanwhile, MYC2 can directly bind to the promoter of the PHYA suppressor – SPA1 (SUPPRESSOR OF PHYTOCHROME A 1) to regulate the expression of *SPA1* (**Chakraborty et al., 2019**).

The range of different light wavelengths captured by the canopy of plants, which can be used for carbohydrate biosynthesis, energy production, and growth, is called photosynthetically active radiation (PAR) (**Hatfield et al., 1984**). Spectral PAR irradiance ranges from 400 to 700 nm under natural conditions, and a reduction of both the amount of PAR (light quantity) and the ratio red to far-red light (light quality) is perceived as a warning signal in plants facing light limiting conditions, thereby triggering adaptive changes in shoot morphology

(**Franklin and Whitelam 2005**; **Franklin, 2008**). To cope with light stress (i.e., low/high PAR conditions, UV radiation), plants evolved a multilevel network of responses and adaptations (**Yang et al., 2019**). The responses can be summarized as regulating light absorption and modulating the captured light energy resulting in altering leaf traits (i.e., leaf orientations, leaf reflectance, and petiole length) (**Yang et al., 2019**). Recent researches proved that plants response to light stress via microRNA-mediated regulation (**Subburaj et al. 2017**; **Achkar et al. 2018**). Besides shoots, light also can affect plant roots (**Walker et al., 2003**; **Lee et al., 2016**). Light signal can be transferred from plant aboveground tissues to roots through the expression of ELONGATED HYPOCOTYL 5 (HY5) in stem triggered by photoactivated phytochrome B (phyB) in shoots to accumulate HY5 protein in roots (**Lee et al., 2016**) confirming the previous founding that light condition in shoots could regulate the metabolism of roots (**Walker et al., 2003**). Recently, the study from Saini and Fricke showed that low PAR affect root and cell hydraulics in barley (**Saini and Fricke, 2020**). These results from previous studies mentioned above suggest light-shoot-root axis does exist and regulate plant growth and development to cope with light stress.

Light has been well known to affect plant defense (**Roden and Ingle, 2009**; **Ballaré 2014**). First, light deficiency affects plant immunity via photoreceptors and the crosstalk with phytohormone (**Manfre et al., 2011**; **Campos et al., 2016**). Manfre et al. showed that both light deficiency and photoreceptors (PHYA and PHYB) impairment increased *N. benthamiana* plants' susceptibility to *Turnip mosaic virus* (TuMV) (**Manfre et al., 2011**). Under continuous light, the blue light photoreceptor CRY1 was shown that be involved in enhanced plant resistance towards *P. syringae* pv. *tomato* (*Pst.*) DC3000 (**Wu and Yang, 2010**). Besides light quantity, the light quality also regulates plant immunity (**Roberts and Paul, 2006**). This regulation mainly depends on the modulation of JA pathway through sensing the ratio between red light and far red light (**Kazan and Manners, 2011**). Under a low ratio of red light to far red-light condition, *Arabidopsis* plants were more susceptible to the necrotrophic pathogen *Botrytis cinerea* which is dependent on COI1 (Coronatine-insensitive 1) and JAZ10 (Jasmonate ZIM domain) – two important components in JA signaling (**Cerrudo et al., 2012**; **Cortés et al., 2016**). Under light deficiency conditions (i.e., low PAR condition, low R:FR condition), shade-intolerant plants were supposed to prioritize growth over defense (**Ballaré 2014**; **Smakowska et al., 2016**). However, some short-term studies in *Arabidopsis* proved that the effect of light on growth is also possible to uncouple with the effect of light on defense (**Cerrudo et al., 2012**; **Cerrudo et al., 2017**). For instance, the *cry1* mutant showed

both a constitutively elongated hypocotyl and resistance to the fungus pathogen *Botrytis cinerea* phenotype (**Cerrudo et al., 2017**). Given the previous studies in trade-offs between growth and defense under light stress mentioned above, a major challenge in the future will be to clarify the underlying mechanisms of different specific photoreceptors (i.e. single specific phytochrome or cryptochrome) regulating plant defense signaling pathways.

1.2 Aboveground stress modulates plant-associated microbes

As discussed in Chapter I, plants in nature live in association with a vast diversity of microorganisms. Besides the effect of aboveground stresses on plant growth and defense mentioned above, the same aboveground stresses also influence plant-associated microbes.

1.2.1 Impact of temperature on soil- and plant-associated microbes

Temperature correlates with microbial diversity in soil and has been shown to be directly linked to microbial metabolism and biochemical processes of microbes (**Gillooly et al., 2001; Brown et al., 2004**). Through sampling the soil microbial communities across North American together with co-cultivation oftwo cyanobacterium strains (*Microcoleus vaginatus* and *M. steenstrupii*) under laboratory conditions, Garcia-Pichel et al. observed that temperature shifted the abundance of these two strains with *M. vaginatus* being more psychrotolerant and *M. steenstrupii* being more thermotolerant (**Garcia-Pichel et al., 2013**). Similarly, by analyzing 126 soil samples from across forest sites with a wide range of temperature gradient using next-generation sequencing technology, Zhou et al. showed that the temperature is a primary factor explaining the composition of soil microbial communities in forest soils and microbes show significantly lower turnover rates across the gradients of temperature compare with plants (**Zhou et al., 2016**). Recently, temperature has been shown to influence arbuscular mycorrhiza fungal diversity and evenness in the roots (**Rasmussen et al., 2018**), root-associated fungal communities (**Rasmussen et al., 2020**), and be one of factors driving bacterial communities in *Arabidopsis* rhizosphere and rhizosplane (**Thiergart et al., 2020**) and in maize roots (**Beirinckx et al., 2020**). Those findings suggested that beyond pH, temperature can also affect composition and function of microbial communities in soil. Therefore, it is likely that temperature also modulates root-associated

microbial communities by modulating the source of root-associated microbes.

1.2.2 Effect of circadian clock and light on plant-associated microbes

As mentioned previously, the circadian clock or the circadian rhythm in plants regulates numerous processes of plant development, growth, and defense. Hence plant metabolism and root exudates are regulated by the circadian clock, thereby affecting plant-associated microbes (**Greenham and McClung, 2015**). It is long well shown that the circadian clock regulates plant immunity, and thereby influences the infection of plant pathogens as summarized previously. Besides plant pathogens, the circadian clock of plants also regulates the commensal and mutualistic microbes (**Staley et al., 2017**; **Hubbard et al., 2018**). Through investigating the bacterial communities in the rhizosphere of *Arabidopsis thaliana* plants (Col-0 and two clock mutants - *toc1-21* and *ztl-30*) at different time points from day to night, Hubbard et al. found that samples from day time points show significant rhizosphere communities compared with samples from night time points and two clock mutants show significant rhizosphere communities compared with Col-0 plants suggesting that the circadian clock of plants influences the structure of rhizosphere communities (**Hubbard et al., 2018**).

Light, one of the major drivers in the circadian clock of plants, influences plant-associated microbes. First as mentioned above, light has been well known to modulate plant defense, and therefore influences endosphere colonization by plant pathogens (**Manfre et al., 2011**). Besides plant pathogens, growth of microbial commensal is also directly influenced by light in the phyllosphere (**Mandalari et al., 2013**; **Beattie et al., 2018**). Light can directly influence some microbes colonized in phyllosphere since some microbes have evolved light sensors and can adjust their metabolisms depending on the surrounding light (**Beattie et al., 2018**). For example, two main photoreceptors in prokaryotic organisms are the bilin-binding phytochrome-related proteins and the flavin-binding proteins (**Mandalari et al., 2013**). Moreover, diurnal light cycle was showed that significantly shift rhizosphere microbiota composition by increasing in the relative abundance of *Proteobacteria*, except for the *Betaproteobacteria*, the *Firmicutes*, and the *Actinobacteria*, and decreasing in the relative abundance of *Acidobacteria* and *Bacteroidetes* compared with dark cycle suggesting carbon metabolism regulated by light is associated with rhizosphere bacterial communities in *Arabidopsis thaliana* (**Staley et al., 2017**); and phenolic compounds increased by UV-B enhancing *Deinococcus citri* strain D61 colonization in *Nicotiana attenuata*

(Santhanam et al., 2017). Similarly, shade-responsive OTUs were reported to be correlated with the phenolic glycoside and sugar metabolism in poplar trees (Timm et al., 2018). However, the extent to which changes in light conditions aboveground can directly or indirectly (i.e. via changes in the host metabolism) modulate the structure of belowground root-associated microbial communities remains unknown.

1.3 Plant-microbiota interaction helps partners cope with aboveground stress

It is well known that microbial symbionts play a role on increasing plants tolerance to extreme temperature (Barka et al., 2006; Acuña-Rodríguez et al., 2020). Barka et al. observed that one of the rhizobacterium strains, *Burkholderia phytofirmans* strain *PsJN*, significantly enhanced grapevine growth under cold stress (Barka et al., 2006). Similarly, Aroca et al. demonstrated that arbuscular mycorrhizal symbiosis improved plants tolerance to cold temperature (Aroca et al. 2007). Recently, a meta-analyses study based on 14 independent experimental studies showed that symbionts significantly increased around 29% of shoot biomass for plants grown at low temperature (from -1°C to 15°C) compared with germ-free plants (Acuña-Rodríguez et al., 2020) indicating that plant symbionts alleviated plant chilling stress.

The circadian clock and light, it is well known that these aboveground factors can regulate plant immunity and modulate plant-associated microbial communities as summarized previously. However, the effect of plant-associated microbes on the extreme condition of air humidity, the circadian clock and light is still unclear.

1.4 Hypothesis and research questions (Chapter II)

Given the fact that the root microbiota rescues plant growth under the suboptimal light condition (chapter I), I first hypothesized that a microbiota-root-shoot axis does exist in plants, allowing them to take advantage of belowground microbial commensals to orchestrate aboveground stress responses. Secondly, I hypothesized that changes in light conditions perceived by leaves can cascade along the shoot-root axis, thereby modulating root microbiota assembly. The major objective was to understand how and by which mechanism plants that are colonized by the synthetic microbiota orchestrate resource investment into shoot under light limiting conditions.

2. Experimental setup

Based on the microbial input ratio experiment and the stress tolerance experiment (see above, chapter I), I chose the input ratio of low level bacteria, low level fungi and low level oomycetes (BFO SynCom with LLL combination) in the FlowPot system using the same experimental setup described in Chapter I to test the extent to which 1) the root microbiota modulates aboveground shoot phenotypic traits under suboptimal light conditions, 2) the root microbiota alters plant responses to light, and 3) the light conditions modulate the structure of the root microbiota.

For the suboptimal light conditions, I chose three different conditions: 1) normal condition with sufficient light (**NC**), 2) reducing partial photosynthetically active radiation (PAR) to get low PAR condition (**LP**, Lomax et al., 2008) , resulting in~55% reduction in photosynthetic photon flux density (PPFD, Mann-Whitney U test, *P* < 2.2e-16) (**Figure 1A and B**) whilst only marginally affecting the R:FR ratio (NC = 9.24, LP = 9.14, **Figure 1C**) and the temperature (NC = 21.02°C, LP = 20.90°C, **Figure 1C**), and 3) by exposing shoot to FR light during 15 minutes at the end of the day (**EODFR**, Dubois et al., 2010).

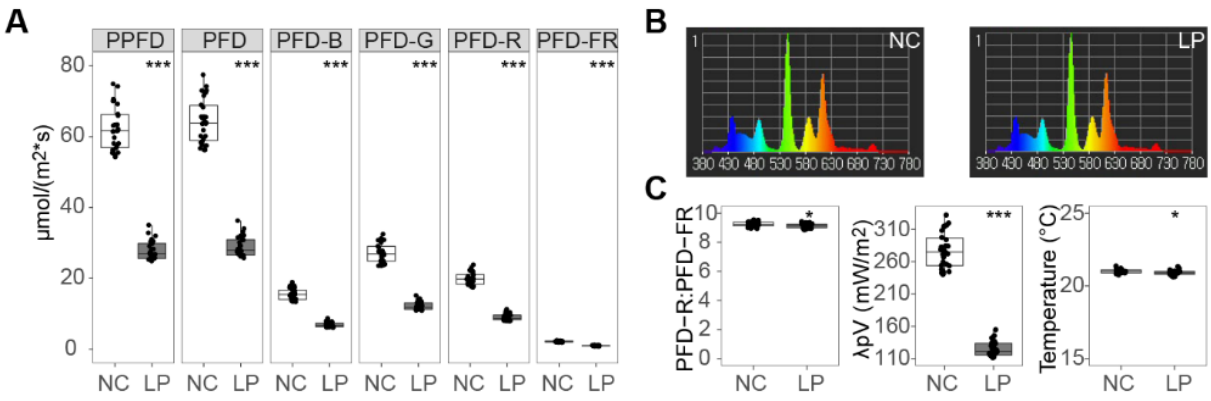

Figure 1. Light parameters and temperature under NC and LP. (A) Light parameters measured in the FlowPot system at different positions in the plant growth chamber (λp = 545 nm). PPFD: Photosynthetic Photon Flux Density defined in 400~700nm, PFD: Photosynthetic Photon Flux Density defined in 380~780nm, PFD-B: Photosynthetic Photon Flux Density in blue field (400~500nm),PFD-G: Photosynthetic Photon Flux Density in green field (500~600nm), PFD-R: Photosynthetic Photon Flux Density in red field (600~700nm),

PFD-FR: Photosynthetic Photon Flux Density in far-red field (700~780nm). Asterisks indicate statistical significance (Mann-Whitney U test, *** $P < 0.001$). **(B)** Spectrum in the FlowPot system under NC (normal light, left) and LP (low PAR, right). **(C)** R:FR ratio (left), λpV(Peak wavelength value: the highest power in the measured spectrum, middle), and temperature (right) measured in the FlowPot system at different positions in the plant growth chamber under different light conditions (NC: normal light and LP: low PAR). Asterisks indicate statistical significance (T-test for R:FR ratio, Mann-Whitney U test for Peak wavelength value and temperature, ***P<0.001, *P<0.05)

3. RESULTS

3.1 Root microbiota confers *A. thaliana* tolerance to light deficiency

Given the fact that root microbiota confers plants growth rescue under suboptimal light condition on chapter I, I continued to test the effect of root microbiota on plant growth under LP (low PAR-low photosynthetic radiation) and EODFR (15 min far red-light treatment end of day). Based on the canopy size **(Figure 2A)** and shoot fresh weight **(Figure 2B)** data, LP and EODFR significant reduced plant canopy size and shoot fresh weight in the absence of root microbiota indicating both LP and EODFR conditions are limiting plant growth in our gnotobiotic system. Notably, the presence of root microbiota rescued LP- and EODFR-mediated reduction in plant canopy size (LP: 2.4-fold, Wilcoxon, P = 5.45e-13; EODFR: 2.1-fold, Wilcoxon, P = 2.88e-4; **Figures 2A and C**) and shoot fresh weight (LP: 2.2-fold, Wilcoxon, P = 2.32e-8; EODFR: 2.2-fold, Wilcoxon, P = 4.11e-5; **Figure 2B**) to the sufficient light condition (NC). These results indicate that the BFO SynCom can rescue plant growth under suboptimal light condition and help plants cope with an aboveground abiotic stress.

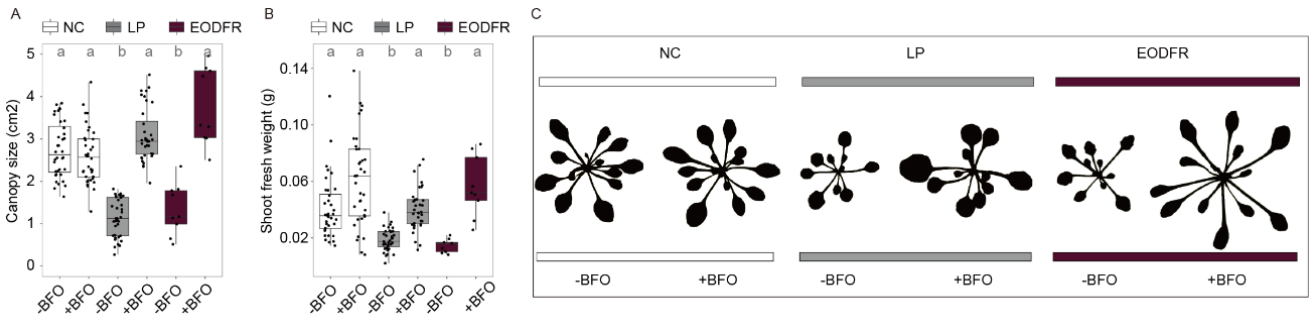

Figure 2. BFO-mediated modulation of shoot growth under LP and EODFR. (A) Canopy size (in cm^2) of five-week-old A. thaliana grown in the FlowPot system in the absence (-) or presence (+) of a synthetic microbial community (SynCom, B = 183 bacteria, F = 24 fungi, O =

7 oomycetes) under either normal light (NC, white), low photosynthetically active radiation (LP, grey), or end-of-day far red (EODFR, dark red). Three independent biological replicates (n = 162 plants). Letters indicate statistical significance corresponding to *Kruskal-Wallis* with *Dunn's* post hoc test (α = 0.05). **(B)** Shoot fresh weight (in g) of five-week-old A. thaliana inoculated with and without the BFO SynCom under NC, LP, and EODFR. Three independent biological replicates (n = 162 plants). Letters indicate statistical significance corresponding to *Kruskal-Wallis* with *Dunn's* post hoc test (α = 0.05). **(C)** Representative images illustrating light- and BFO-induced change in shoot morphology.

From the plant shoot pictures, I observed that plants under LP and EODFR showed different phenotypes (i.e. petiole length, leaf shape and leaf number) (**Figure 2C**). In order to better quantify plant shoot phenotypes, I measured petiole length, ratio of leaf length to leaf width (a proxy of leaf shape) and leaf number after plants five weeks growth in FlowPot. The presence of root microbiota led to a significant increase in petiole length (**Figure 3A**) and leaf number (**Figure 3B**) while showing a lesser extend leaf length/width ratio (**Figure 3C**). Inspection of the magnitude of root microbiota-mediated modification of leaf traits indicated extensive differences among the tested parameters and revealed that root microbiota-induced modification of the leaf length/width ratio, a quantitative measurement of leaf shape, was explaining the least BFO-mediated growth rescue under LP and EODFR (Cohen's d and Hedges'g effect size, **Figure 3D**). Taken together, those results indicate that belowground microbial commensals promote plant´s ability to overcome aboveground light limitation stress by promoting canopy size and to a lesser extent by modulating canopy shape.

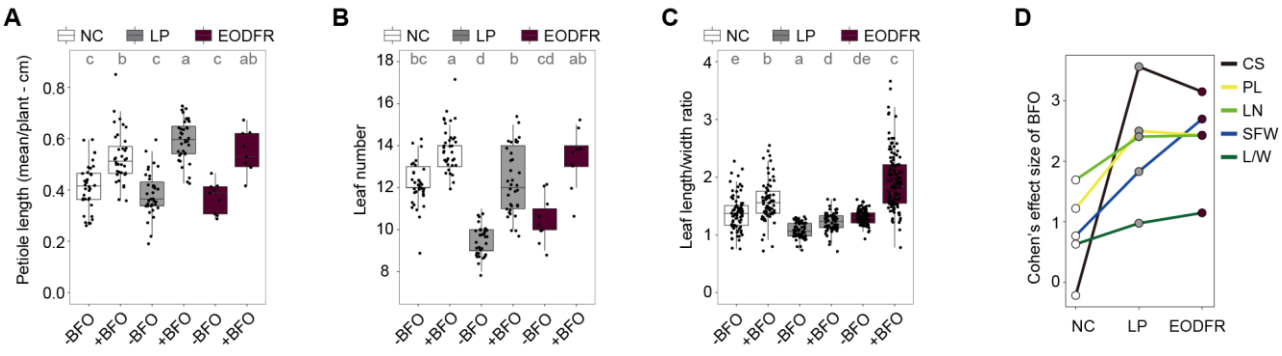

Figure 3. BFO-mediated modulation of leaf traits under LP and EODFR. (A) Mean petiole length (in cm) of five-week-old A. thaliana inoculated with (+) and without (-) the BFO SynCom under NC, LP, and EODFR. Three independent biological replicates (n = 161 plants). Letters indicate statistical significance corresponding to Kruskal-Wallis with Dunn's post hoc test (α = 0.05). **(B)** Leaf length/width ratio of

five-week-old A. thaliana inoculated with (+) and without (-) the BFO SynCom under NC, LP, and EODFR. Note that a ratio close to one reflects round leaves, whereas a ratio close to two reflects elongated leaves. Three independent biological replicates (n = 489 leaves). Letters indicate statistical significance corresponding to Kruskal-Wallis with Dunn's post hoc test (α = 0.05). **(C)** Total leaf number of five-week-old A. thaliana inoculated with (+) and without (-) the BFO SynCom under NC, LP, and EODFR. Three independent biological replicates (n = 161 plants). Letters indicate statistical significance corresponding to Kruskal-Wallis with Dunn's post hoc test (α = 0.05). **(D)** Effect size of BFO on shoot morphological traits under NC, LP, and EODFR. Effect size was computed between -BFO and +BFO conditions for each light condition by adjusting the calculation of the standard deviation with weights of the sample sizes (Cohen´s d, Hedges´g).

3.2 The modification of light modulates root microbiota assembly

After confirming that BFO root commensals promote plant growth under suboptimal light condition, I was wondering whether change in light conditions perceived by leaves can cascade along the shoot-root axis, thereby modulating root microbiota assembly. Using the same strategy described above, I monitored bacterial, fungal and oomycetal community composition in roots and surrounding peat matrix for both LP and NC using amplicon sequencing methods. The 183 bacteria, 24 fungi and 7 oomycetes, respectively, could be discriminated into 115, 17, and 7 strain variants at single nucleotide resolution against reference 16S rRNA and ITS sequences. Inspection of bacterial, fungal, and oomycetal strain variants detected across conditions indicated weak to insignificant effect of the light condition on microbial alpha diversity in both peat soil matrix and root samples (One-Way ANOVA with post hoc Tukey HSD test, **Figure 4**).

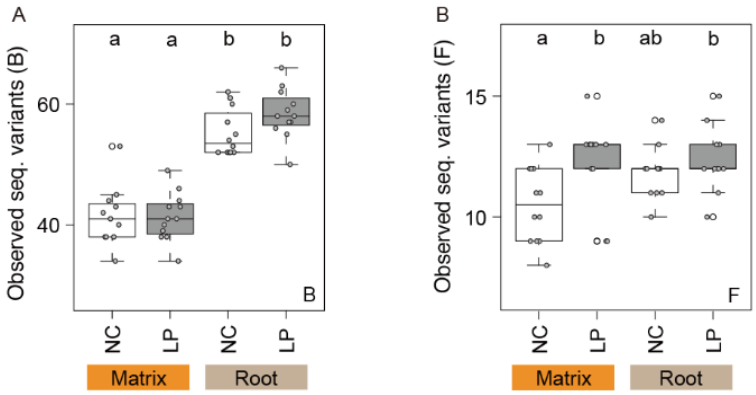

Figure 4. Observed sequenced variants of bacteria (A) and fungi (B). Number of bacterial **(A)** and fungal **(B)** strain variants detected in root and surrounding peat samples five weeks post BFO inoculation in the FlowPot system. Three independent biological replicates (n =

48 samples). Letters indicate statistical significance corresponding to TukeyHSD test (α = 0.05). NC: normal light condition, LP: low PAR.

To clarify the effect of the light condition on microbial beta diversity in both peat soil matrix and root samples, I used principal coordinates analysis of Bray-Curtis dissimilarities (PCoA, **Figure 5**), as well as permutational multivariate analysis of variance (PERMANOVA, **Table 1**). PCoA and PERMANOVA revealed that the factor "compartment" explained a significant part of the variance in bacterial and fungal, but not oomycetal community compositions in the FlowPot system ("compartment", B: $R^2 = 0.40$, $P < 0.001$, F: $R^2 = 0.13$, $P < 0.001$; O: $R^2 = 0.02$, $P = 0.439$, **Table 1**). Overall, the factor "light" did not affect fungal and oomycetal community composition but did significantly shape bacterial community composition in a compartment-dependent manner ("light", $R^2 = 0.07$, $P = 0.002$; "compartment: light" interaction, $R^2 = 0.03$, $P = 0.051$, **Table 1**).

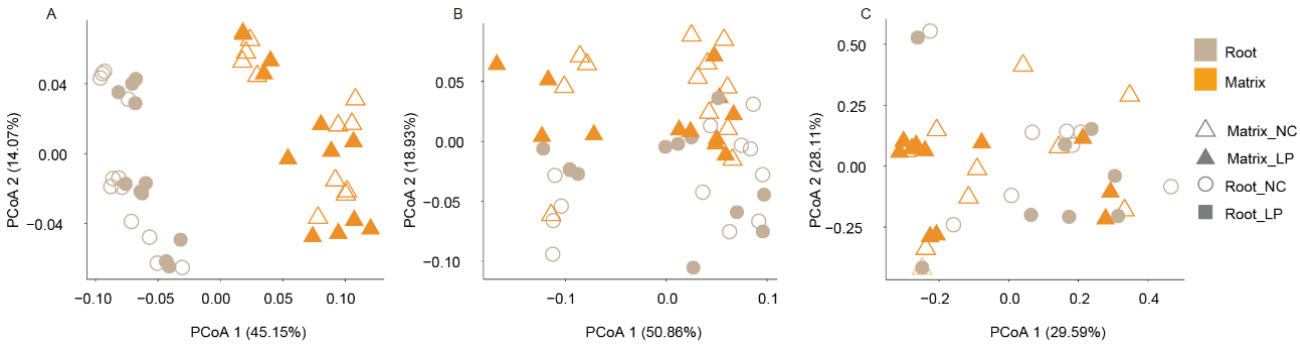

Figure 5. Influence of compartment and light conditions on BFO community composition. Effect of "Compartment" and "Light" on bacterial **(A)**, fungal **(B)**, and oomycetal **(C)** community composition in roots and surrounding peat matrix in the FlowPot system. Data were visualized using a principal-component analysis (PCoA) and the first two dimensions of the PCoA were plotted based on Bray-Curtis dissimilarities. Samples were depicted according to the compartment (matrix: orange triangles; root: brown circles) and the light condition (normal light condition, NC, open symbols; Low PAR, LP, filled symbols).

To further test whether "light" influenced bacterial community composition differentially in root and matrix samples, I used a canonical analysis of principal coordinates (CAP: capscale function in R). CAP analysis constrained by "light" indicated that change in light condition significantly shaped bacterial community composition in roots ("light", 11.9 %, $P < 0.001$), but not in the surrounding soil matrix ("light", $P = 0.606$, **Figure 6D**). In contrast, "light" had no significant effect on fungal and oomycetal community composition in roots ("light", F: $P = 0.105$, O: $P = 0.574$, **Figure 6D**) and a weak impact on fungal community in the matrix

("light", F: $P = 0.023$, O: $P = 0.659$, **Figure 6D**). Partial least squares-discriminant analysis (PLS-DA, **Figure 6A, 6B and 6C**), together with PERMANOVA conducted on root and matrix samples separately (**Table 1**) corroborated the specific and prominent effect of the light condition on the composition of root-associated bacterial communities ("light", root: $R^2 = 0.23$, $P = 0.006$; matrix $R^2 = 0.05$, $P = 0.3$, **Table 1**).

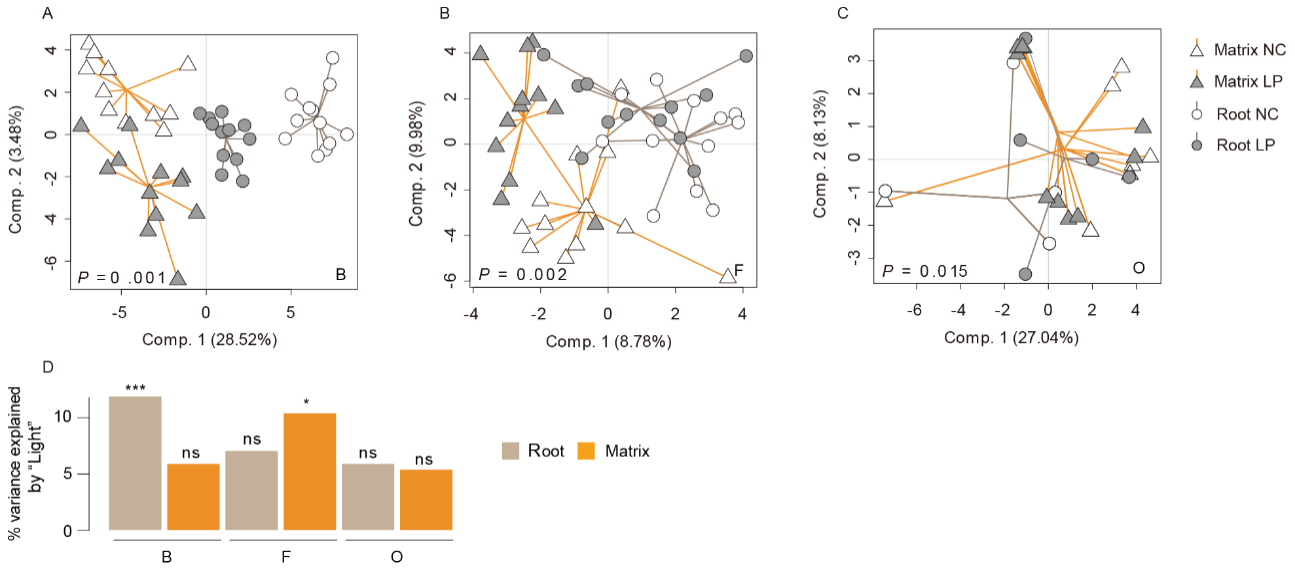

Figure 6. LP-mediated modulation of root microbiota assembly. Between-group variation in microbial community composition using partial least square discriminant analysis (PLS-DA). PLS-DA model testing the significance of the factor light and compartment on bacterial **(A)**, fungal **(B)**, and oomycetial **(C)** community composition. The four following groups were used as "grouping factor" in the model: NC-Root, NC-matrix, LP-root, and LP-matrix. The percentage of variance indicated on each axis represents the variance of the community's composition explained by the grouping factor (n = 48 samples). **(D)** Variation in B, F, and O community composition explained by "Light" (i.e. NC *versus* LP) in root and matrix samples five weeks post BFO inoculation in the FlowPot system. Canonical analysis of principal coordinates was used to quantify the percentage of variance explained by "Light" for each condition. *** $P < 0.001$, * $P < 0.05$.

Table 1 PERMANOVA partitioning of microbial community assemblages based on OTUs distance matrices (Bray Curtis dissimilarities, 999 permutations, with Adonis function in R).

(A) PERMANOVA partitioning of bacterial community assemblages

	Global model			
	Bacteria			
	df	***F***	***R2***	***P***
Compartment	8	4.197	0.39719	**0.001**
Light	1	6.435	0.07474	**0.002**
Compartment:Light	1	2.467	0.02865	0.051
Residuals	43	NA	0.49943	NA
Total	46	NA	1.0	NA

	Model based on roots samples			
	Bacteria			
	df	***F***	***R2***	***P***
Light	1	6.3953	0.2252	**0.006**
Residuals	22	NA	0.77478	NA
Total	23	NA	1.0	NA

	Model based on Matrix samples			
	Bacteria			
	df	***F***	***R2***	***P***
Light	1	1.2002	0.05406	0.3
Residuals	21	NA	0.94594	NA
Total	22	NA	1.0	NA

(B) PERMANOVA partitioning of fungal community assemblages

	Global model			
	Fungi			
	df	***F***	***R2***	***P***
Compartment	8	6.7737	0.12735	**0.001**
Light	1	2.4267	0.04562	0.054
Compartment:Light	1	-0.0093	-0.00017	0.998
Residuals	44	NA	0.82721	NA
Total	47	NA	1.0	NA

	Model based on roots samples			
	Fungi			
	df	***F***	***R2***	***P***
Light	1	0.5279	0.02343	0.674
Residuals	22	NA	0.97657	NA
Total	23	NA	1.0	NA

	Model based on Matrix samples			
	Fungi			
	df	***F***	***R2***	***P***
Light	1	2.4127	0.09883	0.094
Residuals	22	NA	0.90117	NA
Total	23	NA	1.0	NA

(C) PERMANOVA partitioning of oomycetal community assemblages

	Global model			
	Oomycetes			
	df	***F***	***R2***	***P***
Compartment	8	0.89343	0.02282	0.439
Light	1	0.67425	0.01722	0.527
Compartment:Light	1	1.57743	0.04030	0.213
Residuals	36	NA	0.91966	NA
Total	39	NA	1.0	NA

	Model based on roots samples			
	Oomycetes			
	df	***F***	***R2***	***P***
Light	1	2	0.11819	0.142
Residuals	15	NA	0.88181	NA
Total	16	NA	1	NA

	Model based on Matrix samples			
	Oomycetes			
	df	***F***	***R2***	***P***
Light	1	-0.26499	-0.01278	0.999
Residuals	15	NA	0.88181	NA
Total	16	NA	1.0	NA

To further elucidate the structure of bacterial community in root and matrix samples under NC and LP, pairwise-enrichment tests were conducted between LP and NC conditions for root and matrix samples separately. Pairwise-enrichment tests revealed a significant impact of the light condition on the relative abundance of 23 strain variants in root samples and 4 strain variants in matrix samples (**Figure 7**). Notably, multiple *Pseudomonas* isolates were consistently and specifically enriched between LP and NC in the root compartment (**Figure 7**).

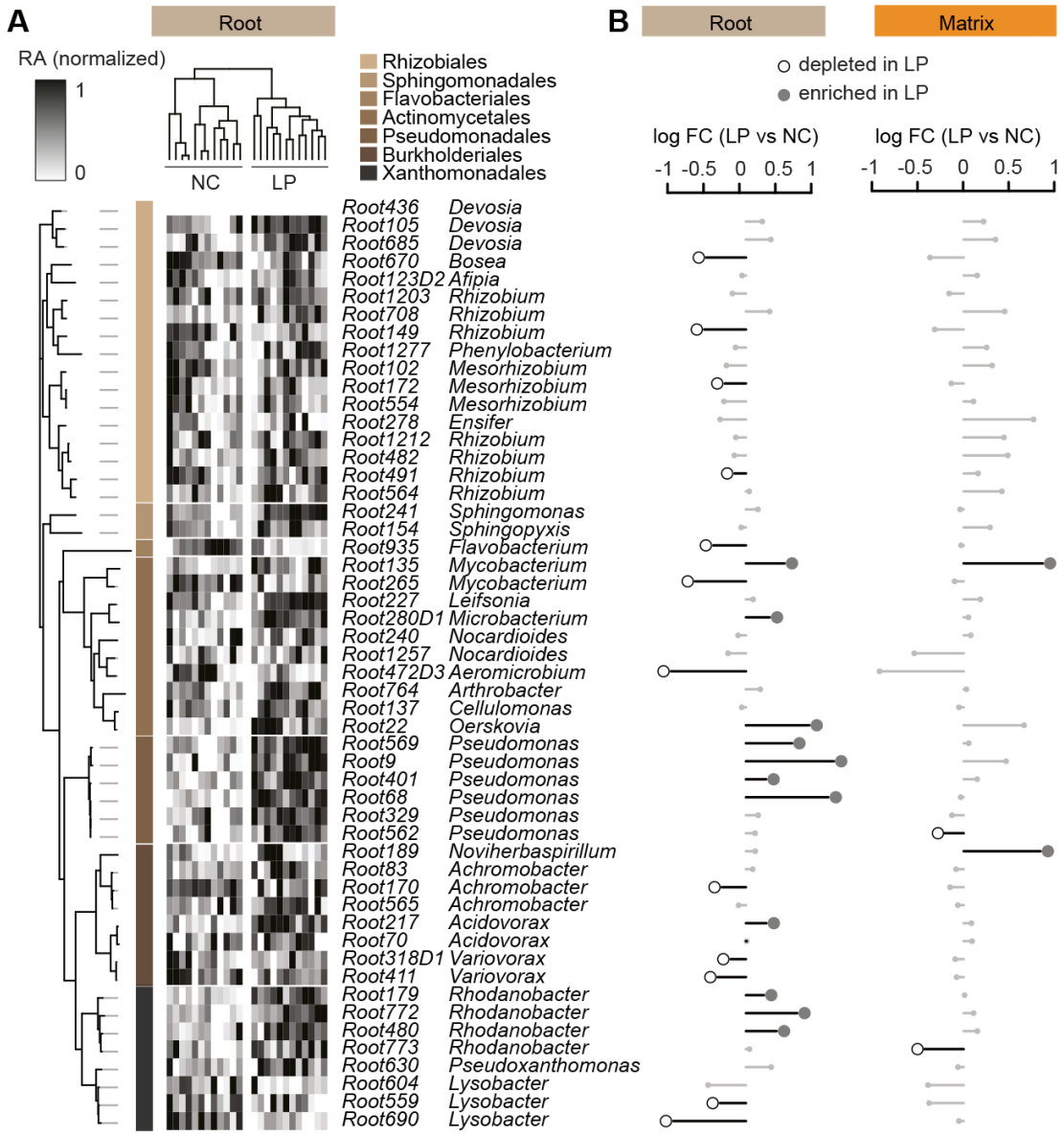

Figure 7. LP-mediated modulation of root bacterial assembly. (A) Normalized relative abundance (RA) of the most prevalent B strain variants detected in roots across NC and LP conditions. Sample-wise normalized RA was calculated for each strain variant and depicted in the heatmap next to the taxonomic tree. Note that only strain variants with an average RA ≥ 0.1% across samples were considered (n = 24 samples). The taxonomic tree was constructed based on a maximum likelihood method using full length 16S rRNA sequences. **(B)** Sample wise log2 fold-change in RA measured for each prevalent strain variant between LP and NC in root and matrix samples (t-test, $P < 0.05$). Log2 fold-changes between LP and NC.

Furthermore, recolonization experiments with Bacterial (B) in the presence or absence of Fungal (F) and Oomycetal (O) communities indicated that B commensals are necessary, but not sufficient for the growth rescue

phenotype in LP (**Figure 8A**). Therefore, the synergistic contribution of B and filamentous eukaryotes is needed to induce full tolerance to LP in the host. Given the fact that multiple *Pseudomonas* isolates enriched under LP compared with NC in the roots (**Figure 7**), I used B removed *Pseudomonas* isolates and *Pseudomonas* isolates alone plus -B and +B as control to evaluate the function of *Pseudomonas* isolates on plant growth under LP. Based on the recolonization experiments with above mentioned microbial communities, I observed that B without *Pseudomonas* isolates lost the function of rescuing plant growth under LP and *Pseudomonas* isolates alone did not rescue plant growth under LP (**Figure 8B**) indicating that *Pseudomonas* isolates are essential but not sufficient to rescue plant growth under LP.

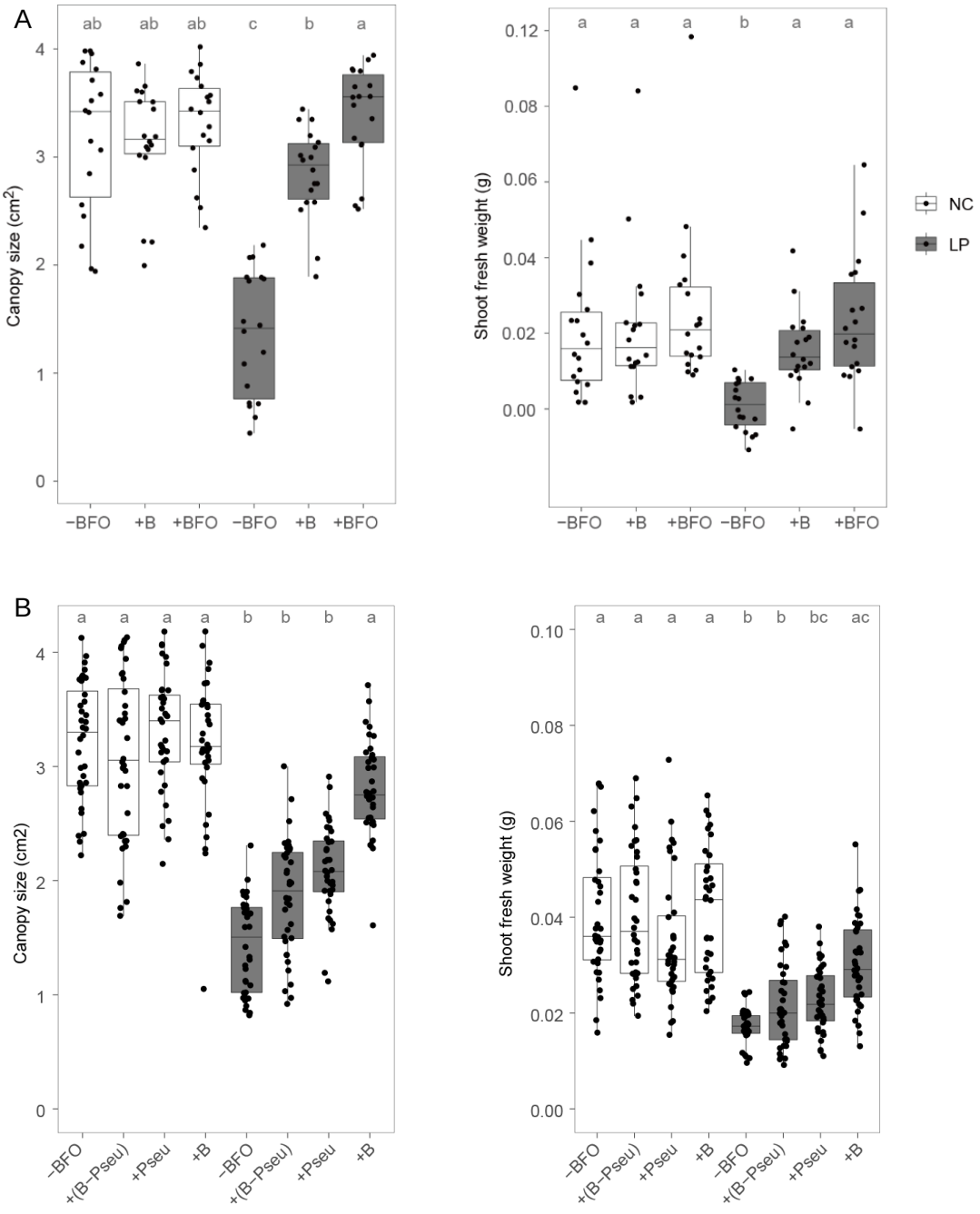

Figure 8. BFO-/B-mediated plant growth under NC and LP. Canopy size (in cm^2) and shoot fresh weight (in g) of five-week-old *A. thaliana* grown in the FlowPot system in the absence (-) or presence (+) of a synthetic microbial community composed of either B or BFO under NC (white) and LP (grey) **(A)** and in the absence (-) or presence (+) of a synthetic microbial community composed of either B without Pseudomonas strains (+(B-Pseu)), or Pseudomonas strains only (+Pseu), or B (+B) under NC (white) and LP (grey) **(B)**. Three independent biological replicates (A: n = 108 plants; B: n = 288 plants). Letters indicate statistical significance corresponding to Kruskal-Wallis with Dunn's post hoc test (α = 0.05). NC: normal light condition. LP: low PAR.

Given the possible ectopic leaf colonization by root microbiota members in our gnotobiotic system (**Bai et al., 2015**), I also tested whether BFO root commensals can be detected in shoots and the extent to which their relative abundance can be modulated by light conditions. Diversity analysis (**Figure 9A**), PCoA (**Figure 9B**) and enrichment tests (**Figure 10**) revealed that 44%, 15%, and 0% of B, F and O strain variants detected belowground were colonizing aboveground shoot tissues, and that the composition of ectopic B assemblage was also modulated by light conditions, with 13 strain variants showing light-dependent differential growth (**Figure 10**).

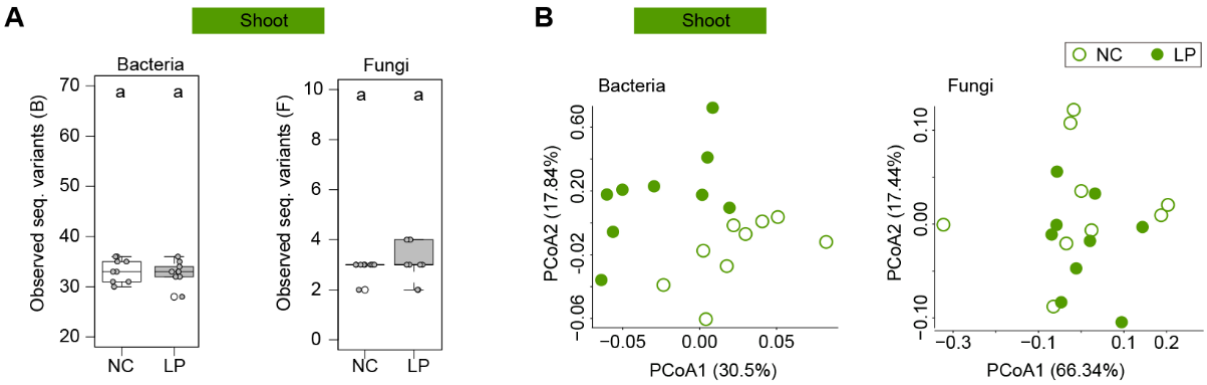

Figure 9. LP-mediated modulation of shoot microbial assembly. (A) Number of bacterial (left) and fungal (right) strain variants detected in plant shoots. Three independent biological replicates (n = 18 samples). Letters indicate statistical significance corresponding to Tukey´s HSD (α = 0.05). NC: normal light condition, LP: low photosynthetically active radiation. (B) Effect of "Compartment" and "Light" on B and F community composition in shoots in the FlowPot system visualized by PCoA (Upper panel: B, Lower panel: F, Empty circles = NC, filled circles LP). Three independent biological replicates (B: n = 18 samples, F: n = 18)

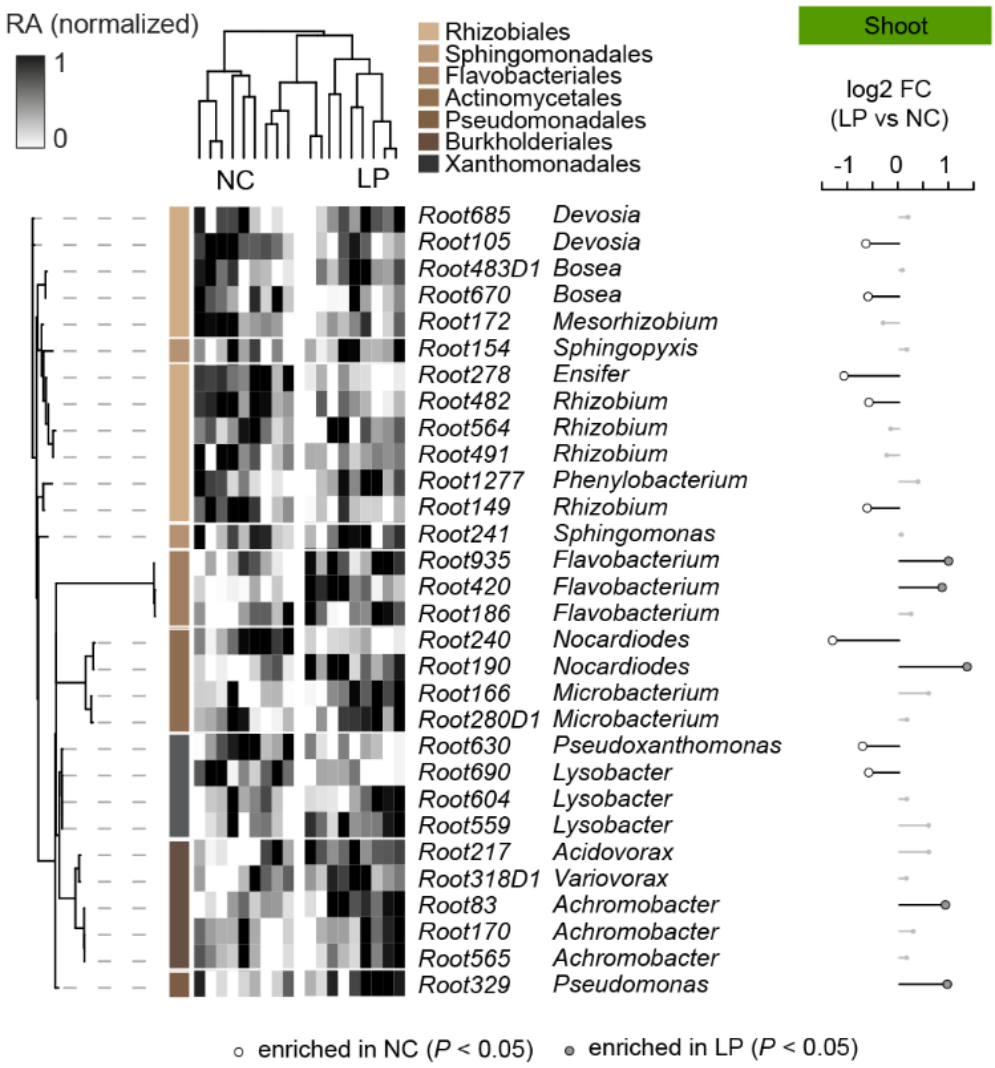

Figure 10. LP-mediated modulation of shoot bacterial assembly. Normalized relative abundance (RA) of prevalent B strain variants detected in shoots across NC and LP conditions. Sample-wise normalized RA was calculated for each strain variant and is depicted in the heatmap next to the taxonomic tree. Only strain variants with an average RA ≥ 0.1% across samples were considered (n = 18 samples). The taxonomic tree was constructed based on a maximum likelihood method using full length 16S rRNA sequences. Sample-wise log2 fold-change in RA measured for each prevalent strain variant between LP and NC in shoot samples. Differential RA with statistically significant P-values are shown (GLM, $P < 0.05$).

Further, the difference of bacterial taxonomic orders between normal light condition (NC) and low PAR condition (LP) was checked. In roots, *Actinomycetales* and *Pseudomonadales* are significantly enriched under LP compared with NC (**Figure 11A**) whereas, in shoots, *Burkholderiales* and *Rhizobiales* are significantly enriched (**Figure 11B**).

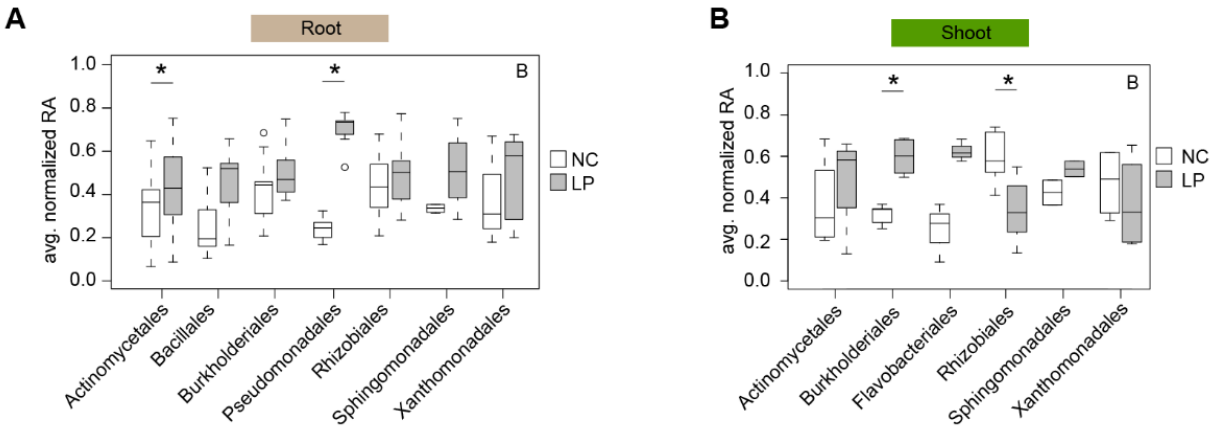

Figure 11. LP mediated bacterial taxonomic orders in roots (A) and shoots (B). (A) Mean normalized RA in LP/NC for bacterial strain variants sorted by taxonomic order. Only strain variants that were consistently found across all samples (n=24) were selected. Bacterial orders with less than one member were not considered (strain variants: Act. n = 28, Bac. n=6, Bur. n=9, Pse. n=7, Rhi. n=20, Sph. n=4, Xan. n=8). Significant differences between norm. RA in LP and NC are shown (Mann-Whitney-U test, $P < 0.05$). **(B)** Mean normalized RA in LP/NC for bacterial strain variants detected in plant shoots sorted by taxonomic order. Only strain variants that were consistently found across all samples (n=18) were selected. Bacterial orders with less than one member were not considered (strain variants: Act. n = 4, Bur. n=5, Fla. n=3, Rhi. n=10, Sph. n=2, Xan. n=4). Significant differences between norm. RA in LP and NC are shown (Mann-Whitney-U test, $P < 0.05$).

Taken together, these results suggest that shoot exposure to LP alters belowground root metabolism, thereby promoting the growth of specific bacterial taxa in a complex multi-kingdom root microbiome.

3.3 Root microbiota triggers plant prioritization of growth over defense under LP

Based on aforementioned results, I hypothesized that plant responses to root commensals and light are interconnected, thereby orchestrating resource investment into shoot under suboptimal light conditions. To test this hypothesis, I profiled the root and shoot transcriptomes of five-week old *A. thaliana* col-0 plants colonized or not by the BFO SynCom and exposed to normal light condition (NC) or low PAR condition (LP) in the gnotobiotic FlowPot system. First, the dissimilarity among samples (Root: n = 12 samples, Shoot: n = 12 samples) using pairwise Pearson´s correlations among samples indicated that presence/absence of the BFO SynCom explained transcriptome differentiation in root samples more than “light”, whereas differentiation in

the shoot transcriptome showed an opposite pattern (**Figure 12A**). This result is consistent with the experimental setup: i.e. microbial inoculation in soil so the root compartment is directly affected by the factor "microbes" and light perception by the shoot compartment so the shoot is directly affected by "light". Then I did pair comparisons ($|\log2FC| \geqslant 1$, Empirical Bayes Statistics, FDR < 0.05) across all samples to determine the number of gene differential regulated between each pairwise comparison. For the comparison of +BFO vs -BFO, the number of differential regulated genes in root samples (2,721 genes) is more than twice as that observed for shoot samples (1,236 genes) (**Figure 12B**) while for the comparison of LP vs NC, the total amount of differential regulated genes in shoot samples (1903 genes) is more than root samples (1784 genes) that is consistent with the result of pairwise Person's correlations (**Figure 12A**). For root samples, the comparison +BFO vs -BFO under LP regulated more genes than NC and similarly the comparison LP vs NC under +BFO regulated more genes than -BFO (**Figure 12B**). The similar result was observed in the comparison LP vs NC for shoot samples (**Figure 12B**). Notably, for shoot samples, the comparison +BFO vs -BFO under LP regulated less genes than NC (**Figure 12B**) indicating that root microbiota triggers less gene expression in shoot under LP.

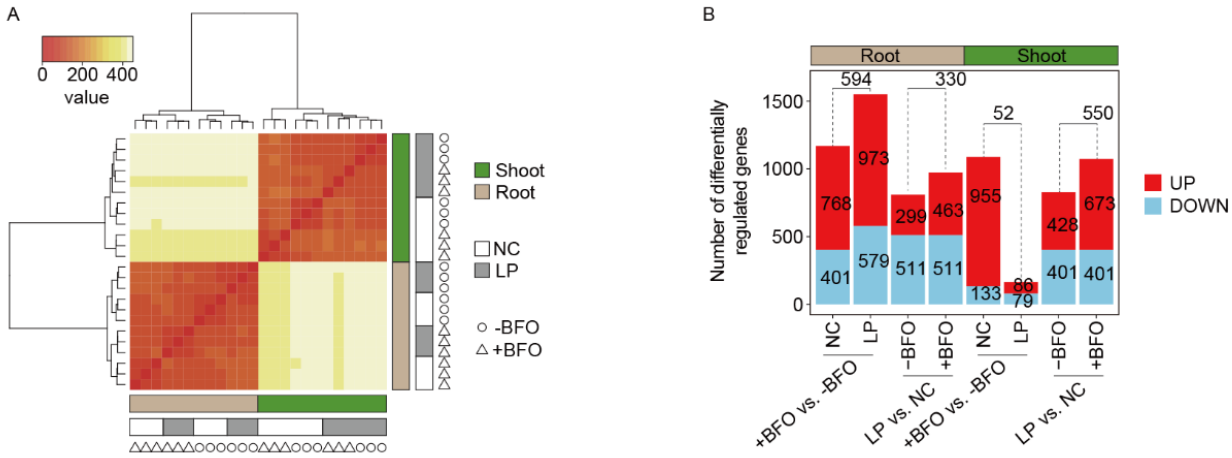

Figure 12. Transcriptional reprogramming in shoot and root in response to light and BFO. (A) Dendrogram showing the hierarchical relationship between samples used for RNAseq. Three independent biological replicates (n = 24 samples). NC: normal light condition, LP: low PAR. -BFO: no microbes (i.e. germ-free), +BFO: with microbes. B: bacteria, F: fungi, O: oomycetes. **(B)** Bar plot showing the numbers of differentially related genes among all paired comparisons. Red colour and blue colour filled bars represent significantly up and down regulated between the corresponding comparison respectively. The black numbers in the bar mean the total number of up or down regulated genes between the corresponding comparison. The black numbers on the top of the bar represent the numbers of overlapped genes between the corresponding conditions.

To determine gene expression patterns in shoot and root samples in response to light and BFO SynCom, a hierarchical clustering was conducted for all genes identified as differentially regulated across conditions (|log2FC| ⩾ 1, Empirical Bayes Statistics, FDR < 0.05). Hierarchical clustering identified 9 gene expression clusters in root (R1-R9, n = 3,013 genes, **Figure 13**) and 8 in shoot (S1-S8, n = 2,790 genes, **Figure 13**).

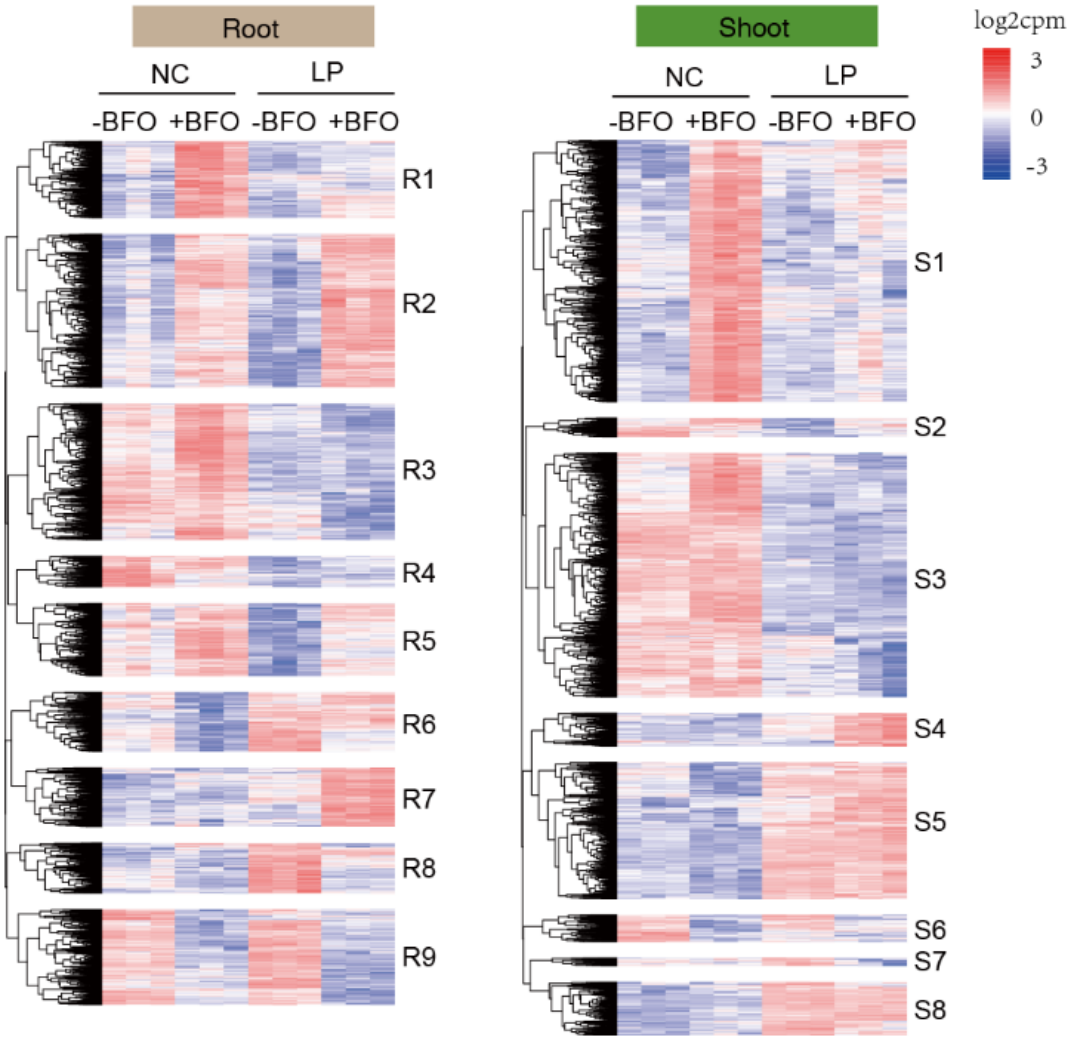

Figure 13. Gene expression pattern of shoot and root in response to light and BFO. Transcript profiling of 3,013 *A. thaliana* genes significantly regulated in root samples (|log2FC| ⩾ 1, Empirical Bayes Statistics, FDR < 0.05) based on all possible pairwise sample comparisons: NC-BFO vs NC+BFO, LP-BFO vs LP+BFO, NC-BFO vs LP-BFO, NC+BFO vs LP+BFO **(Left)**. Over-represented (white to red) and under-represented transcripts (white to blue) are shown across conditions as log2 counts per million (voom-transformed data with limma package in R). The gene set was split into 9 major gene expression clusters, labelled R1 to R9. NC: normal light condition, LP: low PAR, -BFO: no microbes, +BFO: with microbes. Three independent biological replicates (n = 12 samples). Transcript profiling of 2,790 *A. thaliana* genes significantly regulated in shoot samples (|log2FC| ⩾ 1, Empirical Bayes Statistics, FDR < 0.05) based on all possible pairwise

sample comparisons: NC-BFO vs NC+BFO, LP-BFO vs LP+BFO, NC-BFO vs LP-BFO, NC+BFO vs LP+BFO **(Right)**. Over-represented (white to red) and under-represented transcripts (white to blue) are shown. The gene set was split into 8 major gene expression clusters, labelled S1 to S8. Three independent biological replicates (n = 12 samples).

To connect the gene expression clusters identified by hierarchical clustering with biological processes or functions, I did Gene Ontology (GO) term enrichment for each of the clusters depicted in **Figure 13**. Overall, the different gene clusters show different biological functions. By inspecting the top 12 most significant GO terms in each gene clusters, I observed that presence of the BFO SynCom triggered light-independent up-regulation of genes involved in ion homeostasis (root, R2), cell differentiation (root, R2), as well as down-regulation of genes involved in response to salicylic acid (SA; root, R9) and anthocyanin biosynthesis (shoot, S6) (**Figure 14**). In contrast, LP triggered BFO-independent up-regulation of genes involved in response to jasmonic acid and gibberellin (JA, GA; shoot, S5) as well as downregulation of genes involved in flavonoid metabolic process (shoot, S3) and response to high light intensity (root, R4) (**Figure 14**). Furthermore, I identified clusters for which gene expression profiles were modulated by both light and BFO conditions (i.e. R1, R3, R7, R8, S1, S4), likely explaining BFO-mediated host rescue under LP (**Figure 14**).

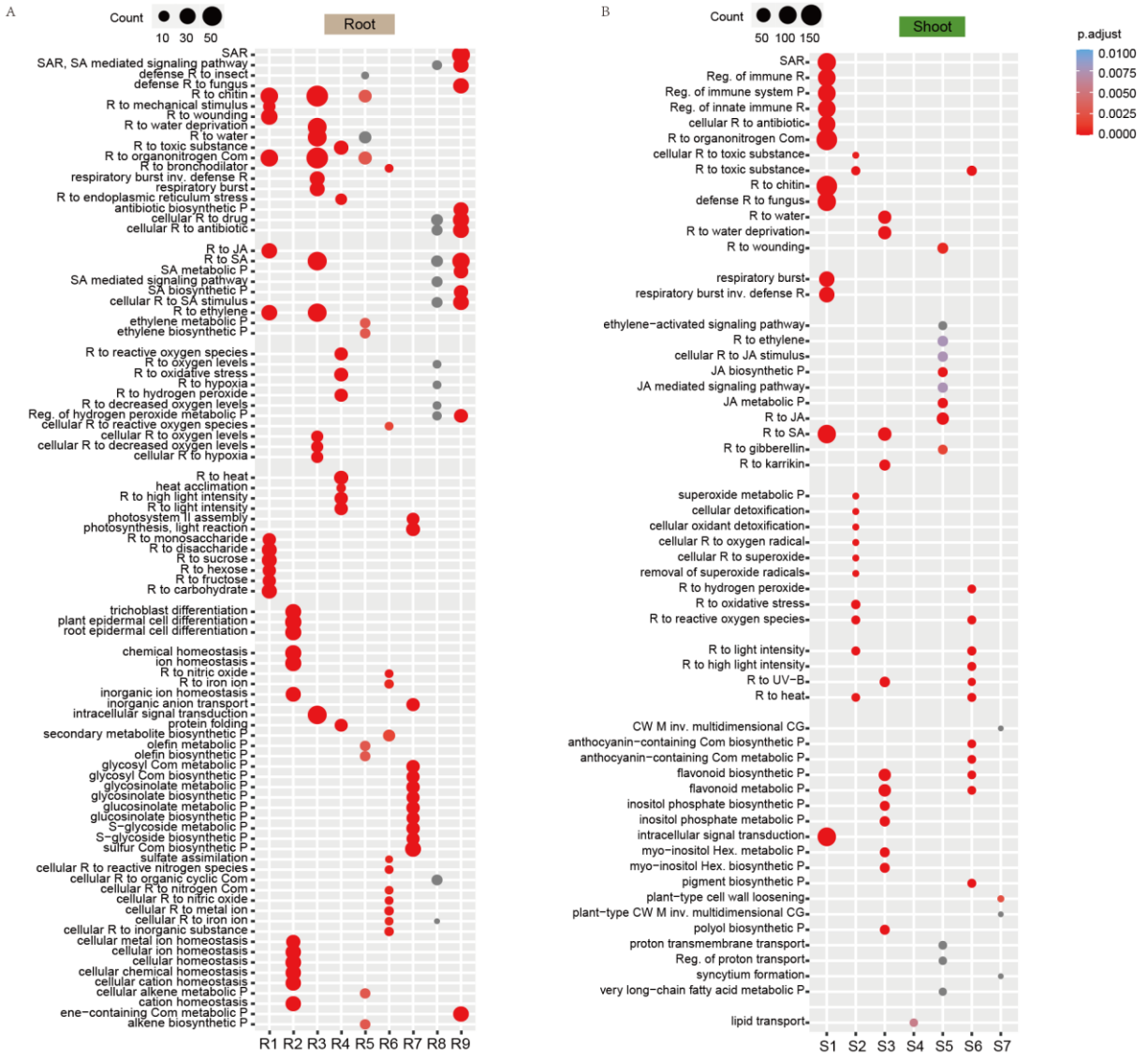

Figure 14. Gene Ontology (GO) term enrichment in shoot and root in response to light and BFO. Gene Ontology (GO) term enrichment depicting the top 12 most significantly enriched GO terms (Hypergeometric test with Bonferroni correction, α = 0.05) detected in all clusters for root samples **(A)** and shoot samples **(B)**. The size of point reflects the amount of gene numbers enriched in this GO term. The colour of point means the p value ((Hypergeometric test with Bonferroni correction). R: response, Reg. Regulation, ET: ethylene, SA: salicylic acid, JA: jasmonic acid, SAR: systemic acquired resistance, CW: cell wall, CG: cell growth, P: process, Com: compound, Hex: hexakisphosphate, inv.: involved in.

Particularly, genes belonging to clusters R1, R3, and S1 were up-regulated by the presence of the BFO SynCom under NC but not under LP (**Figure 15A**). A substantial fraction of the genes (i.e. 227) did overlap between root clusters R1R3 and the shoot cluster S1 (**Figure 15B**), and GO terms analysis revealed consistent enrichments

of immune-related processes, including response to chitin, response to SA, JA, and ethylene, response to organonitrogen compounds, or regulation of immune responses, among others (Hypergeometric test with Bonferroni correction, $P < 0.05$, **Figure 15C**).

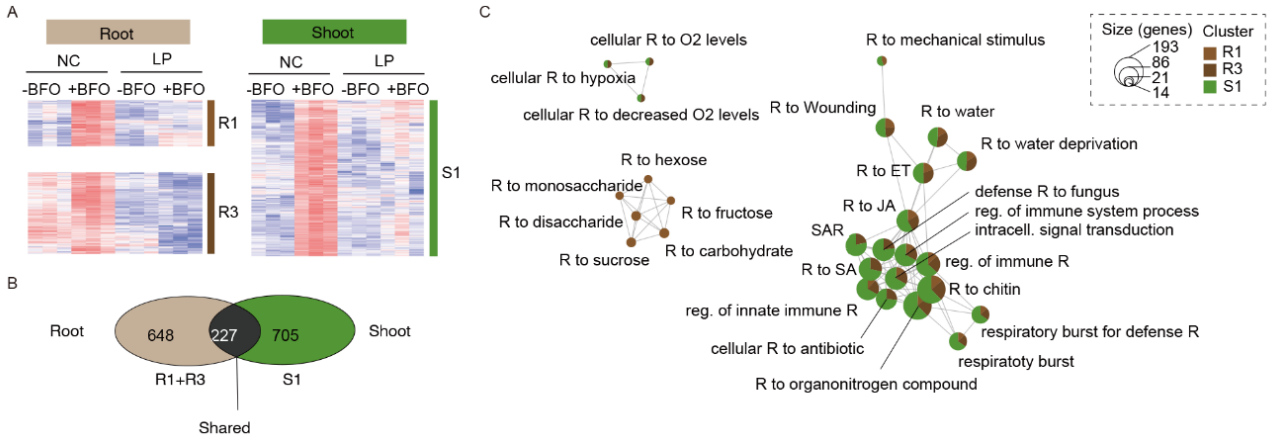

Figure 15. Light- and BFO-mediated transcriptional reprogramming in root and shoot. (A) The heatmap showing the gene expression pattern of gene cluster R1, R3 and S1. **(B)** Number of genes shared between root clusters R1R3 and shoot cluster S1 or specific to each of the two groups. **(C)** Gene Ontology (GO) term enrichment network depicting the top 12 most significantly enriched GO terms (Hypergeometric test with Bonferroni correction, α = 0.05) detected in clusters R1, R3, and S1. Each GO term is represented as a circle and the contribution of each cluster to the overall GO term enrichment is shown. The size of the GO term reflects the number of genes enriched in the GO term. R: response, reg. Regulation, ET: ethylene, SA: salicylic acid, JA: jasmonic acid, SAR: systemic acquired resistance.

To visualize the connections between genes and corresponding GO terms, I used gene-concept network (cnetplot function in R), which depicts linkages between genes and associated top 12 most significantly enriched GO terms detected in clusters R1, R3 and S1. Transcripts with conserved expression patterns in root and shoot encode primarily transcription factors (i.e. WRKY15, WRKY22, WRKY33, WRKY40, WRKY46, SZF1, SZF2, ZAT12, MYB2, MYB15, MYB51, ANAC019, ANAC042, ANAC055), receptor-like protein/kinase (i.e. WAKL10, RLP52, RLK3 LecRK−VI.3, CRK9), ethylene-responsive elements (ERF6, ERF11), or calmodulin binding proteins (CBP60G, CML38) (**Figure 16**). Immune response activation in response to the BFO SynCom under NC was more extensive aboveground than belowground and involved several well-known immune-related genes that act through multiple pathways (**Figure 16**). These genes encode transcription

factors/proteins/enzymes involved in indole glucosinolate biosynthesis (MYB51, CYP81F2), camalexin production (CYP71B15), SA response (PR1, BGL2, FRK1, EDS5 and PAD4), systemic acquired resistance (SAR; SARD1, ALD1, AZI1 and DOX1), and to a lesser extend ethylene/JA responses (PDF1.2b). Overall, the genes in cluster R1, R3, and S1 were involved in multiple plant immune responses.

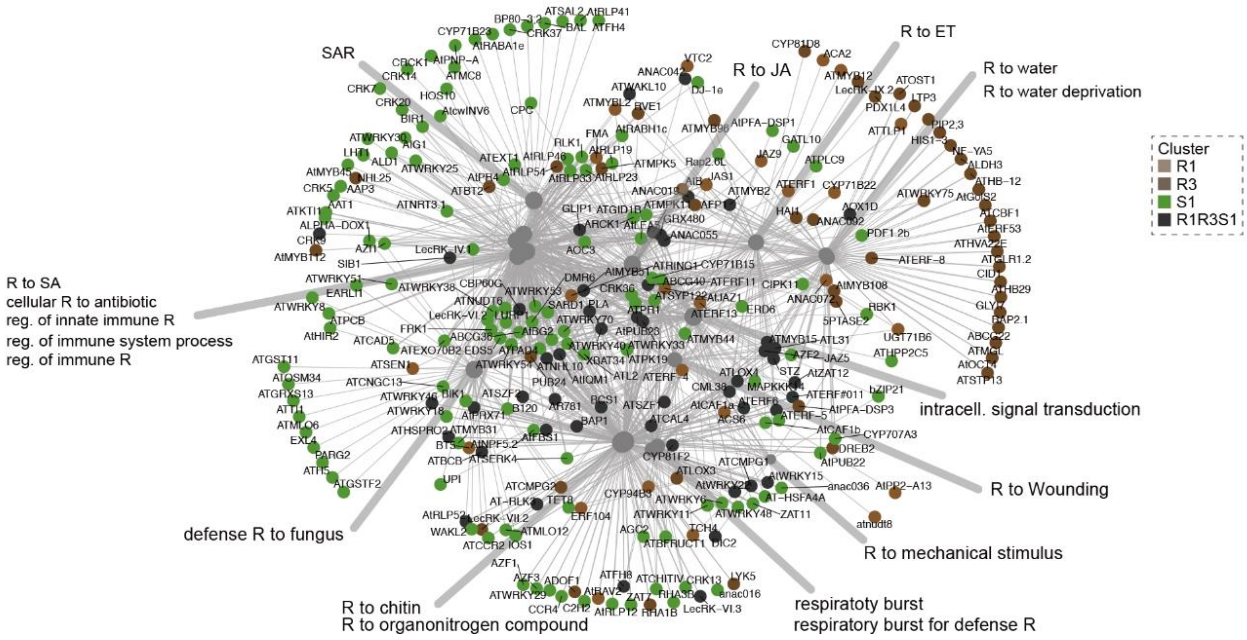

Figure 16. Genes in the transcriptional reprogramming of root and shoot mediated by light and BFO. Gene-concept network (cnetplot function in R) depicting linkages between genes and associated top 12 most significantly enriched GO terms detected in clusters R1, R3 and S1. Each node represents a gene and is colour-coded according the different cluster names. R: response, reg. Regulation, ET: ethylene, SA: salicylic acid, JA: jasmonic acid, SAR: systemic acquired resistance,

Transcriptional shut down of these BFO-induced immune responses in LP (S1, R1, R3) were accompanied by transcriptional up-regulation of specific genes in cluster R7 and S4 (**Figure 17A**). To clarify which biological processes are activated in clusters R7 and S4 and, I did GO term network and gene-concept network analyses. Based on the network of GO terms, I observed that cluster R7 was related with gluconeogenesis and cluster S4 was involved in lipid transport (**Figure 17B**).

Taken together, these results demonstrate that *A. thaliana* responses to root commensals and light are interconnected along the root-shoot axis, thereby allowing prioritization of microbiota-induced growth over defence responses under LP.

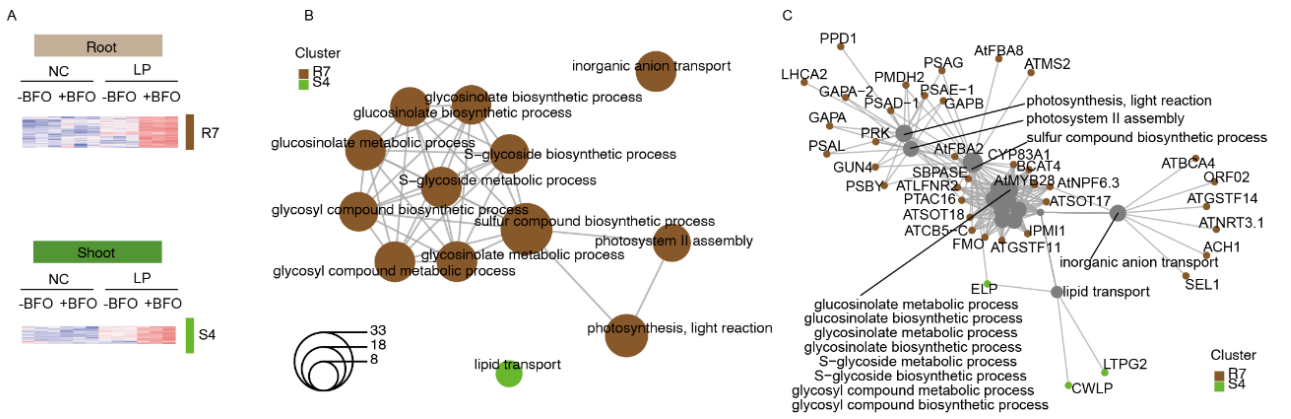

Figure 17. Transcriptional reprogramming mediated by light and BFO in root and shoot. (A) The heatmap showing the gene expression pattern of gene cluster R7 and S4. **(B)** Gene Ontology (GO) term enrichment network depicting the top 12 most significantly enriched GO terms (Hypergeometric test with Bonferroni correction, α = 0.05) detected in clusters R7 and S4. Each GO term is represented as a circle and the contribution of each cluster to the overall GO term enrichment is shown. The size of the GO term reflects the number of genes enriched in the GO term. **(C)** Gene-concept network (cnetplot function in R) depicting linkages between genes and associated top 12 most significantly enriched GO terms detected in clusters R7 (root) and S4 (shoot). Each node represents a gene and is colour-coded according the different cluster names.

Based on the transcriptional data reported above, I hypothesized that BFO-triggered defense responses in shoot can protect *A. thaliana* against leaf pathogens in a light-dependent manner. To test this hypothesis, I inoculated leaves of four weeks-old *A. thaliana* (NC-BFO, NC+BFO, LP-BFO, LP+BFO) with the necrotrophic fungal pathogen *Botrytis cinerea* B05.10 (*Bc*, droplet inoculation, 2 µl droplets containing $1x10^3$ spores) or the biotrophic bacterial pathogen *Pseudomonas syringae pv. tomato* DC3000 (*Pst*, spray inoculation, OD = 0.2). Evaluation of pathogen growth *in planta* by quantitative PCR (*Bc*) or colony counting (*Pst*) revealed extensive influence of both light and SynCom conditions on disease resistance five days post pathogen inoculation (One-Way ANOVA with post hoc Tukey HSD test, $P < 0.05$, **Figures 18**). Plants colonized with the BFO SynCom under NC are the most resistant to both pathogens, consistent with the diverse and extensive BFO-triggered aboveground immune responses observed in the RNAseq data (**Figure 15** and **Figure 16**). In contrast, germ-free plants facing LP were the most susceptible to both pathogens and failed to mount effective immune responses, indicating that root commensals are needed for effective leaf immunity. Although BFO-induced leaf protection is weakened under LP compared to NC (One-Way ANOVA with post hoc Tukey HSD test, $P < 0.05$),

these plants remained able to limit pathogen proliferation whilst massively investing into shoot growth (**Figure 2**). Therefore, root commensals simultaneously confer aboveground host tolerance to unrelated biotic (pathogen) and abiotic (light) stresses.

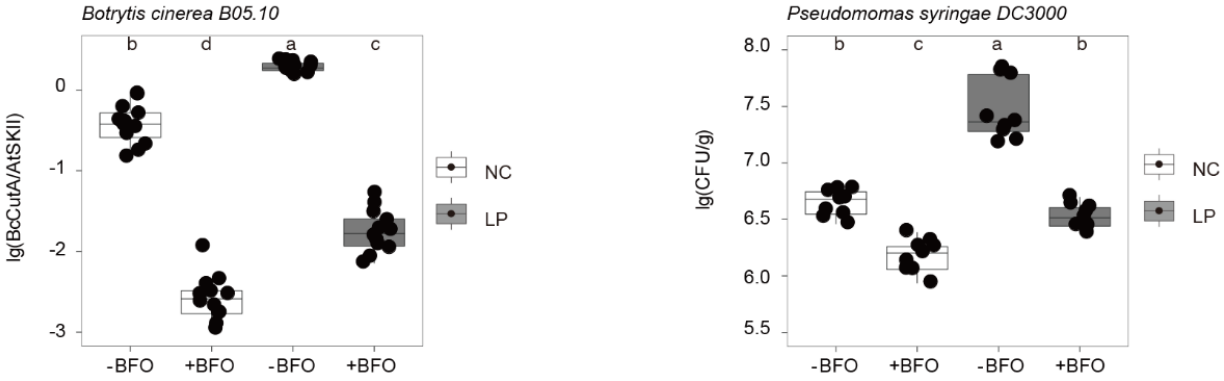

Figure 18. Plant immunity changed by light and BFO in shoot. qPCR-based quantification of *Botrytis cinerea B05.10* growth **(Left)** in *A. thaliana* leaves five days post pathogen inoculation in the FlowPot system. For inoculation, 2 µl droplets containing $1x10^3$ spores were applied to leaves of four weeks-old *A. thaliana* grown in the presence/absence of the BFO SynCom under either NC or LP. The relative growth of *B. cinerea* and *A. thaliana* was determined by amplification of the *BcCutinaseA* gene and the *AtSkII,* respectively. Four independent biological replicates (n = 48 plants). Letters indicate statistical significance corresponding to One-Way *ANOVA* with *post hoc Tukey* HSD test (α = 0.05). Colony count-based quantification of *Pseudomonas syringae pv. tomato DC3000* growth **(Right)** in *A. thaliana* leaves five days post pathogen inoculation in the FlowPot system. For inoculation, bacterial suspension was adjusted to OD = 0.2 and spray-inoculated on leaves of four weeks-old *A. thaliana* grown in the presence/absence of the BFO SynCom under either NC or LP. For colony counting, 20 µl dilution series (10^{-1}, 10^{-2}, 10^{-3}, 10^{-4}, 10^{-5} with 10 mM Mgcl2) spot on NYGA plate, counting colonies after two days incubation at 28 °C. Three independent biological replicates (n = 36 plants). Letters indicate statistical significance corresponding to One-Way *ANOVA* with *post hoc Tukey* HSD test (α = 0.05).

3.4 Microbiota-mediated plant growth rescue under LP depends on JA, cryptochromes, and BR.

Given the fact that the root microbiota rescued plant growth under suboptimal LP condition, I hypothesized that the balance between growth and defense was involved in this phenotype. Previous studies identified two phytohormone-dependent crosstalkbetween growth and defense pathways (**Guo et al., 2018**). One balance is

mediated by the antagonism between gibberellin- dependent (GA) growth and jasmonate acid-dependent (JA) defense. Another balance involves interplay between brassinosteroids- dependent (BR) growth and jasmonate acid-dependent (JA) defense. To identify host components required for prioritization of microbiota-induced growth over defense in LP, I monitored plant growth, *Bc* colonization, and *Pst* colonization across several mutants in our gnotobiotic system. These include mutants impaired in SA and JA biosynthesis (SA: *sid2-2*, JA: *dde2-2;* **Wildermuth et al., 2001; von Malek et al., 2002**), JA and GA signalling (JA: *myc2-3 – jazQ;* GA: *dellaP;* **Shin et al., 2012; Campos et al., 2016; Park et al., 2013**), brassinosteroid signal transduction (*bri1-301*), light perception (*cry1cry2*, **Mockler et al., 1999**), and indole-3-pyruvic-acid-dependent auxin biosynthesis (*sav3-3*) (**Figure 19**).

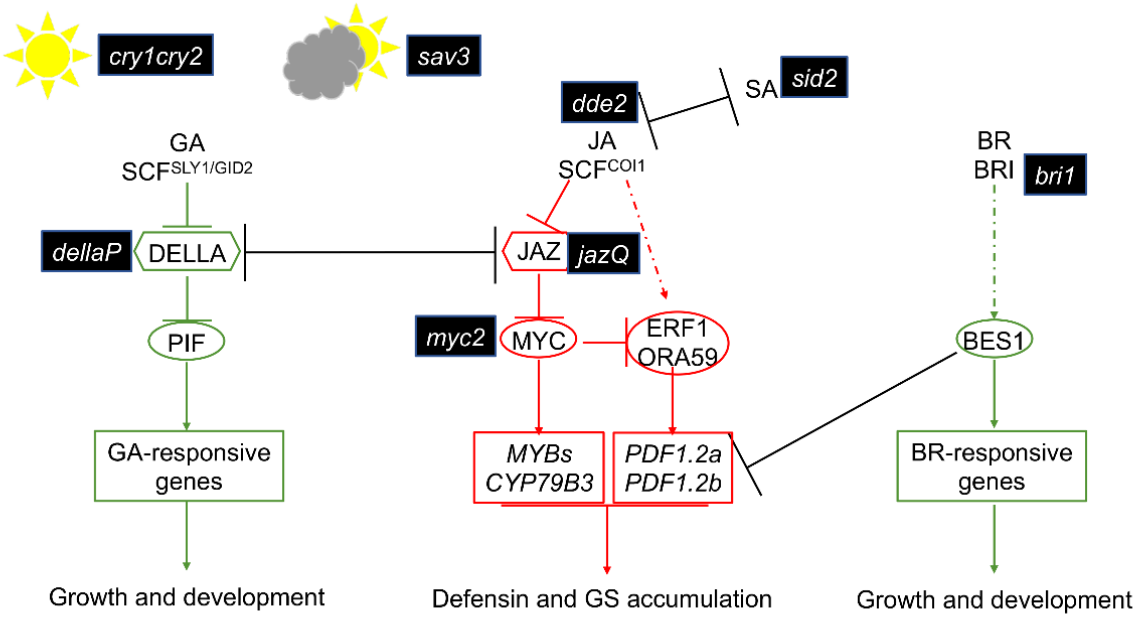

Figure 19. The gene-connected model of gibberellin (GA), jasmonate acid (JA) and brassinosteroids (BR) pathway. The black filled boxes mean the mutants I chose and used in this chapter. Mutants used are *i*mpaired in SA and JA biosynthesis (*sid2-2*, *dde2-2*), JA and GA signaling (*myc2-3, jazQ and dellaP*), BR-mediated signal transduction (*bri1-301*), cryptochromes (*cry1cry2*), and indole-3-pyruvic-acid-dependent auxin biosynthesis (*sav3-3*).

For plant growth, I measured the canopy size of individual five-week old plants across all mutants under NC

and LP in the presence and the absence of the BFO SynCom. Consistent with previous work (**Campos et al., 2016; Park et al., 2013**), I observed mutant-to-Col-0 variation in vegetative growth under the control condition (NC-BFO), with enhanced growth for the *dellaP* mutant and reduced growth for the *jazQ* mutant (**Figure 20**). Since DELLA family proteins repress the GA-dependent growth pathway, the *dellaP* mutant shows enhanced growth compared with Col-0 plants. Oppositely, the *jazQ* mutant shows reduced growth compared to Col-0 plants due to the strong activation of JA-mediated immune responses. For the canopy size of Col-0 plants (**Figure 20**), the result is consistent with the data shown before (**Figure 2**) validating that root microbiota-dependent rescue of plant growth under suboptimal light condition is robust and reproducible. Overall, for each mutant tested individually under normal light condition, we observed that canopy size of plants with root microbiota did not show significant difference compared with plants without root microbiota (**Figure 20**). However, under LP, we observed remarkable differences in canopy size between BFO-colonized and germ-free plants forCol-0, *sid2-2*, and *dellaP* (**Figure 20**). Notably, under LP, the mutants *jazQ*, *dde2-2*, *myc2-3*, *bri1-301*, *cry1cry2*, and *sav3-3*did not show BFO-mediated growth increase in canopy size (**Figure 20)**

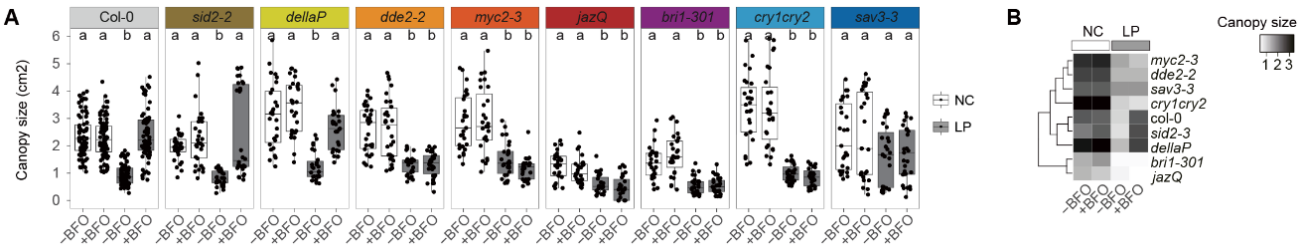

Figure 20. Canopy size of all mutants under NC and LP in the absence or presence of the BFO SynCom in the FlowPot system. **(A)** Canopy size (in cm^2) of *A. thaliana* Col-0 and eight mutants grown under NC and LP in the absence (-BFO) or presence of the BFO SynCom (+BFO) in the FlowPot system. The canopy size of five-weeks old plants was measured using Fiji and data from three independent biological replicates are shown (n = 1188 plants across replicates and genotypes). Statistical significance across conditions for each genotype is indicated with letters, corresponding to *Kruskal-Wallis* with *Dunn's post hoc* test (α = 0.05). NC: normal light condition, LP: low PAR. **(B)** Summary heatmap depicting the mean canopy size (in cm^2) measured across plant genotypes and conditions.

Given the fact that LP showed different effect on canopy size of all tested lines between -BFO and +BFO (**Figure 20**), I was wondering what the degree of LP affected plant canopy size for each mutant -BFO and +BFO. To clarify this question, I calculated the ratio of canopy size between LP and NC for each mutant -BFO and in

+BFO separately. Irrespective of these differences in growth rate, LP-mediated reduction in canopy size was quantitatively similar across all mutant tested in the absence of the BFO SynCom (0.48 – 0.71-fold decrease in canopy size), except for the *sav3-3* mutant that retained high growth in LP (Kruskal-Wallis with Dunn's post hoc test). BFO-mediated growth rescue observed in LP for Col-0 was retained in the *sid2-2*, *dellaP*, and *sav3-3* mutants, indicating that the corresponding genes are dispensable for BFO-mediated canopy size enhancement in LP (**Figure 21**). Remarkably, this growth rescue phenotype was abolished in the *dde2-2*, *myc2-3*, *jazQ*, *bri1-301* and *cry1cry2* mutants, indicating that JA biosynthesis/signalling, BR signal transduction, and cryptochromes are needed for BFO-mediated tolerance to low PAR (**Figure 21**). Meanwhile, I measured the shoot fresh weight and observed the same results as canopy size (**Figure 22**) which is consist with the result of canopy size (**Figure 20**).

These results suggest that integration of belowground response to microbiota and aboveground response to light involves multiple points of control along the root-shoot axis.

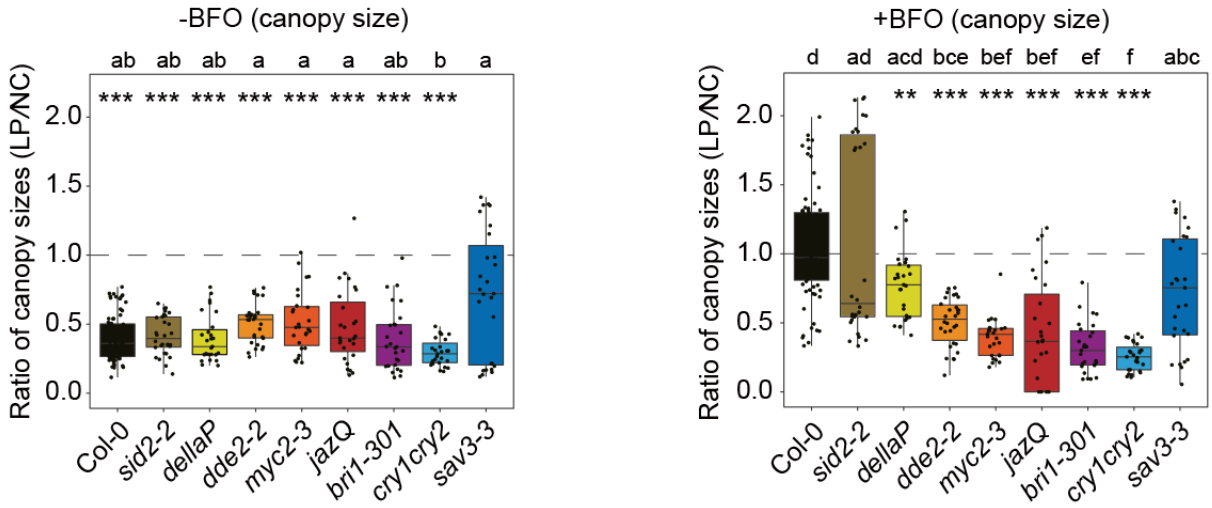

Figure 21. The comparison of canopy size LP vs NC in the absence and presence of the BFO SynCom for all mutants separately in the FlowPot system. Differential canopy size between LP and NC for *A. thaliana* Col-0 and eight mutants grown in the FlowPot system under germ-free conditions (-BFO, **Left**) or in the presence of the BFO SynCom (+BFO, **Right**). The selected mutants are impaired in SA and JA biosynthesis (*sid2-2*, *dde2-2*), JA and GA signaling (*myc2-3, jazQ and dellaP*), BR-mediated growth-defense tradeoffs (*bri1-301*), cryptochromes (*cry1cry2*), and auxin synthesis (*sav3*). Ratio in canopy size (five-weeks old plants) was computed between LP and NC across three independent biological replicates (n = 594 for -BFO samples and 594 for +BFO samples). Datapoints below (or above) the

dashed line showed canopy size decrease (or increase) in LP compared to NC. Statistical significance across genotypes is indicated with letters, corresponding to *Kruskal-Wallis* with *Dunn's post hoc* test (α = 0.05). Statistical significance between LP and NC is indicated with stars, corresponding to Mann-Whitney U test (** $P < 0.01$, * $P < 0.05$).

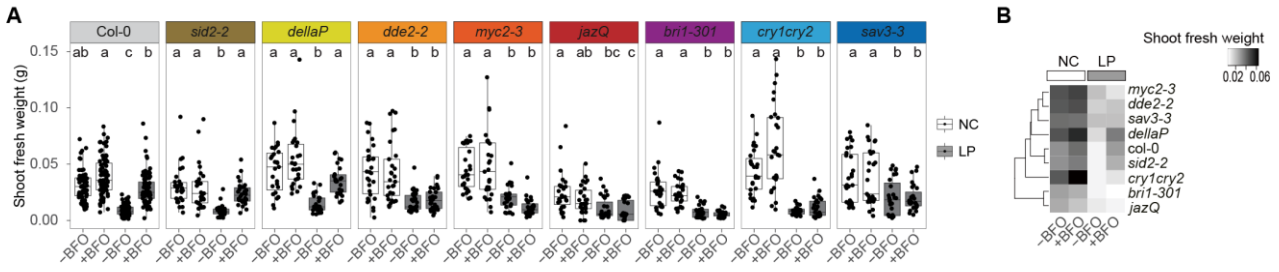

Figure 22. Shoot fresh weight of all mutants under NC and LP in the absence or presence of the BFO SynCom in the FlowPot system. (A) Shoot fresh weight (in g) of five-week-old A. thaliana Col-0 and eight mutants grown under NC and LP in the absence (-BFO) or presence of the BFO SynCom (+BFO) in the FlowPot system. Three independent biological replicates are shown (n = 1188 plants across replicates and genotypes). Statistical significance across conditions for each genotype is indicated with letters (Kruskal-Wallis with Dunn's post hoc test, α = 0.05). NC: normal light condition, LP: low PAR. **(B)** Summary heatmap depicting the mean shoot fresh weight (in g) measured across plant genotypes and conditions.

To further quantify plant shoot phenotypes, I measured petiole length, ratio of leaf length to leaf width (a proxy of leaf shape) and leaf number of five-week-old plants grown in the FlowPot system. For Col-0, the presence of root microbiota led to a significant increase in petiole length, leaf number and the leaf length/width ratio (**Figure 23A**) which is consistent with previous data (**Figure 3A**). In contrast, most of these BFO-induced phenotypic differences under LP were largely abolished in the *dde2-2*, *myc2-3*, *jazQ*, *bri1-301*, *cry1cry2*, and *sav3-3* mutants (**Figure 23**) indicating that the corresponding genes are also needed for root microbiota-mediated modification of these traits.

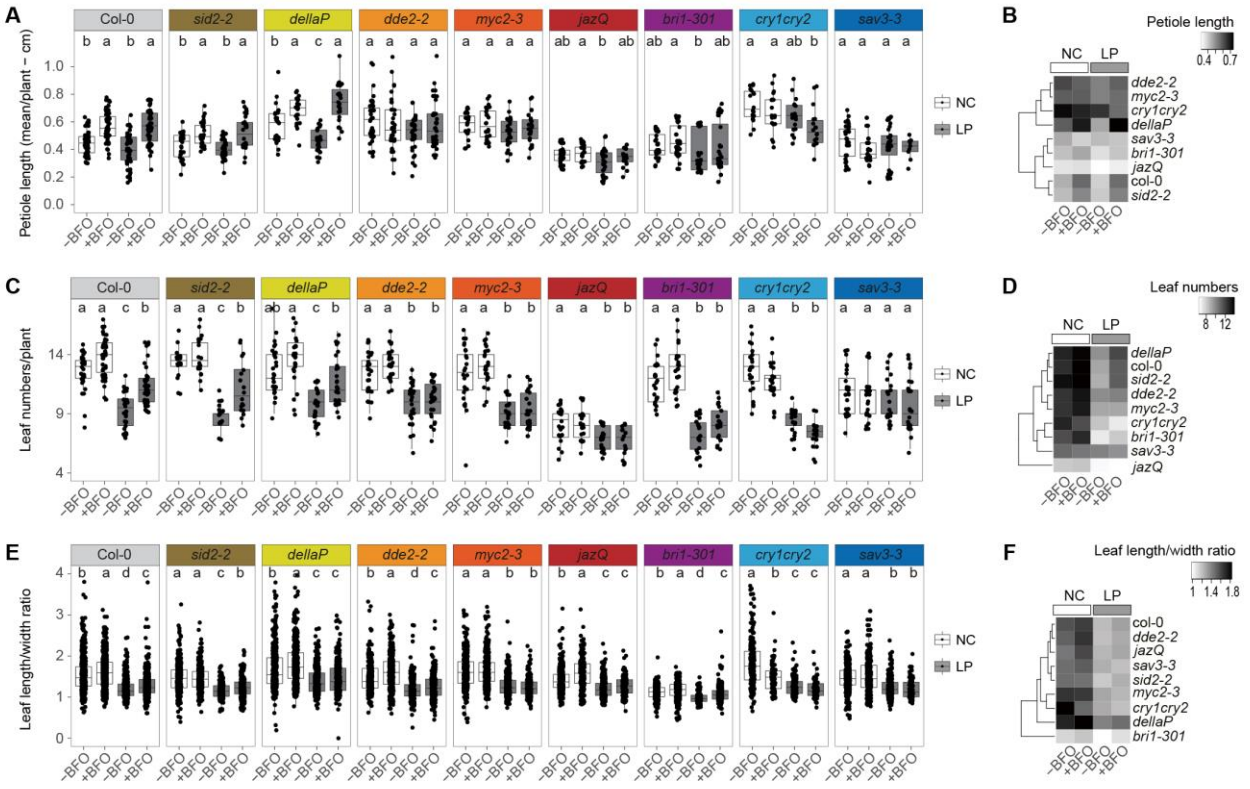

Figure 23. Leaf traits of all mutants under NC and LP in the absence or presence of the BFO SynCom in the FlowPot system. (A) Mean petiole length (in cm) of five-week-old A. thaliana Col-0 and eight mutants grown under NC and LP in the absence (-BFO) or presence of the BFO SynCom (+BFO) in the FlowPot system. Three independent biological replicates are shown (n = 1095 plants across replicates and genotypes). Statistical significance across conditions for each genotype is indicated with letters (Kruskal-Wallis with Dunn's post hoc test, α = 0.05). NC: normal light condition, LP: low PAR. **(B)** Summary heatmap depicting the mean value of mean petiole length per plant (in cm) measured across plant genotypes and conditions. **(C)** Total leaf number of five-week-old A. thaliana Col-0 and eight mutants grown under NC and LP in the absence (-BFO) or presence of the BFO SynCom (+BFO) in the FlowPot system. Three independent biological replicates are shown (n = 925 plants across replicates and genotypes). Statistical significance across conditions for each genotype is indicated with letters (Kruskal-Wallis with Dunn's post hoc test, α = 0.05). NC: normal light condition, LP: low PAR. **(D)** Summary heatmap depicting the mean total leaf number measured across plant genotypes and conditions. **(E)** Leaf length/width ratio of five-week-old A. thaliana Col-0 and eight mutants grown under NC and LP in the absence (-BFO) or presence of the BFO SynCom (+BFO) in the FlowPot system. Three independent biological replicates are shown (n = 9708 leaves across replicates and genotypes). Statistical significance across conditions for each genotype is indicated with letters (Kruskal-Wallis with Dunn's post hoc test, α = 0.05). NC: normal light condition, LP: low PAR. **(F)** Summary heatmap depicting the mean value of mean leaf length/width ratio measured across plant genotypes and conditions.

The results of canopy size and shoot fresh weight presented above suggest that integration of belowground response to microbiota and aboveground response to light involves multiple points of control along the root-shoot axis. Further to clarify the immunity status of tested mutants in the FlowPot gnotobiotic system using exactly the same experimental setup (NC+BFO, NC-BFO, LP-BFO, LP-BFO), I then inoculated leaves of four-week-old *A. thaliana* Col-0 and aforementioned mutant plants with *B. cinerea* (*Bc*). After five days, I quantified *Bc* growth in leaves of *A. thaliana* Col-0 and mutants grown under NC and LP in the absence (-BFO) or presence of the BFO SynCom (+BFO) in the FlowPot system using qPCR (specific primers targeting *Bc* cutinase A and *A. thaliana* SKII, **Liu et al., 2009**). First, I observed genotype-specific difference in *Bc* susceptibility/resistance phenotypes in control conditions (NC-BFO, **Figure 24A**), with the *dde2-2* mutant being the most susceptible and the *sid2-2* mutant being the most resistant, which is consistent with previous work (**Wildermuth et al., 2001; von Malek et al., 2002**). It is well known that plant defense towards to *Bc* is mediated, at least partially via the JA phytohormone branch. Since JA biosynthesis is abolished in the *dde2-2* mutant, the increased insusceptibility to *Bc* was expected (**Figure 24A**). Oppositely, the *sid2-2* mutant is impaired in SA biosynthesis which likely promotes induction of the JA branch that restrict *Bc* growth via the well-known antagonism between SA and JA (**Figure 24A**). I tested another unrelated leaf pathogen, the biotrophic bacterial pathogen *Pseudomonas syringae pv. tomato* DC3000 (*Pst*). I inoculated leaves of four weeks-old *A. thaliana* (NC-BFO, NC+BFO, LP-BFO, LP+BFO) with *Pst* (spray inoculation, OD = 0.2) and evaluated *in planta* pathogen growth by colony counting. I observed genotype-specific difference in *Pst* susceptibility/resistance in control conditions (NC-BFO, **Figure 24C**), with the *sid2-2* and *jazQ* mutants being the more susceptible and the *myc2-3* mutant being most resistant compared with Col-0 plants, which is consistent with previous work (**Shin et al., 2012**; **Cui et al., 2018**). This is consistent with the fact that defense towards to *Pst* is mediated by the SA branch (i.e. abolished in sid2-2) (**Cui et al., 2018**) (**Figure 24C**). It is also well known that *Pst* secretes coronatine to stimulate the plant JA signaling pathway to dampen the SA branch (**Journot-Catalino et al., 2006**). Similarly, Given the fact that JAZ family proteins repress the JA signaling pathway, the *jazQ* mutant constitutively and strongly actives JA signaling and therefore activation of the SA branch is compromised in this mutant. The *myc2-3* mutant is JA insensitive plants so the above talked strategies failed and that is the reason for the result that the *myc2-3* mutant is more resistance to *Pst* compared with Col-0.

Bc growth and *Pst* growth across all tested mutants, I calculated the mean value for each parameter under each

condition and used heatmap to illustrate that. Based on the heatmap of canopy size data, the lines Col-0, *sid2-2* and *dellaP* show similar trend under four different conditions (NC-BFO, NC+BFO, LP-BFO, LP+BFO) (**Figure 20B**) indicating that the phenotype of plant growth rescued by root microbiota under LP is not dependent on *SID2* gene and DELLA protein family genes. However, the mutants *myc2-3*, *dde2-2*, *sav3-3*, *cry1cry2*, *bri1-301*, and *jazQ* show different pattern of canopy size with Col-0 plants (**Figure 20B**) indicating that the phenotype of plant growth rescued by root microbiota under LP might be related with *MYC2*, *DDE2*, *CRY1*, *CRY2*, *BRI1* and JAZ family genes. Based on the heatmap of *Bc* growth, the *dellaP* mutant shows similar pattern with Col-0 plants (**Figure 24B** and **24D**) indicating that the plant defense towards *Bc* modulated by root microbiota and light is not depend on DELLA family genes. Based on the heatmap of *Pst* growth, the *sav3-3* mutant shows similar pattern with Col-0 plants (**Figure 24D**) indicating that the plant defense towards *Pst* modulated by root microbiota and light is not depend on *SAV3* gene.

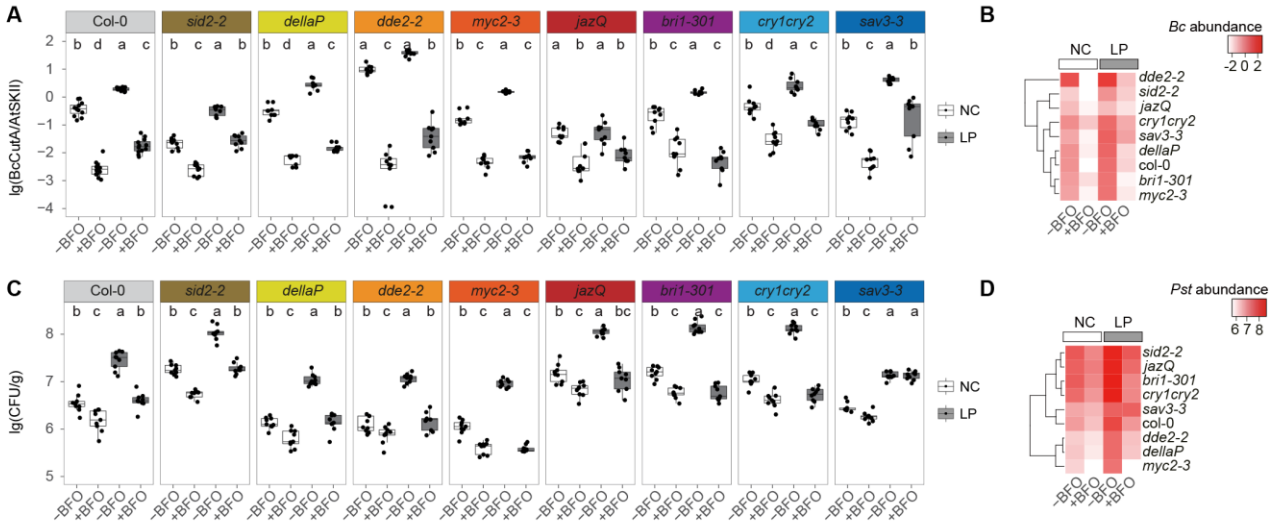

Figure 24. Pathogen growth in leaves of all mutants under NC and LP in the absence or presence of the BFO SynCom in the FlowPot system. (A) *B. cinerea* growth in leaves of *A. thaliana* Col-0 and eight mutants grown under NC and LP in the absence (-BFO) or presence of the BFO SynCom (+BFO) in the FlowPot system. *Botrytis cinerea B05.10* growth was quantified by qPCR in *A. thaliana* leaves five days post pathogen inoculation. For inoculation, 2 µl droplets containing $1x10^3$ spores were applied to leaves of four weeks-old *A. thaliana* grown in the presence/absence of the BFO SynCom under either NC or LP. The relative growth of *B. cinerea* and *A. thaliana* was determined by amplification of the *BcCutinaseA* gene and the *AtSkII,* respectively. data from three independent biological replicates are shown (n = 336 samples across replicates and genotypes). Statistical significance across conditions for each genotype is indicated with

letters, corresponding to *Kruskal-Wallis* with *Dunn's post hoc* test (α = 0.05). **(B)** Summary heatmap depicting relative *B. cinerea* growth (lg (BcCutA/AtSKII)) measured across plant genotypes and conditions. **(C)** *Pseudomonas syringae pv. tomato* DC3000 (*Pst*) growth in leaves of A. thaliana Col-0 and eight mutants grown under NC and LP in the absence (-BFO) or presence of the BFO SynCom (+BFO) in the FlowPot system. *Pst* growth was quantified by colony counting in *A. thaliana* leaves five days post pathogen inoculation. *Pst* inoculation was carried out by spaying *Pst* at OD 0.2 in 10 mM $MgCl_2$ on leaves of four weeks-old *A. thaliana* grown in the presence/absence of the BFO SynCom under either NC or LP. The data from three independent biological replicates are shown (n = 324 samples across replicates and genotypes). Statistical significance across conditions for each genotype is indicated with letters (Kruskal-Wallis with Dunn's post hoc test, α = 0.05). **(D)** Summary heatmap depicting relative *Pst* growth (lg (CFU/g)) measured across plant genotypes and conditions.

To better illustrate the difference of *Bc* growth between NC and LP conditions, I calculated the ratio of *Bc* growth between LP and NC for each mutant in the absence of BFO (-BFO) and in the presence of BFO (+BFO) separately. (**Figure 25**). For all mutants tested except *jazQ*, a significant and consistent increase in *Bc* load was observed in LP compared to NC (3.70 – 25.69-fold increase in susceptibility), indicating that LP-mediated reduction in canopy size in the absence of microbial root commensals (**Figure 21**) was also associated with impaired resistance towards *Bc* (**Figure 24**). Among the five mutants impaired in BFO-mediated growth rescue in LP, *myc2-3* and *bri1-301* mutants also showed enhanced resistance towards *Bc* whereas *cry1cry2* and *dde2-2* mutants remained highly susceptible to *Bc* under suboptimal light conditions (Mann-Whitney-U test).

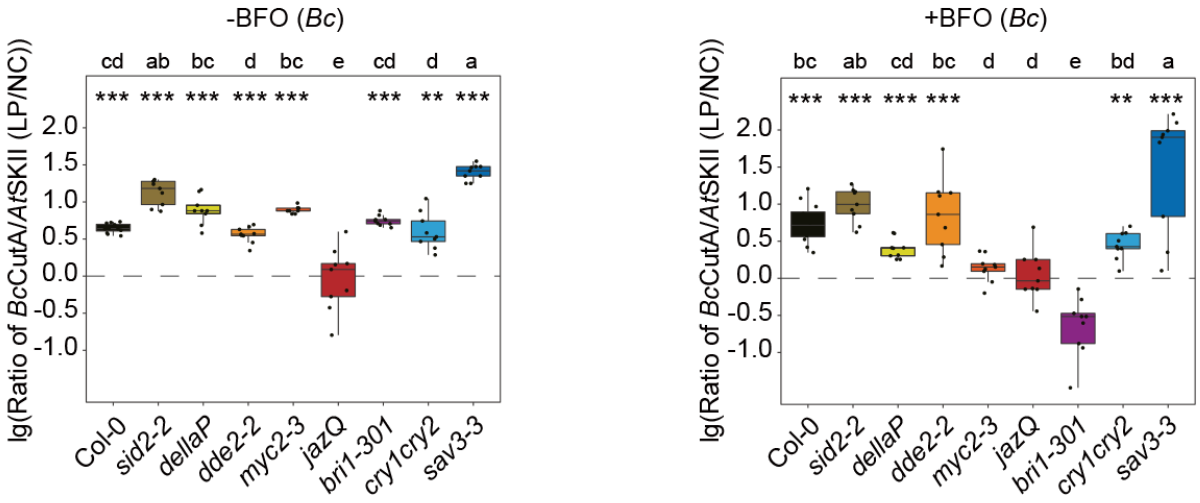

Figure 25. The comparison of *B. cinerea* growth in leaves LP vs NC in the absence and presence of the BFO SynCom for all mutants separately in the FlowPot system. Differential *B. cinerea* growth between LP and NC in leaves of *A. thaliana* Col-0 and eight

mutants grown in the FlowPot system either under germ-free conditions (-BFO, **Left**) or in the presence of the BFO SynCom (+BFO, **Right**). *Botrytis cinerea B05.10* growth was quantified by qPCR in *A. thaliana* leaves five days post pathogen inoculation. For inoculation, 2 µl droplets containing $1x10^3$ spores were applied to leaves of four weeks-old *A. thaliana* grown in the presence/absence of the BFO SynCom under either NC or LP. The relative growth of *B. cinerea* and *A. thaliana* was determined by amplification of the *BcCutinaseA* gene and the *AtSkII,* respectively. Ratio in *B. cinerea* load (five-week-old plants) was then computed between LP and NC across three independent biological replicates for each genotype (n = 168 for -BFO samples, n = 168 for +BFO samples). Datapoints above (or below) the dashed showed *B. cinerea* growth increase (or decrease) in LP compared to NC. Statistical significance across genotypes is indicated with letters, corresponding to *Kruskal-Wallis* with *Dunn's post hoc* test (α = 0.05). Statistical significance between LP and NC is indicated with stars, corresponding to Mann-Whitney U test (** $P < 0.01$, * $P < 0.05$).

A similar analysis was performed to assess differential *Pst* growth between NC and LP conditions, I calculated the ratio of *Pst* growth under LP vs NC for each mutant in the absence of BFO (-BFO) and in the presence of BFO (+BFO) separately. Based on **Figure 26**, all mutant tested showed a significant and consistent increase in *Pst* load in LP compared to NC (-BFO condition, 4.66 – 11.94 fold increase in susceptibility), indicating that LP-mediated reduction in canopy size in the absence of microbial root commensals (**Figure 21**) was also associated with impaired resistance towards *Pst* (**Figure 26**). Among the six mutants impaired in BFO-mediated growth rescue in LP, *myc2-3*, *bri1-301* and *cry1cry2* mutants also showed enhanced resistance towards *Pst* (Mann-Whitney-U test). Therefore, lack of BFO-induced growth in LP in the *myc2-3* and *bri1-301* mutants is associated with increase resistance to phylogenetically diverse biotrophic bacterial and necrotrophic fungal pathogens.

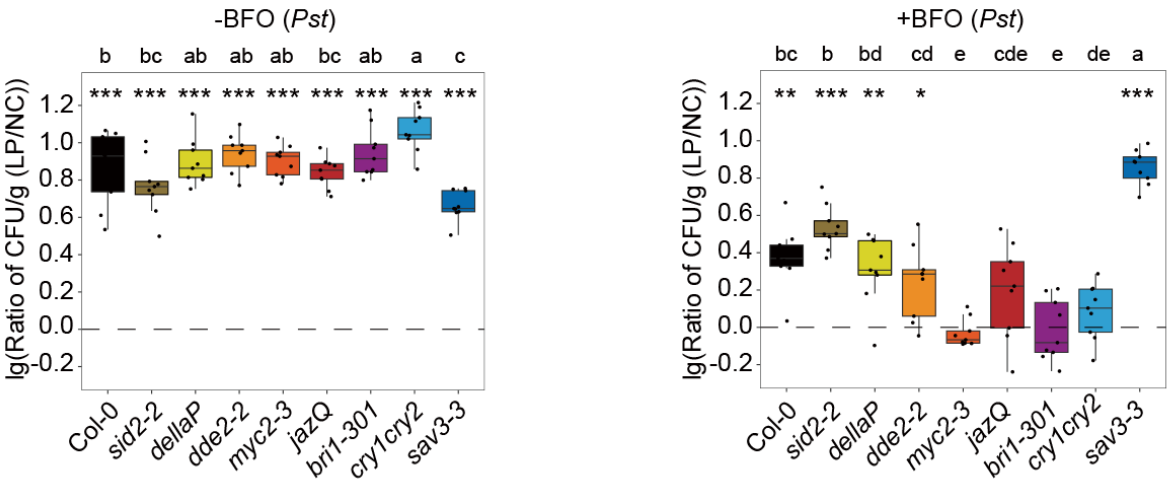

Figure 26. The comparison of *Pst* growth in leaves LP vs NC in the absence and presence of the BFO SynCom for all mutants separately in the FlowPot system. Differential *Pst* growth between LP and NC in leaves of *A. thaliana* Col-0 and eight mutants grown in the FlowPot system either under germ-free conditions (-BFO, **Left**) or in the presence of the BFO SynCom (+BFO, **Right**). Pst growth was quantified by colony counting in *A. thaliana* leaves five days post pathogen inoculation. *Pst* inoculation was carried out by spaying *Pst* at 0.2 OD in 10 mM MgCl2 on A. thaliana leaves of four weeks-old *A. thaliana* grown in the presence/absence of the BFO SynCom under either NC or LP. The data from three independent biological replicates are shown (n = 324 samples across replicates and genotypes). Ratio in *Pst* load (five-week-old plants) was then computed between LP and NC across three independent biological replicates for each genotype (n = 162 for -BFO samples, n = 162 for +BFO samples). Datapoints above (or below) the dashed showed *Pst* growth increase (or decrease) in LP compared to NC. Statistical significance across genotypes is indicated with letters, corresponding to *Kruskal-Wallis* with *Dunn's post hoc* test (α = 0.05). Statistical significance between LP and NC is indicated with stars, corresponding to Mann-Whitney U test (** $P < 0.01$, * $P < 0.05$).

Further analysis of BFO effect size on plant phenotypic traits and pathogen growth under NC and LP (Cohen's d effect size) supported the role of MYC2 as a potential regulatory node balancing microbiota-induced defense (broad-spectrum) and growth under LP (**Figure 27**).

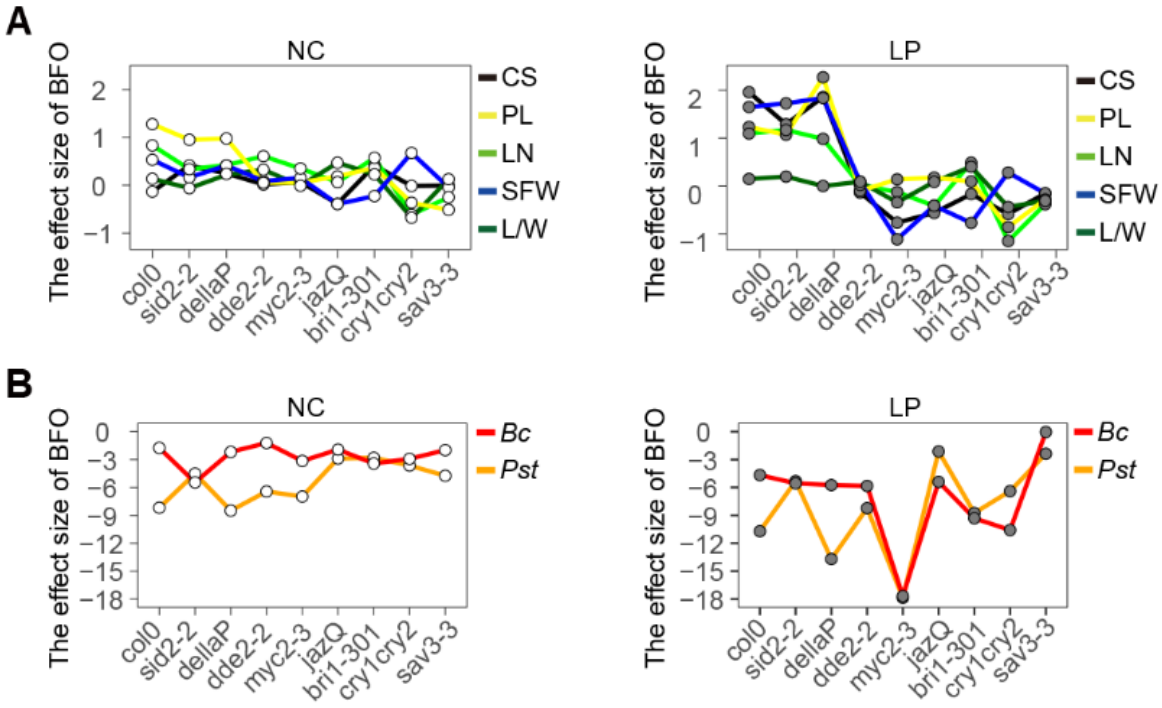

Figure 27. Effect size of BFO on shoot morphological traits and pathogen growth of *A. thaliana* Col-0 and eight mutants grown in the FlowPot system. (A) Effect size of BFO on shoot morphological traits of *A. thaliana* Col-0 and eight mutants grown in the FlowPot system under NC (left) and LP (right). Effect size was computed between -BFO and +BFO conditions for each light condition by adjusting the calculation of the standard deviation with weights of the sample sizes (Cohen´s d). Different colors of lines respect different shoot morphological traits. CS: canopy size, PL: petiole length (mean/plant), LN: leaf number, SFW: shoot fresh weight, L/W: leaf length/width ratio. **(B)** Effect size of BFO on Botrytis cinerea B05.10 (Bc) growth (red line) and *Pseudomonas syringae pv. tomato* DC3000 (Pst) growth (orange line) in leaves of *A. thaliana* Col-0 and eight mutants grown in the FlowPot system under NC (left) and LP (right). Effect size was computed between -BFO and +BFO conditions for each light condition by adjusting the calculation of the standard deviation with weights of the sample sizes (Cohen´s d).

Taken together, the above results point towards MYC2 as potential regulatory nodes balancing microbiota-induced growth or defense in a light-dependent manner.

3.5 Shifts in the structure of root bacterial community explain plant growth rescue under LP condition

Then I asked whether differentiation in bacterial community composition observed between LP and NC in roots

of Col-0 plants (**Figure 7**) is altered in the different mutants and explained differential growth phenotypes. I took advantage of the previous experiment in which the different mutants were grown in the gnotobiotic system under NC and LP (+BFO/-BFO) to simultaneously monitor microbial assemblages in root and peat matrix in output samples five-week post BFO inoculation. PERMANOVA confirmed the effect of the light condition on B community composition in roots, but not in matrix samples (root, "light": R^2 = 0.014, P = 0.024) and revealed that B community differentiation was more extensively shaped by "genotype" than by "light" (root, "genotype": R^2 = 0.117, P < 0.001, Table 2). Pairwise-enrichment tests conducted between LP and NC conditions for each genotype (edgeR, generalized linear model, P < 0.05, F**igure 28**) validated the increase in RA of root-associated *Pseudomonas* observed in the WT context, but also revealed mutant-specific differences in abundance profiles at the strain (**Figures 28**) and class (**Figure 29**) levels.

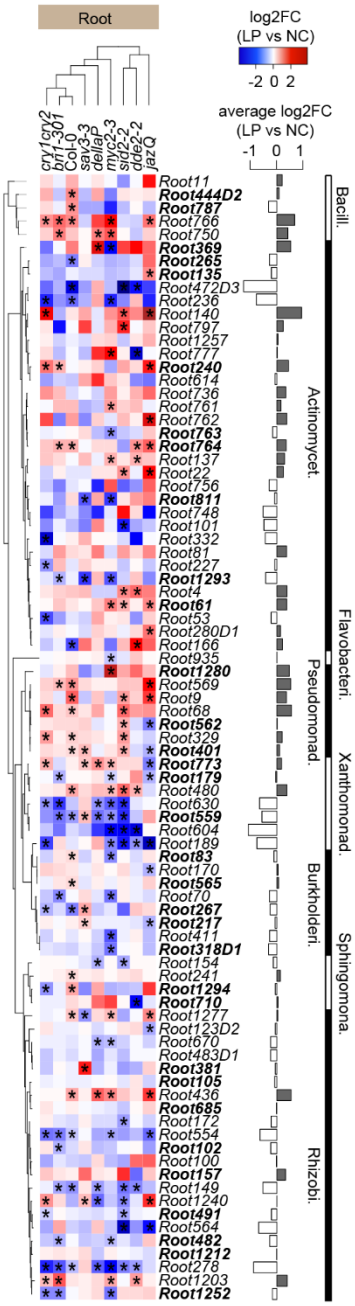

Figure 28. The shift and relationship of bacterial community for each plant lines (LP vs NC). Phylogeny-based heatmap showing differential normalized relative abundance (norm. RA, root samples) between LP and NC for each strain variant across different A. thaliana genotypes. The Maximum likelihood tree includes only strain variants (n = 85) that were consistently present across genotype samples (number of samples per genotype: n = 9, except jazQ: n = 6 and Col-0: n = 21). Differences between LP and NC were calculated based on mean values and are shown as a gradient from blue (norm. RA in LP < NC) to red (norm, RA in LP > NC). Taxonomy is shown at the class level with alternating white and black colours. Samples (i.e. genotypes) were ordered based on hierarchical clustering. Significant differences in RA between LP and NC are indicated by Asterisks (GLM, $P < 0.05$). The barplot next to the heatmap represents the mean

difference in norm. RA between LP and NC measured across all genotypes. Strain variants belonging to the genus Pseudomonas are highlighted in bold.

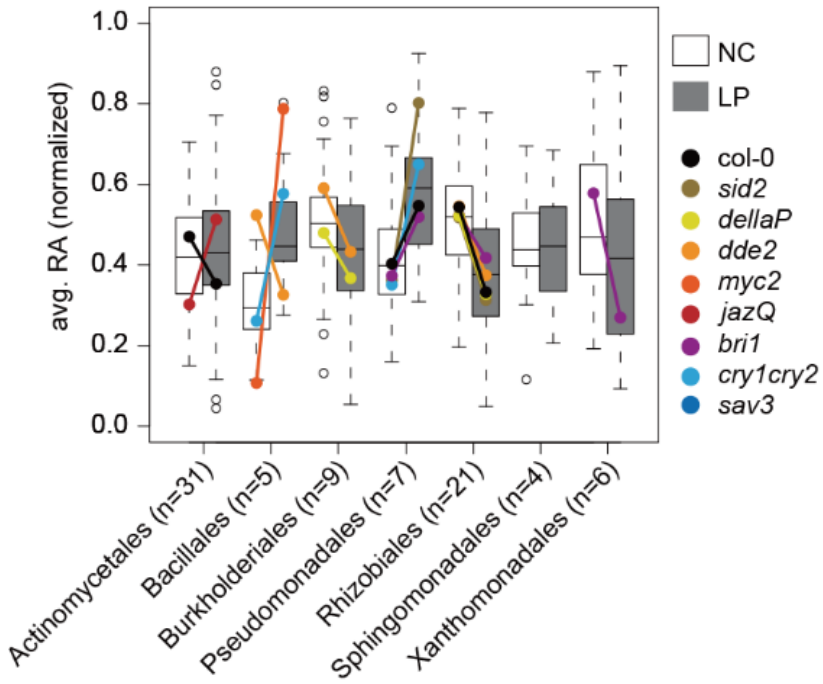

Figure 29. The mean of relative abundance under NC and LP. Mean normalized RA in LP/NC samples for bacterial strain variants for all all genotypes, sorted by taxonomical order. Boxplot depicting all genotypes together, to show general trends. Colored dots depict means within genotypes that are significantly different (Mann-Whitney-U test, $P < 0.05$).

To test for potential associations between aboveground canopy phenotypes and belowground community composition, BFO-induced differential in canopy size were calculated for each mutant between LP-BFO and LP+BFO conditions. In a second step, I asked whether these quantitative differences measured across genotypes were significantly linked to corresponding variations in root microbiota composition under LP. Using a linear regression model, a significant link between BFO-induced canopy size across mutants and B community composition was observed in root (46.9% of the variance based on Bray Curtis distances), which explained 47.7% of the variation in B community composition along PCoA1 ($R^2 = 0.4776$, $F_{1,7} = 8.314$, $P = 0.02353$, **Figure 30A**). Given the two distinct plant phenotypes observed under LP between -BFO and +BFO (rescued: BFO-induced growth in LP; not rescued: lack of BFO-induced growth in LP) the 8 genotypes were divided into these two groups. To identify strain variants which variation in RA allowed the best discrimination of the two groups, with the help of F. Mesny and Nathan Vannier, we trained a Support Vector Machines model with

Recursive Feature Elimination (SVM-RFE) based on strain RA data in LP. This approach led to the identification ofa set of 37 strain variants that are sufficient to accurately associate one sample to one phenotypic group: $R^2 = 0.83$ (**Figure 30B**).

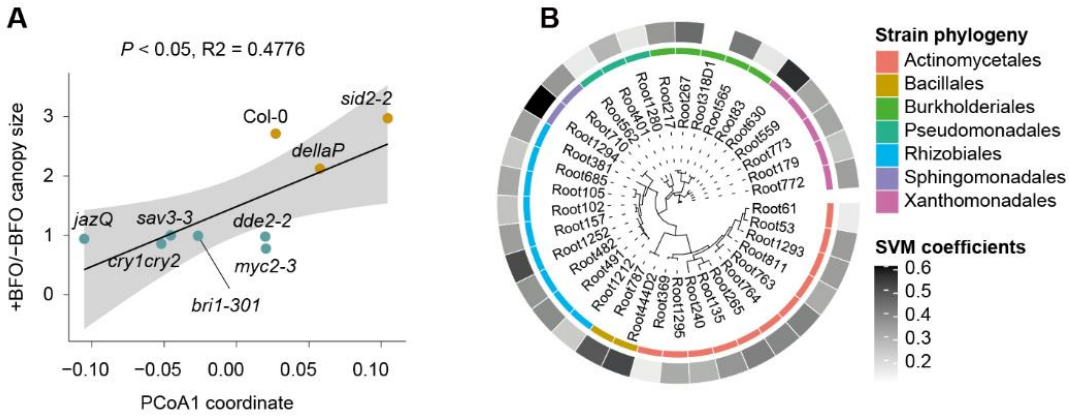

Figure 30. Bacterial composition shifts in LP explain plant growth rescue. (A) Linear regression between BFO-induced canopy size in LP and bacterial community composition. BFO-induced canopy size was calculated as a ratio between the plant weight under LP in +BFO and mean plant weight of the respective mutant under LP in -BFO. Coordinates on the first axis of a PCOA based on Bray-Curtis dissimilarities between samples was used as a proxy of bacterial community composition. P-value and R2 obtained with ANOVA are indicated in the figure. **(B)**

Using relative abundance data of these 37 strain variants selected by SVM-RFE (**Figure 30 B**) as an input for PLS-DA greatly improved model prediction (PLS-DA, P <0.001, classification error = 20.4% when all strain variants were considered, **Figure 31A**, classification error = 8.1%, when the 37 strain variants were considered, **Figure 31B**). In contrast, a similar analysis with the strain variants not selected by the SVM model (n = 68) no longer discriminated the two groups (PLS-DA, P > 0.05, classification error > 40%, data not shown).

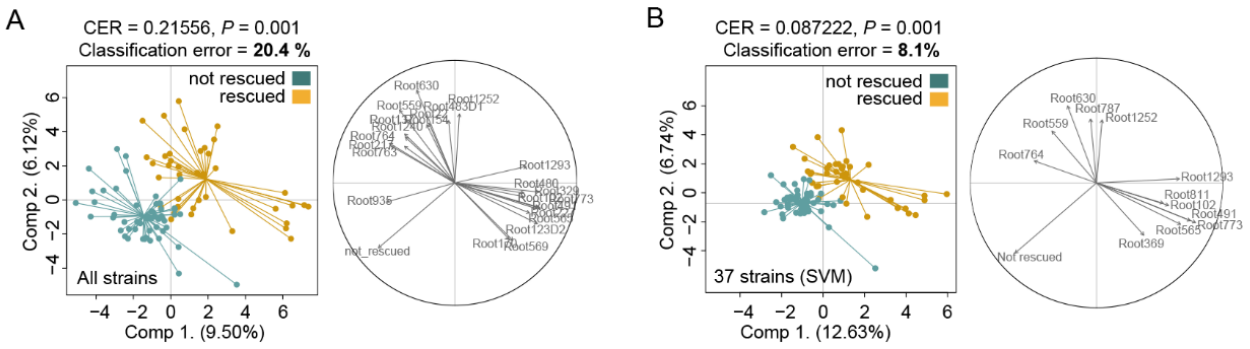

Figure 31. Differentiation between bacteria rescued and non-rescued plant phenotypes. (A) Partial least square discriminant analysis (PLS-DA) testing the differentiation between rescued and non-rescued plant phenotypes in LP based on the composition of the bacterial communities across all mutants (i.e. strains RA; 109 stains, samples n=90). The correlation circle shows the strains participating to the differentiation of the two groups (only strains with a correlation to the axes >0.5 are shown). Quality parameters of the analysis (P-value, CER and mean misclassification rate) are indicated in the figure. (B) SVM-guided Partial least square discriminant analysis (PLS-DA) testing the differentiation between rescued and non-rescued plant phenotypes in LP based on the composition strains RA using the subset of strains identified in the System Vector Machine (SVM) (37 stains, samples n=90). The correlation circle shows the strains participating to the differentiation of the two groups (only strains with a correlation to the axes >0.5 are shown). Quality parameters of the analysis (P-value, CER and mean misclassification rate) are indicated in the figure.

Further PERMANOVA confirmed the specific effect of "light" on bacterial community composition in root, but not in matrix samples (root: $R^2 = 0.014$, $P = 0.024$) and revealed that bacterial community differentiation was more extensively shaped by "genotype" than by "light" (root: $R^2 = 0.117$, $P < 0.001$) (**Table 2**). However, interaction between "genotype" and "light" was insignificant (root: $R^2 = 0.039$, $P = 0.506$), suggesting that light-driven changes in belowground bacterial community composition were not extensively influenced by gene mutations in the respective mutants (**Table 2**).

Table 2 PERMANOVA partitioning of microbial community assemblages based on OTUs distance matrices (Bray Curtis dissimilarities, 999 permutations, with Adonis function in R).

	Global model			
	Bacteria			
	df	***F***	***R2***	***P***
Genotype	8	4.116	0.06667	**0.001**
Compartment	1	99.203	0.20085	**0.001**
Light	1	1.761	0.00357	0.107
Genotype:Compartment	8	1.615	0.02615	**0.011**
Genotype:Light	8	0.970	0.01571	0.495
Compartment:Light	1	3.127	0.00633	**0.014**
Genotype:Compartment:Light	8	0.403	0.00653	1.000
Residuals	333	NA	0.67420	NA
Total	368	NA	1.0	NA

	Model based on roots samples			
	Bacteria			
	df	***F***	***R2***	***P***
Genotype	8	2.90677	0.11690	**0.001**
Light	1	2.79874	0.01407	**0.024**
Genotype:Light	8	0.98324	0.03954	0.506
Residuals	165	NA	0.82948	NA
Total	182	NA	1.0	NA

	Model based on Matrix samples			
	Bacteria			
	df	***F***	***R2***	***P***
Genotype	8	2.89801	0.11751	**0.001**
Light	1	2.28485	0.01158	0.083
Genotype:Light	8	0.47755	0.01936	0.993
Residuals	168	NA	0.85154	NA
Total	185	NA	1.0	NA

Taken together, these results suggest a clear link between belowground B community composition and aboveground growth phenotypes under LP. However, it remains unclear whether these compositional shifts in root commensal community are the cause or the consequence of canopy size phenotypes under LP.

3.6 Priority to microbiota-induced growth over defense under LP requires MYC2

Given the fact that MYC2 is a central regulatory node controlling the crosstalk between JA and other phytohormone signaling pathways (i.e. GA, SA, ABA, IAA), and is also regulating responses to light and circadian clock (**Kazan and Manners, 2013**), we hypothesized that this transcription factor might coordinate prioritization of microbiota-induced growth over defense under suboptimal light conditions. To test this hypothesis, I used the lines Col-0, *myc2-3*, and *jin1-8* pMYC2:MYC2-FLAG in which a MYC2-FLAG fusion protein is expressed under control of the native MYC2 promoter (MYC2-FLAG, *myc2* background, **Hou et al. 2010**) and grow these plants using exactly the same experimental setup as described before. As expected, BFO-mediated growth rescue under LP is abolished in the *myc2-3* mutant and growth phenotypes are similar between the lines Col-0 and *jin1-8* pMYC2:MYC2-FLAG (**Figure 32**) validating that this complementation line can be used for deeper inspection of the MYC2 molecular function. Remarkably, we observed that the BFO SynCom significantly increased plant canopy size and shoot fresh weight not only under LP, but also under EODFR (**Figure 32**), indicating that MYC2-dependent rescue of plant growth by BFO is robust across multiple light-limiting conditions.

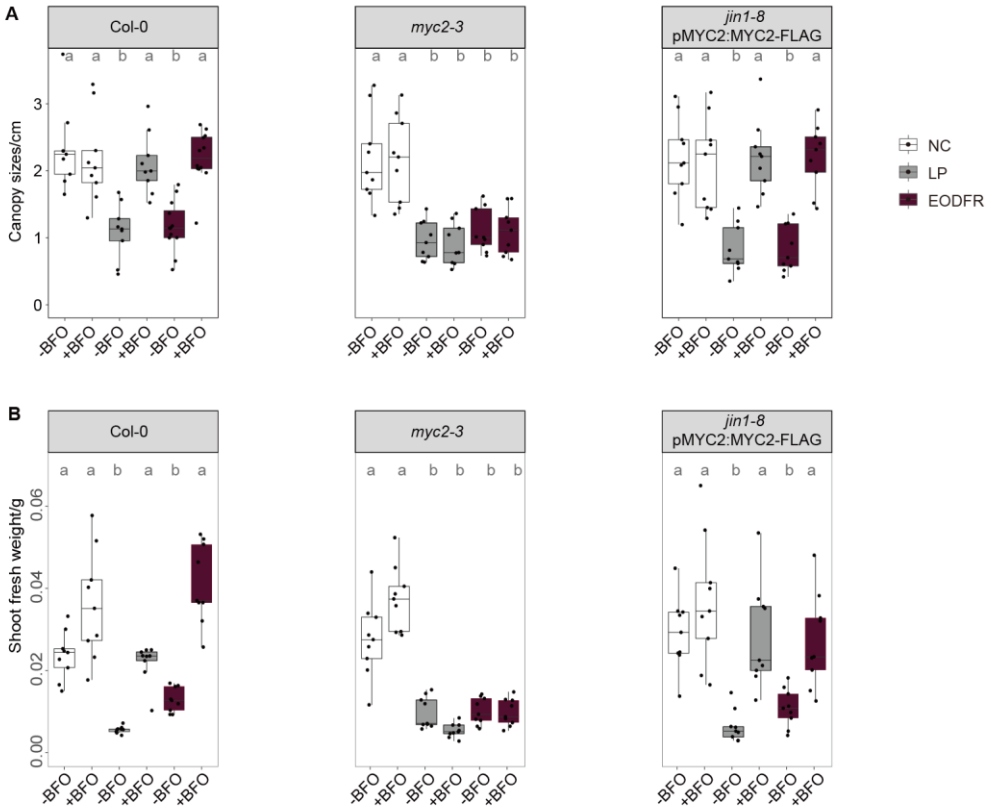

Figure 32. MYC2-dependent prioritization of BFO-induced growth over defense in LP. (A) Canopy size (in cm^2) of five-week-old WT (Col-0), mutant (*myc2-3*), and complemented (*jin1-8* pMYC2:MYC2-FLAG) *A. thaliana* grown in the FlowPot system in the absence (-) or presence (+) of the BFO SynCom under either normal light (NC, white), low photosynthetically active radiation (LP, grey), or end-of-day far red (EODFR, dark red). Three independent biological replicates (Col-0: n = 60 plants, *myc2-3*: n = 54 plants, *jin1-8 pMYC2:MYC2-FLAG*: n = 54 plants). Letters indicate statistical significance corresponding to *Kruskal-Wallis* with *Dunn's post hoc* test (α = 0.05). **(B)** Shoot fresh weight (in g) of five-week-old WT (Col-0), mutant (*myc2-3*), and complemented (*jin1-8* pMYC2:MYC2-FLAG) *A. thaliana* grown in the FlowPot system in the absence (-) or presence (+) of the BFO SynCom under either normal light (NC, white), low photosynthetically active radiation (LP, grey), or end-of-day far red (EODFR, dark red). Three independent biological replicates (Col-0: n = 60 plants, *myc2-3*: n = 60 plants, *jin1-8 pMYC2:MYC2-FLAG*: n = 60 plants). Letters indicate statistical significance corresponding to *Kruskal-Wallis* with *Dunn's post hoc* test (α = 0.05).

To clarify the function of MYC2 on plant growth rescue by BFO commensals under LP, I performed RNA sequencing experiments with the *myc2-3* mutant and the *jin1-8* pMYC2: MYC2-FLAG. First, I calculated the distance between samples (Root: n = 12 samples, Shoot: n = 12 samples) for the *myc2-3* mutant and the *jin1-8* pMYC2: MYC2-FlAG line separately. Pairwise Pearson´s correlations among *jin1-8* pMYC2: MYC2-FlAG

samples indicated that presence/absence of the BFO SynCom explained transcriptome differentiation in root samples more than "light", whereas differentiation in the shoot transcriptome showed an opposite pattern (**Figure 33**) which is similar with the data from Col-0 samples (**Figure 8A**) indicating that *jin1-8* pMYC2: MYC2-FlAG plants show an overall similar response to light and root microbiota. Notably, for the *myc2-3* mutant, the factor "root microbiota" explained transcriptome differentiation in shoot samples more than the factor "light" (**Figure 33**), suggesting that MYC2 is involved in plant response to LP in the shoot compartment.

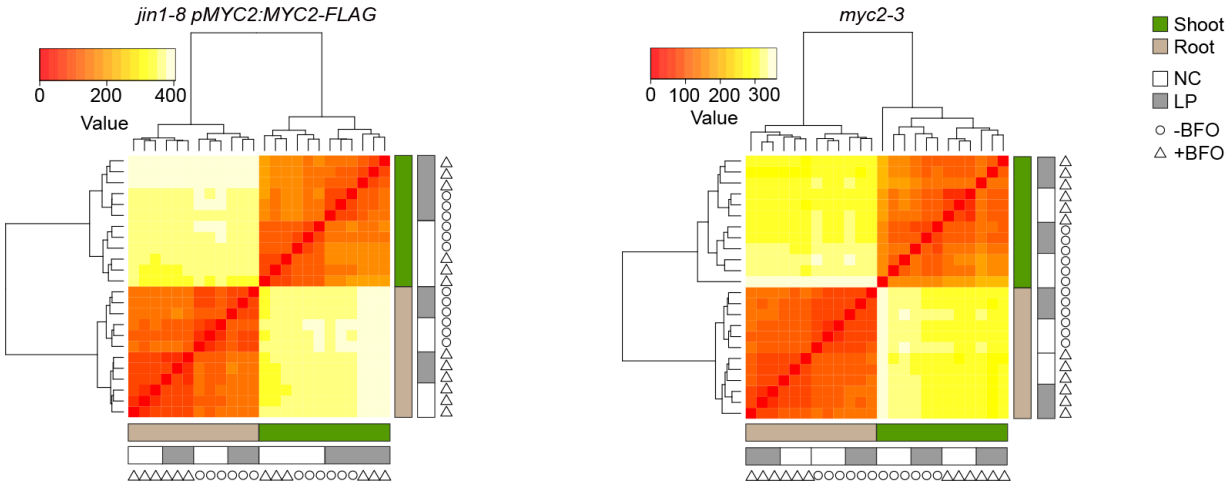

Figure 33. Transcriptional reprogramming in shoot and root of *jin1-8* pMYC2:MYC2-FLAG and *myc2-3* in response to light and BFO. Dendrogram showing the hierarchical relationship between samples used for RNA sequencing. Three independent biological replicates (n =48 samples). NC: normal light condition, LP: low PAR. -BFO: no microbes (i.e. germ-free), +BFO: with microbes. B: bacteria, F: fungi, O: oomycetes.

To determine the extent to which gene expression patterns are different between the *myc2-3* mutant and the *jin1-8* pMYC2: MYC2-FlAG line (NC-BFO, NC+BFO, LP-BFO, LP+BFO), I calculated the fold-change between the *myc2-3* mutant and the *jin1-8* pMYC2: MYC2-FLAG line for each condition and filtered all significantly regulated genes (referred to as *MYC2*-Differentially Expressed - MDEs, $|\log2FC| \geqslant 1$, Empirical Bayes Statistics, FDR < 0.05). Then, I performed hierarchical clustering using expression profiles of all genes identified as differentially regulated across conditions ($|\log2FC| \geqslant 1$, Empirical Bayes Statistics, FDR < 0.05). Hierarchical clustering identified 8 gene expression clusters in root (MDER1-MDER8, **Figure 34**) and 8 in shoot (MDES1-MDES8, **Figure 34**).

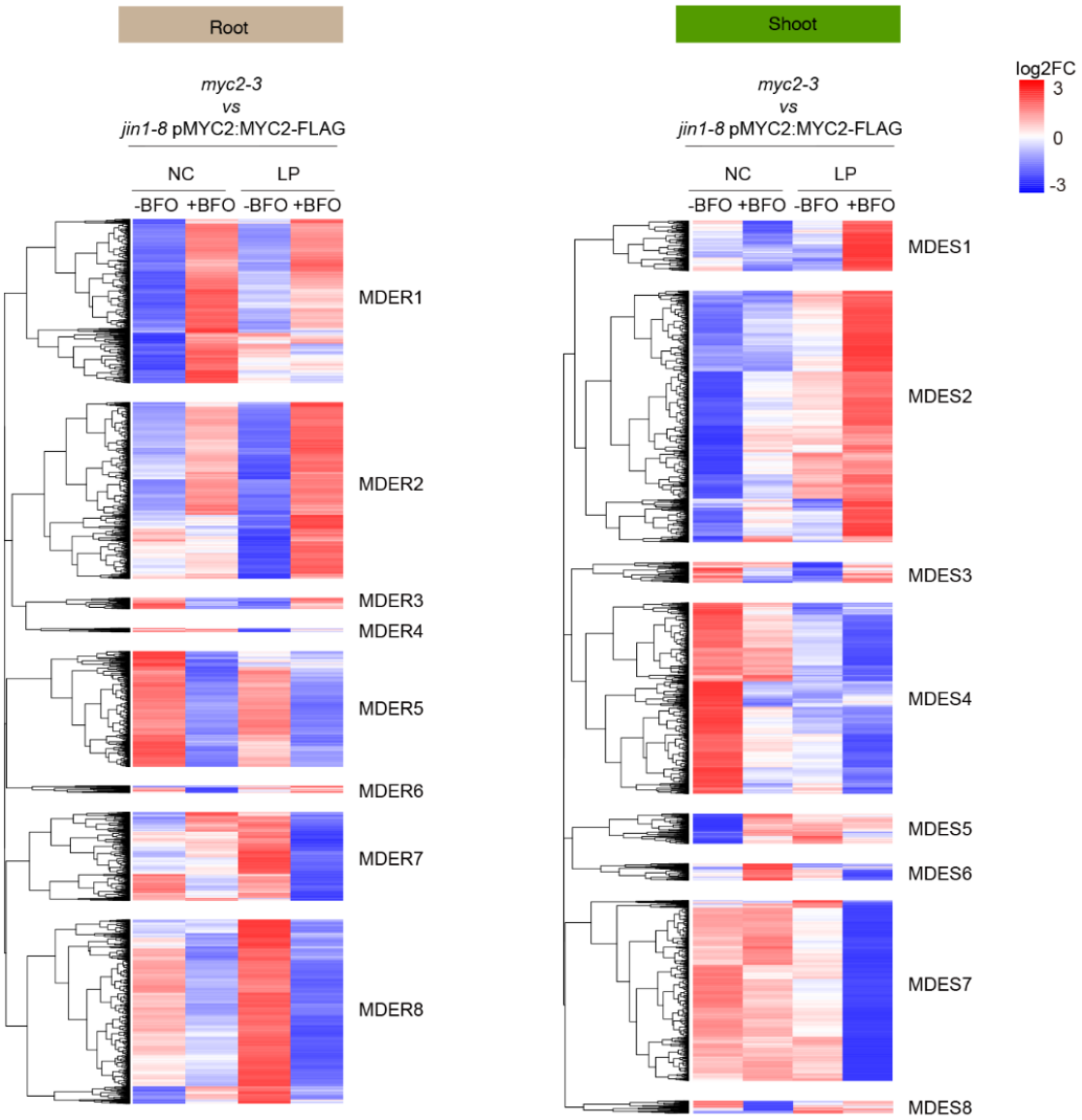

Figure 34. Gene expression pattern of shoot and root in response to light and BFO. Transcript profiling of 5,231 *A. thaliana* genes significantly regulated in root samples **(Left)** between *A. thaliana myc2-3* and *jin1-8* pMYC2:MYC2-FLAG mutant lines (|log2FC| ⩾ 1, Empirical Bayes Statistics, *FDR* < 0.05). Over-represented (white to red) and under-represented transcripts (white to blue) are shown across conditions as mean log2 counts per million (TMM-normalized voom-transformed data with limma package in R). The gene set was split into eight major MYC2 differentially-expressed gene expression clusters in root, labelled MDER1 to MDER8. NC: normal light condition, LP: low PAR, -BFO: no microbes, +BFO: with microbes. Three independent biological replicates (n = 24 samples). Transcript profiling of 5,038 *A. thaliana* genes significantly regulated in shoot samples **(Right)** between *A. thaliana myc2-3* and *jin1-8* pMYC2:MYC2-FLAG mutant lines (|log2FC| ⩾ 1, Empirical Bayes Statistics, *FDR* < 0.05). Over-represented (white to red) and under-represented transcripts (white to blue) are shown across conditions as mean log2 counts per million (TMM-normalized voom-transformed data with limma package in R). The gene set was split into eight major MYC2 differentially-expressed gene expression clusters in shoot, labelled MDES1 to MDES8. NC:

normal light condition, LP: low PAR, -BFO: no microbes, +BFO: with microbes. Three independent biological replicates (n = 24 samples).

To connect the gene clusters generated by hierarchical clustering with gene biological processes and functions, I performed Gene Ontology (GO) term enrichment for individual gene clusters depicted in **Figure 34**. In roots, GO terms enrichment analyses of MDEs revealed that processes related to ion homeostasis and circadian rhythm (MDE-R6), response to sugar (MDE-R2), defense (MDE-R5), photosynthesis and response to light (MDE-R6), or cytokinesis processes (MDE-R6) were modulated by MYC2 across the different conditions (**Figure 35**). In shoots, GO terms related to photosynthesis (MDE-S1), defense (MDE-S2), cytokinesis (MDE-S3), secondary metabolite biosynthesis (MDES4), response to JA (MDE-S5), or starch and sugar biosynthesis (MDE-S7) were also altered in the *myc2-3* mutant (**Figure 35**). Notably, clusters MDES2 and MDES7 contained GO terms for which the most significant enrichments were observed and genes in these clusters were either induced (MDE-S2) or repressed (MDE-S7) in the *myc2-3* mutant compared to MYC2-FLAG in the condition LP+BFO (**Figure 35**).

Figure 35. Gene Ontology (GO) term enrichment in root and shoot in response to light and BFO. Gene Ontology (GO) term enrichment depicting the top 12 most significantly enriched GO terms (Hypergeometric test with Bonferroni correction, α = 0.05) detected in all clusters for root samples **(Left)** and shoot samples **(Right)**. The size of point reflects the amount of gene numbers enriched in this GO term. The colour of point means the p value ((Hypergeometric test with Bonferroni correction). R: response, Reg. Regulation, ET: ethylene, SA: salicylic acid, JA: jasmonic acid, SAR: systemic acquired resistance, CW: cell wall, CG: cell growth, P: process, Com: compound, Hex: hexakisphosphate, inv.: involved in.

Based on the GO enrichment from shoot samples, I observed that MDES2 and MDES7 clusters contain the most significantly enriched GO terms (**Figure 35**). To obtain deeper insights into the biological functions associated with these the corresponding genes, I generated GO term networks for top 12 most significant GO terms in clusters MDES2 and MDES7. From the GO network analysis, I observed that genes in the MDES2

cluster are associated with plant defense, for example, systemic acquired resistance, defense response to fungus, or response to chitin (**Figure 36B**). However, the MDES7 cluster is associated with plant growth, especially starch biosynthesis and metabolism (**Figure 36B**). Under LP, genes in the cluster MDES2 cluster are significantly upregulated in the presence of BFO under LP whilst those in the cluster MDES7 are downregulated (**Figure 36A**), indicating that defense is prioritized over growth under LP in the *myc2-3* mutant, which is consistent with the loss of plant growth rescue phenotype observed for this mutant in LP.

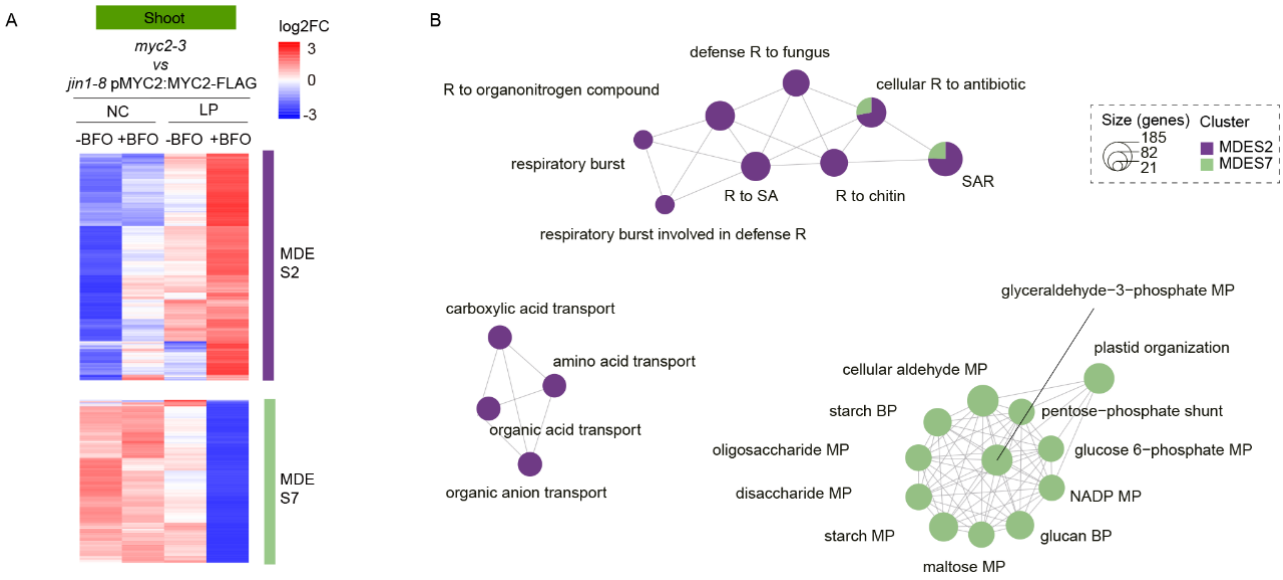

Figure 36. MYC2-dependent ttranscriptional reprogramming mediated by light and BFO in shoot. (A) The heatmap showing the gene expression pattern of gene cluster MDES2 and MDES7. **(B)** Gene Ontology (GO) term enrichment network depicting the top 12 most significantly enriched GO terms (Hypergeometric test with Bonferroni correction, α = 0.05) detected in clusters MDES2 and MDES7. Each GO term is represented as a circle and the contribution of each cluster to the overall GO term enrichment is shown. The size of the GO term reflects the number of genes enriched in the GO term.

Given the extensive activation of defense-related genes observed under LP in the *my2-3* mutant, I asked how many of these genes do overlap with the previously identified genes in the cluster S1 (See **Figure 13**). To clarify this question, I calculated the percentage of overlapped genes between MDES2/ MDES7 and gene clusters previously defined in the context of Col-0 plants (See **Figure 13**). Based on the pie plots (**Figure 37**), we observed that 28% of the genes are shared between the cluster MDES2 and the previously identified the cluster S1 from Col-0 samples (see **Figure 13**). Meanwhile, 11% of the genes in the cluster MDES7 were shared

between the cluster MDES7 and the previously identified the cluster S3 (see **Figure 13**) from Col-0 samples.

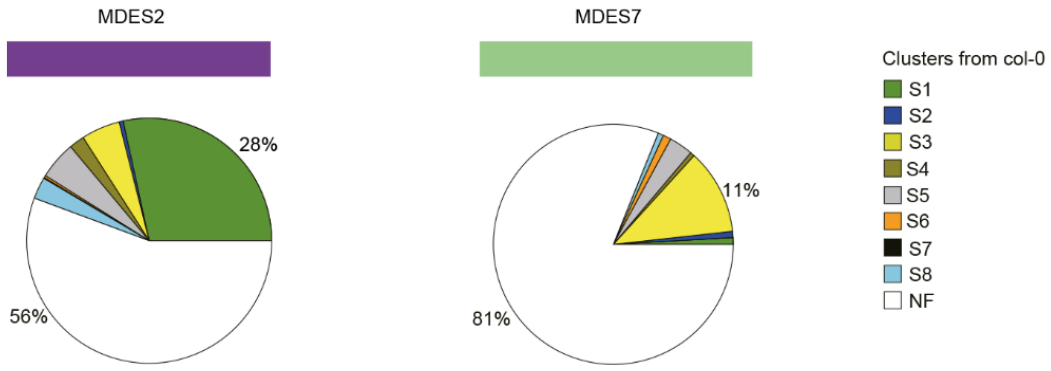

Figure 37. The overlap of genes in MDES2 and MDES7 cluster with col-0 data. Percentage of genes shared between shoot clusters MDES2 **(Left)** and MDES7 **(Right)** and shoot clusters (S1 to S8) of col-0 data previously defined.

Then, I inspected the genes and associated GO terms in the cluster MDES2 and MDES7 using a gene-concept network analysis. From the gene-concept network (**Figure 38**), I observed that genes in the cluster MDES2 are largely SA-responsive genes (i.e. PR1, BGL2, FRK1, EDS5) or involved in SAR (i.e. SARD1, AZI1 and FMO1), confirming that the *myc2-3* mutant colonized by the root microbiota massively invests into shoot defense under LP. In contrast, genes from the cluster MDES7 are involved in starch and sugar metabolic processes (**Figure 38**), These genes encode enzymes that are primarily involved in starch biosynthesis (i.e. SS1, SS3), are required for starch accumulation (i.e. ADG1, PGI), or starch breakdown (i.e. LSF1, LSF2, PTPKIS1, BAM3) in leaves. The results illustrate that priority to defense in the *myc2*-3 mutant is associated with altered sugar metabolic processes in shoot.

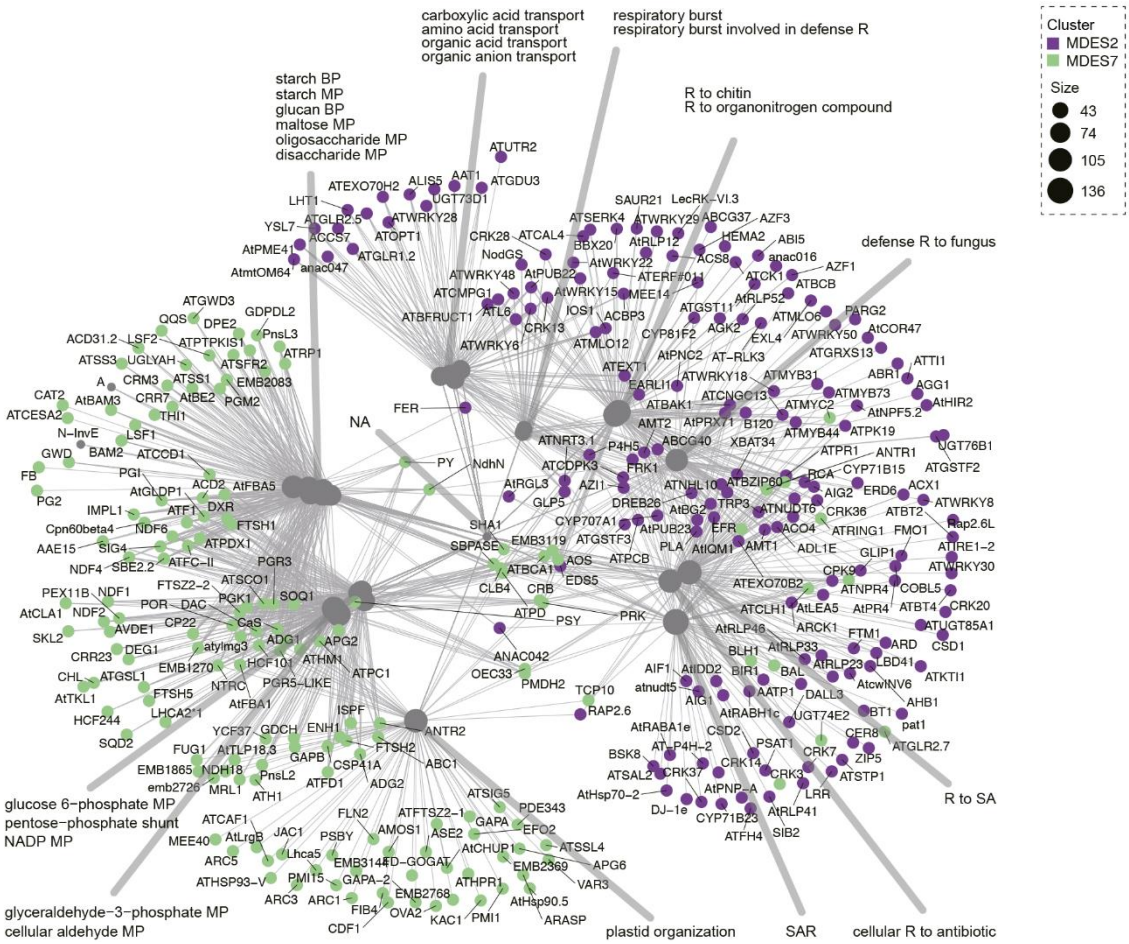

Figure 38. Gene-concept network of genes in MDES2 and MDES7 clusters. Gene-concept network (cnetplot function in R) depicting linkages between genes and associated top 12 most significantly enriched GO terms detected in clusters MDES2 and MDES7. Each node represents a gene and is colour-coded according the different cluster names. R: response, SA: salicylic acid, SAR: systemic acquired resistance, BP: biosynthetic process, MP: metabolic process.

To further validate that BFO-induced plant defense is retained in the *myc2-3* under LP, I inoculated leaves of four-week old *myc2-3* and *jin1-8* pMYC2-FLAG plants (NC-BFO, NC+BFO, LP-BFO, LP+BFO) with the necrotrophic fungal pathogen *Botrytis cinerea* B05.10 (*Bc*, droplet inoculation, 2 µl droplets containing $1x10^3$ spores) or the biotrophic bacterial pathogen *Pseudomonas syringae pv. tomato* DC3000 (*Pst*, spray inoculation, OD = 0.2). Evaluation of pathogen growth *in planta* by quantitative PCR (*Bc*) or colony counting (*Pst*) validated the extensive influence of both light and SynCom conditions on disease resistance five days post pathogen inoculation (One-Way ANOVA with post hoc Tukey HSD test, $P < 0.05$, **Figures 39**). However, the increase in plant susceptibility towards both pathogens observed between NC and LP in the *jin1-8* pMYC2-FLAG (+BFO

condition) was no longer visible in the *myc2-3* mutant, validating that priority to defense explains lack of BFO-mediated growth promotion in LP on one hand and increased resistance to leaf pathogens on another hand(**Figure 39**) which is consistent with the transcriptome data (**Figure 36**).

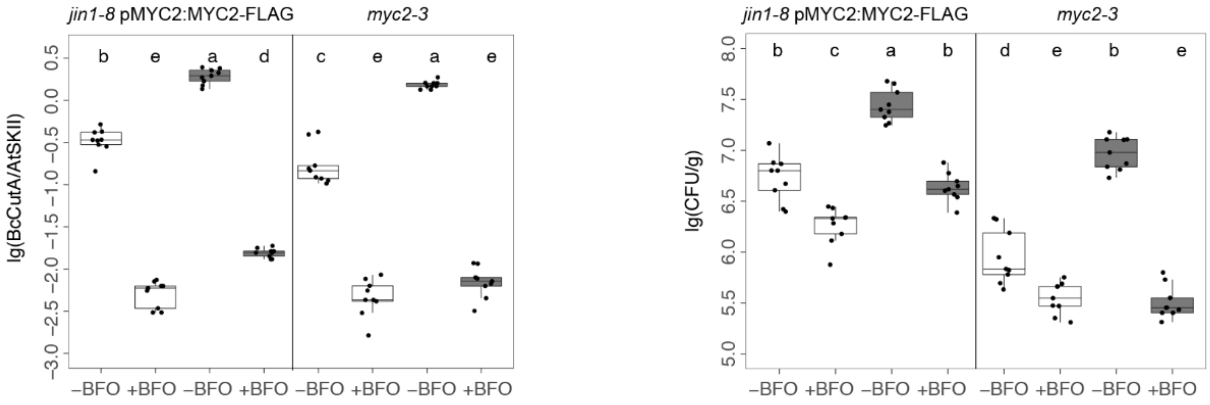

Figure 39. The immunity of *jin1-8* pMYC2:MYC2-Flag and *myc2-3* plants changed by light and BFO in shoot. qPCR-based quantification of *Botrytis cinerea B05.10* growth **(Left)** in *A. thaliana* leaves five days post pathogen inoculation in the FlowPot system. For inoculation, 2 µl droplets containing $1x10^3$ spores were applied to leaves of four weeks-old *A. thaliana* grown in the presence/absence of the BFO SynCom under either NC or LP. The relative growth of *B. cinerea* and *A. thaliana* was determined by amplification of the *BcCutinaseA* gene and the *AtSkII,* respectively. Four independent biological replicates (n = 72 plants). Letters indicate statistical significance corresponding to One-Way *ANOVA* with *post hoc Tukey* HSD test (α = 0.05). Colony count-based quantification of *Pseudomonas syringae pv. tomato DC3000* growth **(Right)** in *A. thaliana* leaves five days post pathogen inoculation in the FlowPot system. For inoculation, bacterial suspension was adjusted to OD = 0.2 and spray-inoculated on leaves of four weeks-old *A. thaliana* grown in the presence/absence of the BFO SynCom under either NC or LP. For colony counting, 20 µl dilution series (10^{-1}, 10^{-2}, 10^{-3}, 10^{-4}, 10^{-5} with 10 mM Mgcl2) spot on NYGA plate, counting colonies after two days incubation at 28 °C. Three independent biological replicates (n = 72 plants). Letters indicate statistical significance corresponding to One-Way *ANOVA* with *post hoc Tukey* HSD test (α = 0.05).

Taken together, those above results indicate that the trade-off between starch/carbon metabolism and defense in leaves is modulated by light in a MYC2-dependent manner.

4. DISCUSSION

It is well known that the root microbiota plays an important role in alleviating plant abiotic stresses (**Castrillo et al., 2017**; **Fitzpatrick et al., 2018**; **Harbort et al., 2020**). For example, Castrillo et al. demonstrated that a synthetic bacterial community (SynCom) significant enhanced the expression of *PHR1* gene which is the master regulator of phosphate starvation responses (PSRs) under limited phosphate conditions (**Castrillo et al., 2017**) indicating the root microbiota promote the phosphate starvation response in plants. Fitzpatrick et al. reported that the root microbiota promoted drought tolerance in diverse lineages of plant species. Particularly the abundance of one sequence variant belonging to the the genus *Streptomyces* was positively correlated with the ability of plants to resistance the drought stress (**Fitzpatrick et al., 2018**). Reciprocally, it has been demonstrated that some abiotic factors alter the component of root microbial communities (**Oldroyd et al., 2011**; **Walitang et al., 2018)** For example, phosphate availability for legume plants is directly related with the colonization-efficiency of arbuscular mycorrhiza in plants (**Oldroyd et al., 2011**). Walitang *et al.* revealed salt stress shifts rice endophytic communities and found *Pantoea, Flavobacterium, Microbacterium, Enterobacter, Kosakonia* and *Curtobacterium* are dominant bacterial groups under salt stress (**Walitang et al., 2018**). Recently, Harbort et al reported that the beneficial interaction between root microbiota and *Arabidopsis thaliana* under iron deficiency depending on the secretion of host-derived coumarins (**Harbort et al., 2020**). However, previous studies mainly focused on the role of the root microbiota for alleviating belowground abiotic stresses such as drought, salt, or nutrient stresses. I first demonstrated that root microbiota conferred Arabidopsis thaliana tolerance to light suboptimal conditions. By monitoring the component of root microbial communities under different light condition (NC and LP), I proved that change in light condition significantly shaped bacterial community composition in roots, but not in the surrounding soil matrix (**Figure 6D**). This result indicates that light perception in leaves likely has cascading consequences on root metabolism, and that these light-induced changes in the host are directly responsible for the compositional shifts observed in root samples. These results are consistent with previous work (**Lee et al., 2016**) and our RNAseq data, which suggest that aboveground light has important consequences on belowground root functions.

Previous studies showed that the interplay between root-associated microbes, plant immunity, and plant response to abiotic stresses is key to promote plant survival in nature (**Hiruma et. al., 2016**; **Hacquard et al., 2016**; **Castrillo et al., 2017**). Hacquard et al. demonstrated that the colonization of *Colletotrichum tofieldiae* triggered *Arabidopsis* prioritization of growth over defense responses under phosphate sufficient conditions (**Hacquard et al., 2016**). In contrast, under phosphorous limiting conditions, these plant immune responses were shut downbased on the *Arabidopsis* transcriptome data (**Hacquard et al., 2016**). Similarly, Castrillo et al. demonstrated that the root microbiota drives integration of plant response to phosphate and immunity, thereby promoting the starvationover defense responses (**Castrillo et al., 2017**). Recently, Harbort et al. found that a bacterial SynCom improved Arabidopsis thaliana iron nutrition and modulated a subset of defense genes in a Coumarin-dependent manner (**Harbort et al., 2020**). In my results, I observed that BFO root commensals and ectopic leaf colonizers induce extensive immune responses in leaves when light conditions are optimal. This result is consistent with the idea that plants grown with their microbial commensals activate a state of alert in plants that is referred to as a priming of plant defense (**Selosse et al., 2014**; **Hu et al., 2018**). Through inoculation with two different types of pathogen (the necrotrophic fungal pathogen *Botrytis cinerea* B05.10 and the biotrophic bacterial pathogen *Pseudomonas syringae pv. tomato* DC3000), I observed that the presence of the root microbiota indeed extensively protected leaves from phylogenetically distinct pathogens. This result is remarkable and suggest that commensals are at least as important as the immune system itself to restrict pathogen growth in nature. This protective activity can be explained by direct microbe-microbe competition (i.e. ectopic leaf commensals) or by microbiota-induced priming of immunity (**Durán et al., 2018**; **Berendsen et al., 2018**; **Vannier et al., 2019**; **Carrión et al., 2019**). However, our results suggest that *A. thaliana* can modulate these microbiota-induced immune responses according to the light condition. Therefore, the discovery of this light-dependent growth-defense trade-off is likely critical for decision making in plants growing in their natural environments.

During the last decade, two classic phytohormone dependent pathways involved in the balance between growth and defense in *Arabidopsis* have been extensively studied including GAs – JA antagonism and BRs – JA antagonism (**Guo et al., 2018**). Through screening 8 mutants impaired in the phytohormone dependent balance between growth and defense under NC and LP in the absence and the presence of root microbiota in the FlowPot system, I observed that in the presence of root microbiota (+BFO), the mutants *bri1-301*, *dde2-2*, *myc2-3*, *jazQ*

and *cry1cry2* lost the phenotype of growth rescue by root microbiota under light suboptimal condition and show maintained defense and compromised growth under low PAR condition (**Figure 21, Figure 25,** and **Figure 26**). These results suggest that the phenotype of plant prioritization growth over defense by root microbiota under light suboptimal condition is consistent with the previous reported phytohormone depend growth – defense tradeoff (**Guo et al., 2018**). Meanwhile, based on the result of *cry1cry2* mutant lost the growth rescue by root microbiota under light suboptimal condition and show maintained defense under LP (**Figure 21, Figure 25,** and **Figure 26**), I demonstrated that this observed tradeoff between growth and defense is light receptor dependent since CRY1 and CRY2 are cryptochromes for the light perception in *Arabidopsis* (**Somers and Fujiwara, 2009**).

An important question is whether there is a direct link between microbial community composition in plant roots and alleviation of *A. thaliana* growth deficiency under LP. In the context of biotic stresses, it has been shown that leaf colonization by microbial pathogens or herbivores resulted in shifts in the rhizosphere microbiota through host-induced modulation of root exudation profiles (**Rudrappa et al., 2008**; **Yuan et al., 2018**; **Hu et al., 2018**). Using manipulation experiments, these pathogen/herbivore-induced shifts in rhizosphere commensal communities were shown to be the direct cause protecting the next plant generation through the promotion of systemic defense responses (**Berendsen et al., 2018**; **Yuan et al., 2018**; **Hu et al., 2018**). Therefore, modulation of the rhizosphere microbiota via leaf pathogen-induced change in root exudation profiles appears to dictate survival and performance of the offspring. Here, I observed that multiple *Pseudomonas* isolates were consistently and specifically enriched in plant roots under LP compared to NC (**Figure 7**). One important question is whether this enrichment is directly responsible (i.e. the cause) of BFO-induced growth in LP. Based on microbiota manipulation experiments, I first observed that the bacterial community is needed for the phenotype (**Figure 8**). Remarkably, a microbiota drops out experiment with 177 bacterial strains lacking all 7 *Pseudomonas* isolates did no longer rescue plant growth under LP, indicating that *Pseudomonas* are necessary for the growth rescue in LP (**Figure 8**). Therefore, it is highly possible that the host-driven recruitment of root-associated *Pseudomonas* observed under LP at least contributes to the phenotype. However, additional work is still needed to clearly disentangle the extent to which shifts in bacterial community composition observed in plant roots between LP and NC are the cause or the consequence of canopy phenotypes.

It is long well shown that the phytohormone jasmonate (JA) plays essential roles in plant defense towards

pathogens and pests and meanwhile regulating plant development processes (**Wasternack, 2007**). Under non-stress condition, JA responses are restrained by JASMONATE-ZIM-DOMAIN (JAZ) family proteins which is well known as the repressor in JA signaling pathway through Skp-Cullin-F-box (SCF) interaction with CORONATINE INSENSICTIVE1 (COI1, a F-box protein) (**Chini et al., 2007**; **Yan et al., 2007**). Under some stress condition, for example pathogen attack, wounding, the biosynthesis of JA is rapidly activated in plants (**Wasternack and Kombrink, 2010**). JA-Ile binds to JAZ-COI1 complexes resulting the degradation of JAZ protein via the 26S proteasome (**Thines, et al., 2007**; **Sheard et al., 2010**). During the degradation of JAZ protein, MYC2, one of the major transcription factor (TF) in JA signaling, is released and trigger downstream JA response in plants (**Dombrecht et al., 2007**). Hence, the *jazQ* (*jaz* quintuple) mutant maintains continuous strong defense at the cost of losing growth since JA signaling is continuously activated (**Major et al., 2017**). Consistent with this work, I observed that, the *jazQ* mutant show significant reduced canopy size under the control condition (NC-BFO) compared with Col-0 plants (**Figure 21**). Meanwhile, I observed that *jazQ* mutant is more susceptible to pathogen *Pseudomonas syringae pv. tomato* DC3000 (*Pst*) while *myc2-3* mutant is more resistance to *Pst* which is consistent with the study from Major et al. since the *jazQ* mutant maintains continuous strong defense and the *myc2-3* mutant is JA insensitive (**Major et al., 2017**). Notably, the *myc2-3* mutant lost the phenotype of growth rescued by root microbiota under light suboptimal conditions (both low PAR and end of day far red-light treatment) (**Figure 32**) suggesting that plant growth rescued by root microbiota under light suboptimal conditions requires *MYC2*.

MYC2, a basic-helix-loop-helix (bHLH) TF, regulates multiple processes in plants (**Major et al., 2017**). Besides modulation of JA signaling, MYC2 is also involved in light signaling and might orchestrate the regulation of plant growth and development by light quality (**Robson et al., 2010**; **Hong et al., 2012**; **Shin et al., 2012**; **Kazan and Manners 2013**). Robson et al. reported that the *myc2* mutant showed an attenuated growth inhibition under continuous far red-light condition suggesting MYC2 is involved in the plant response to far red light (**Robson et al., 2010**). Further study from Hong et al. demonstrated that MYC2 directly binds to promoters of *TPS21* and *TPS11* (the sesquiterpene synthase genes) which are regulated by red light indicating that MYC2 is involved in plant response to light quality (**Hong et al., 2012**). These results together with our results mentioned above suggest MYC2 coordinates a complex network of plant growth in response to light quality and light quantity. Meanwhile, based on the transcriptome data, I observed that the *myc2-3* mutant shoot lost

the ability of sensing the light change which is consistent with above mentioned previous studies (**Robson et al., 2010**; **Hong et al., 2012**) and further indicates MYC2 is involved in plant response to light. Our data proved that the *myc2-3* mutant maintains strong immune response compared with the control line *jin1-8* pMYC2: MYC2-FlAG under LP (**Figure 38**) which explained that root microbiota lost the ability of rescuing plant growth under LP suggesting that LP-dependent down-regulation of microbiota-induced defense in leaves is orchestrated through MYC2 via a cross talk between photoreceptor signaling and defense signaling. Our results suggest that interference of MYC2 (JA signaling pathway) with light, SA/SAR and GA signaling pathways is key to orchestrate investment in shoot growth over shoot defense in LP. In our gene expression network (**Figure 38**), I identified few genes connecting the clusters MDE_S2 (growth cluster) and MDE_S7 (defense cluster). Remarkably, these MDEGs include EDS5 (**Serrano et al., 2013**), a transporter required for SA export from chloroplast and needed for SA signaling (induced in *myc2-3* in LP); AOS (**Sanders et al., 2000**), a key chloroplast enzyme needed for JA biosynthesis (repressed in *myc2-3* in LP); and RGL3 (**Dill and Sun 2001**), a repressor of GA responses (induced in *myc2-3* in LP). As these genes are well-known MYC2 target genes (**Mine et al., 2017**; **Wild et al., 2012**; **von Moerkercke et al., 2019**; **Zander et al., 2020**), it is conceivable that differential regulation of the expression of these genes by MYC2 orchestrates a complex cross talk between JA, SA, and GA to either prioritize microbiota-induced growth or defense according to the surrounding light conditions.

Taken together, our results filled up the previous studies ant further indicate that the root microbiota triggered trade-off between growth and defense modulated by light is in a MYC2-dependent manner. Moreover, the data presented suggest that plant growth and survival in nature likely depends on the ability of these sessile organism to utilize belowground microbial signals to either prioritize growth or defense depending on light quantity/quality perceived by leaves. Therefore, phenotypic plasticity and aboveground stress responses in plants can be modulated by signals from microbial root commensals.

5. Conclusions

I demonstrated that a synthetic root microbiota confers *Arabidopsis* tolerance to LP. I also showed that aboveground light condition modulates root microbiota assembly. Further, I proved that *A. thaliana* responses to root commensals and light are interconnected along the root-shoot axis, thereby allowing prioritization of microbiota-induced growth over defense responses under LP. Moreover, I demonstrated that light and root microbiota modulate plant defense towards pathogens. Through screening 8 mutants impaired in phytohormone-dependent balance between growth and defense, I demonstrated that root microbiota-mediated plant rescue depends on JA biosynthesis and signaling, cryptochromes and BR. Further, I proved that root microbiota-induced canopy size significantly linked with root bacterial community composition. Finally, I demonstrated that priority to microbiota-induced growth over defense under LP requires MYC2.

Based on the results, I provide the hypothetical model explaining the underlying mechanism in the plant growth rescued by root microbiota under LP (**Figure 40**). In the absence of BFO commensals, plants prioritize growth over refence, especially under LP. However, LP restricts both growth and defence responses, leading to small plants that are highly susceptible to leaf pathogens. In the presence of BFO root commensals, extensive activation of immunity response was observed in leaves, thereby effectively protecting leaves against microbial pathogens. However, under LP, root microbiota-induced systemic immune responses in leaves are shut down in a MYC2-dependent manner, thereby giving priority to microbiota-induced growth.

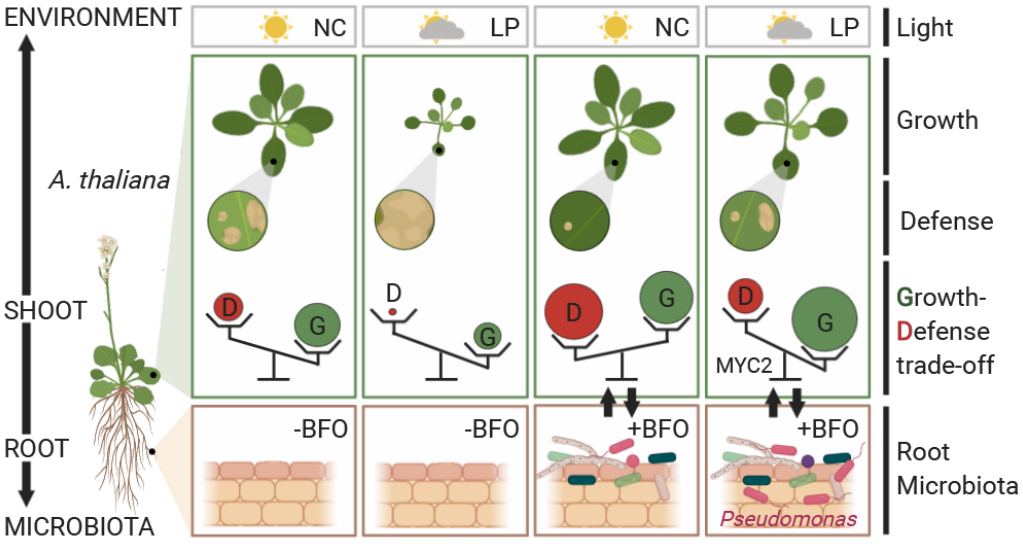

Figure 40. Model for root microbiota-induced growth-defence trade-off between NC and LP. Graphical summary illustrating the bidirectional communication mechanisms along the microbiota-root-shoot-environment axis in *A. thaliana*. In the absence of BFO commensals, plants prioritize growth over defence, especially under LP. However, suboptimal light conditions restrict both growth and defence responses, leading to small plants that are highly susceptible to leaf pathogens. In the presence of BFO root commensals, extensive activation of immunity response was observed in leaves, thereby effectively protecting leaves against microbial pathogens. BFOs also promote growth responses under this condition, which likely compensates the fitness cost associated with this elevated immune status. Under suboptimal light conditions, root microbiota-induced systemic immune responses in leaves are shut down in a MYC2-dependent manner, thereby giving priority to microbiota-induced growth. However, although these plants massively invest into shoot growth in LP, they remain more resistant to leaf pathogens than corresponding germ-free control plants.

6. MATERIALS AND METHODS

6.1 Experimental model

6.1.1 Microbial strains

The bacterial strains used in this study have been previously reported (**Bai et al., 2015**) and are summarized in Chapter I. The fungal and oomycetal strains used in this study are outlined in Chapter I already. *Pseudomonas syringae* pv. *tomato* DC 3000 strain used in this study was a gift from Dr. Jane Parker's laboratory (MPIPZ, Cologne, Germany) and have been described before (**Buell et al., 2003**). *Botrytis cinerea* B05.10 strain used in this study was a gift from Dr. Rainer P. Birkenbihl and have already been reported (**Staats et al., 2012**).

6.1.2 *A. thaliana* strains

A. thaliana Col-0 wild-type (N60000) was obtained from the Nottingham Arabidopsis Stock Centre (NASC). *dellaP* (the *della* pentuple mutant) was generated by crossing *ga-28*, *rgl1-SK62*, *rgl2-SK54*, *rgl3-3*, and introgressed *gai-t6* and have been previously reported (**Park et al., 2013**). *jazQ* mutant was generated by transferring DNA (T-DNA) insertion mutants of *jaz1-2*, *jaz3-4*, *jaz4-1*, *jaz9-4* and *jaz10-1*and have been described (**Campos et al., 2016**). Mutant lines *myc2-3* (**Shin et al., 2012**), mutant *myc234* line (**Fernandez-Calvo et al., 2011**) and line *jin1-8* pMYC2:MYC2-FLAG (**Hou et al., 2010**) were obtained from Dr. Jane Parker's laboratory (MPIPZ, Cologne, Germany). Mutant lines *dde2-2* (**von Malek et al., 2002**) and s*id2-2* (**Wildermuth et al., 2001**) were obtained from Dr. Kenichi Tsuda's laboratory (MPIPZ, Cologne, Germany). Mutant lines *bri1-301* and *sav3-3* were gifts from Dr. Youssef Belkhadir's laboratory (GMI, Vienna, Austria). Mutant line *cry1-304 cry2-1* (**Mockler et al., 1999**) was provided by Dr. Zhoubo Hu (Geneva University, Switerland).

6.1.3 Culture conditions for microbial strains in vitro

Bacterial strains were stored in 30% glycerol at −80°C and routinely cultured at 20°C in liquid 50% TSB media

(Sigma-Aldrich, USA). Fungal strains were cultured at 20°C in solid PGA media (Sigma-Aldrich, USA) and agar plugs with mycelia were stored in 30% glycerol at −80°C. Oomycetal strains were continuously propagated in solid PGA media. *Pseudomonas syringae* pv. *tomato* DC 3000 strain was stored in 7% Dimethyl sulfoxide (DMSO) at −80°C. *Botrytis cinerea* B05.10 strain spores were stocked at -80°C at a concentration of 10^7 spores mL^{-1} in Vogelbuffer (in 1L: 15 g sucrose, 3 g Na-citrate, 5 g K_2HPO_4, 0.2 g $MgSO_4$ $7H_2O$, 0.1 g $CaCl_2$ $2H_2O$, 2 g NH_4NO_3).

6.1.4 *Arabidopsis* growth condition

Seeds were surface-sterilized in 70% ethanol for 18 min followed by a brief wash with 100% ethanol (1 min). Seeds were dried out under sterile bench and were incubated for two days at 4°C in the dark. Individual seeds were sown onto the surface of FlowPots by pipetting one seed at a time. FlowPots containing seeds were inoculated with half-strength Murashige and Skoog (MS) medium without sucrose (pH 5.5). Combiness boxes containing FlowPots with plants (Kremer et al., 2018) were incubated under short-day conditions at 21°C with two light intensity (NC: PPFD 61.24, LP: PPFD 43.32) (10 hr) and at 19°C in the dark (14 hr).

6.2 Method Details

6.2.1 Microbiota reconstitution experiments in the FlowPot system

Bacterial strains were cultivated from glycerol stock (pellets of bacterial colonies stored in 50% glycerol at −80°C) in deepwell 96-well- plates containing 400 µl of 50% TSB (Tryptic Soy Broth, Sigma) with 180 rpm shaking speed for seven days at 25°C and subsequently pooled (in equal ratios). This bacterial pool was centrifuged at 4,000 xg for 10 min and re-suspended in 10 mM $MgCl_2$ to remove residual media and bacteria-derived metabolites. Prior to inoculation, OD600 was adjusted to 0.5. Fungal individual strains were cultivated from their glycerol stocks (pieces of fungal mycelium stored in 30% glycerol stock at −80°C) in PGA (Potato Glucose Agar, Sigma-Aldrich) for fourteen days. 100 mg mycelium per stain was harvested into 2 ml Eppendorf tube containing 1 ml $MgCl_2$ and one sterile stainless-steel bead (3.2 mm) using sterile tips. Mycelium were subsequently crushed with a paint shaker (SK450, Fast & Fluid Management, Sassenheim, Netherlands) for 10 min and pooled with equal volume. Oomycetal strains were cultured from PGA stock individually in new PGA

plates for fourteen days and treated as described for fungal strains. Procedures of setting up the gnotobiotic FlowPot system were carried out as previously described (**Kremer et al., 2018**; **Durán et al., 2018**).

For experiments of clarifying the initial difference in relative abundance among bacterial, fungal and oomycetal groups did not affect output root microbiota assembly and plant growth five weeks post inoculation, each group was designed two levels: high level and low level. High levels of bacteria, fungi and oomycetes are 2 ml bacterial liquid (OD600 = 0.5), 100 mg fungal mycelium and 40 mg oomycetal mycelium. Low levels of each group were diluted 10 times from high levels (0.2 ml bacterial liquid, 10 mg fungal mycelium and 40 mg oomycetal mycelium in 50 ml 1/2 MS separately). Eight possible combinations of bacteria-fungi-oomycetes relative abundance were then assembled and used to repopulate sterile matrix in the FlowPot system. For other microbiota reconstitution experiments, 50 ml 1/2 MS contained 0.2 ml bacterial liquid (OD600 = 0.5), 10 mg fungal mycelium and 40 mg oomycetal mycelium.

After microbial inoculation, sterile *A. thaliana* seeds described as before were sown on the surface of the matrix (10 seeds per pot). Then the closed boxes were incubated at 21°C, for 10 hours with different light conditions (NC: PPFD 61.24, LP: PPFD 43.32) at 19°C and 14 hours in the dark. After one-week incubation, redundant seedlings were pulled under sterile bench and three seedlings per pot were left. Then the closed boxes were continually incubated at the same condition described above for another four weeks.

After incubation, plant shoots were cut for plant observation described following. For community profiling, plant roots were thoroughly washed with sterile Milli-Q water and dried with sterilized Whatman glass microfiber filters (GE Healthcare Life Sciences). Meanwhile, matrix samples (only substrate in the pot without plant roots) were taken (around 0.5 ml volume of matrix per pot). Then plant roots and matrix were transferred into individual lysing matrix E tubes (MP Biomedicals), frozen in liquid nitrogen and stored at −80°C.

6.2.2 Plant observations

To quantify plant growth and plant phenotype, first individual plant shoot was cut and measured shoot fresh weight. Then individual plant shoot was adhered to white paper using Polyester, non-sterile film (VMR, USA) and scanned for following parameters. Canopy size, petiole length of each leaf, the ratio of each leaf length to

width and leaf numbers of each plant were conducted using Fiji (**Schindelin et al., 2012**).

6.2.3 Microbial community profiling

The aforementioned samples of matrix and roots were harvested in a 2 ml tube with screw lip separately were crashed using the Precellys®24 tissue lyzer (Bertin Technologies, Montigny-le-Bretonneux, France). For matrix samples, 978 µl SPB (Sodium Phosphate Buffer) with 122 µl MT-Buffer were added to each tube. The tubes were crashed (Nr. 5) 1×30 sec. For root samples, the tubes were crashed (Nr. 5) 1×30 sec fist and then added 978 µl SPB (Sodium Phosphate Buffer) with 122 µl MT-Buffer. The tubes with buffer were crashed again (Nr. 5) 1×30 sec. All the tubes were centrifuge 15 minutes at 14000×g (rcf). Then all samples of matrixes and roots were performed DNA isolation using the FastDNA® SPIN for soil kit (MP Biomedicals, Solon, USA).

After DNA isolation, the concentration of sample DNA was measured by PicoGreen method. First 1×TE Buffer was prepared. Then the dye of PicoGreen was added into 1×TE Buffer (PicoGreen: Pico Working Solution=1:200), mixed, this was the working Pico solution. 40 µl working Pico solution was added into QPCR plate wells. 4 µl DNA sample was added to the well. The fluorescence of samples was measured by QPCR machine (IQ5 real-time PCR Thermocycler, Biorad, Munich, Germany). The procedure of QPCR was 30 sec at 25 °C, 3x30 seconds at 25 °C for measuring fluorescence, 30 seconds at 15 °C. Finally, all of samples DNA were adjusted to 3.5 ng/µl.

Sample library preparation started with two steps of PCR for bacteria, fungi and oomycetes separately. For bacteria, the first step PCR used 25 cycles with primer V5-V6 (799F/1192R). For fungi, the first step PCR used 25 cycles with primer ITS1 (ITS1F/ITS2). For oomycetes, the first step PCR used 25 cycles with primer ITS1 (ITS1-O/5.8s-O-Rev). The first step PCR in total contains 25 µL containing 3 µL sample DNA, 1x incomplete reaction buffer, 1.25 U DFS-Taq DNA Polymerase, 2 mM of MgCl2, 0.3 % BSA, 200 µM of dNTPs and 400 nM of each primer. The procedure of PCR was 94 °C for 2 minutes, 94 °C for 30 seconds, 55 °C for 30 seconds, 72 °C for 30 seconds and 72 °C for 10 minutes in total 25 cycles. After the first step PCR, digestion was conducted to remove the enzyme and primers in the first step PCR. For digestion step, a mixture of 1 µl Antarctic phosphatase, 1 µl Exonuclease I and 2.44 µl Antarctic phosphatase buffer was added to 20 µl of the pooled first step PCR product. The procedure of digestion was 37 °C for 30 minutes and 85 °C for 15 minutes. After the

digestion, 3 µl liquid was taken as the sample for the second step PCR. The second step PCR was used the same PCR mixture solution except primers that barcode primes including barcodes and Illumina adaptors (B5-barcodes for bacteria, Ft-barcodes for fungi, Ot-barcodes for oomycetes). The procedure of second step PCR was 94 °C for 2 minutes, 94 °C for 30 seconds, 55 °C for 30 seconds, 72 °C for 30 seconds and 72 °C for 10 minutes in total 10 cycles.

After two steps PCR, 5 µl PCR product was mixed with 5 µl 6×Orange G DNA Loading Dye for each sample. Then the mixture mixed with 5 µL of Gel Loading Dye (Orange G, 6X, Sigma, Hamburg, Germany) was run on the 1 % agarose gel with TAE to check the DNA bind. After control gel checking, for bacteria, all PCR product (around 70 µL) was mixted with 20 µL Gel Loading Dye (Orange G) and run on a 1.5 % agarose gel for 2 hours at 80 V. Bands with the 500 bp size were cut and purified using the QIAquick gel extraction kit (Qiagen, Hilden, Germany). After gel extraction, DNA concentration was measured using the PicoGreen method as described already. For fungi and oomycetes, the purification was used Agencourt AMPure XP-PCR Purification (AMPure XP-PCR Purification, Beckman Coulter, Krefeld, Germany). The pure DNA samples concentration was measure by the PicoGreen method described before. For each kingdom (bacteria, fungi and oomycetes), 30 ng DNA of each sample was mixed. Then for each kingdom, the mixture was purified with Agencourt AMPure XP-PCR Purification (AMPure XP-PCR Purification, Beckman Coulter, Krefeld, Germany) twice. The DNA concentration was measured by the Quantus™ Fluorometer (Promega, Manheim, Germany). 100 ng DNA from bacteria, fungi and oomycetes was mixed. The mixture DNA concentration was measure by the Quantus™ Fluorometer (Promega, Manheim, Germany).

Finally, paired-end Illumina DNA sequencing was performed using the Illumina MiSeq system at the Department of Plant-Microbe Interactions, Max Planck Institute for Plant Breeding Research.

6.2.4 16S rRNA and ITS read processing

Paired amplicon sequencing reads were joined using Qiime (join_paired_reads, Caporaso et al. 2010). In case of ITS reads, for un-joined read pairs all forward reads where retained for demultiplexing. Demultiplexing and quality filtering was done using Qiime (split_libraries_fastq, phred=30). All quality filtered and demultiplexed reads were trimmed to an equal length. Reference sequences were obtained from all used Strains (Bacteria = xx,

Fungi=xx, Oomycetes=XX, see Table XX) using respective resources of sequenced genomes if available. Reference sequences were then trimmed to contain only the amplified region. Trimmed reference sequences that were 100% identical, were grouped in so called strain variants. This led to xx bacterial, xx fungal and xx oomycetal strain variant sequences. Reference sequences of strain variants were mapped against all trimmed amplicon reads using usearch (Edgar et al. 2010), allowing one mismatch (usearch –usearch_global, with max diff = 1). Unmapped reads were discarded. Count tables were made from these mapping results.

6.2.5 Microbial community profile statistical analysis

To calculate alpha diversity indices, count tables were rarefied to 1000 reads. Significant differences were determined by an ANOVA and post-hoc Tukey test ($p<0.05$). Distance matrices were calculated by using a normalized count table (CSS, Paulson et al, 2013) as an input for Bray Curtis distance calculation. These distance tables were used as an input for constrained principal coordinate analysis (CPCoA, capscale function in R) and partial least square discriminant analysis (PLSDA). The condition function was used to correct for batch effects and when applicable for treatments (LP/NC) when performing CPCoA,

To determine differences in abundance across all experiments for individual strains, relative abundances were rescaled to be in range from 0 to 1. For this read counts per sample were transformed to relative abundances by division by total sum of reads per sample. Then for all samples belonging to one experiment, RA of each individual strain variant across desired samples to analyze (e.g. only root samples, only wt and mutant samples) were rescaled using this general equation $x-(\min(x))/(\max(x)-\min(x))$, where x represents all RA values per strain variant from one experiment. Strain variants that where not consistently found across samples were discarded from downstream analysis. Rescaled abundances were used to calculate LP/NC ratios, whereas means were calculated across all samples from all experiments. Significance of differences in standard RA and re-scaled RA were tested using the Wilcoxon rank sum test ($p<=0.05$).

To find possible correlation of LP/NC ratios of individual strain variants with phenotype effects (?), mean ratios per mutant were calculated (mean of each experiment first, then mean across all experiments). Same was done for values of canopy size, Bt growth and Pst growth. Mean values were then tested for correlation using spearman correlation ($p<0.05$, fdr corrected).

6.2.6 Transcriptome sequencing experiments

A. thaliana col-0, *myc2-3* and *jin1-8* pMYC2:MYC2-FLAG plants growing in the FlowPot system under NC/ LP conditions as described before were harvested after 5 weeks -BFO/ +BFO inoculation. A. thaliana col-0, *myc2-3* and *jin1-8* pMYC2:MYC2-FLAG shoots and roots were harvested separately under laboratory conditions at 10 am. Root samples were washed quickly to remove the matrix attached on the roots using 10% RNAlater (Qiagen, Valencia, CA) in 1X PBS as the capture buffer to mitigate RNA degradation. Total RNA from all samples were extracted using the RNeasy® Plant Mini Kit (Qiagen, Germany). RNA-seq libraries were prepared and sequenced at the Max Planck Genome Centre (Cologne, Germany) with an Illumina HiSeq2500.

6.2.7 Transcriptome sequencing data analysis

The FastQC suite (http://www.bioinformatics.babraham.ac.uk/projects/fastqc/) was performed to check the quality of the sequenced reads. Subsequently, the RNA-seq reads were mapped to the annotated genome of *A. thaliana* (TAIR10) using Tophat2 (**Kim et al., 2013**, tophat2 -p 20 -a 10 -g 10) with Bowtie2 (**Langmead et al., 2012**) building genome index. The mapped RNA-seq reads were subsequently transformed into a fragment count per gene per sample using the htseq-count script (s=reverse, t=exon) in the package HTSeq (**Anders et al., 2015**). Count tables of col-0 samples were concatenated to one count matrix. Count tables of *myc2-3* and *jin1-8* pMYC2:MYC2-FLAG samples were concatenated to one count matrix. To normalize count data, raw counts first were calculated normalization factor via TMM-normalization. Then the genes with more than 100 counts were extracted. The extracted TMM-normalized count data were transformed to log2cpm via voom function in limma package (**Ritchie et al., 2015**) in R (**R version 3.6.3**). Subsequently, log2cpm data were used to calculate log2 fold changes and p-values (F-test) for individual comparisons. Resulting p-values were adjusted for false discoveries (FDR) due to multiple hypotheses testing via the Benjamini-Hochberg procedure. To identify significant different expression genes, a threshold of $|\log2FC| \geq 1$ and $FDR < 0.05$ was applied. Heatmaps of significantly regulated genes expression profiles were generated using pheatmap package (**Kolde 2015**) in R. The Euclidean distance was used to show the distance among clustering rows. The values in heatmaps were scaled by row. Gene Ontology (GO) enrichment analysis was conducted by enrichGO function in clusterProfiler package (**Yu et al., 2012**) in R. Biological Process (BP) and 0.05 p-values cutoff were chosen.

P-values were adjusted via the Benjamini-Hochberg method.

6.2.8 Pathogen inoculation and symptom quantification

For *Botrytis cinerea* B05.10 inoculation of *Arabidopsis* plants, the spores were diluted in Vogelbuffer (in 1 L: 15 g of Suc, 3 g of Na-citrate, 5 g of K_2HPO_4, 0.2 g of $MgSO_4 \cdot 7H_2O$, 0.1 g of $CaCl_2 \cdot 2H_2O$, and 2 g of NH_4NO_3) to 5×10^5 spores mL^{-1}. For droplet inoculations, 2 µl droplets containing $1x10^3$ spores were applied to each leaves of four weeks-old *A. thaliana* grown in the presence/absence of the BFO SynCom under either NC or LP. The entire infection processes were conducted under sterile clean bench. After plant leaves five days post pathogen inoculation in the FlowPot system, plant shoots were washed using Milli-Q water twice and dried with sterilized Whatman glass microfiber filters (GE Healthcare Life Sciences). Surface sterile plant shoots were weighted and put into 2 mL sterile Eppendorf tubes for DNA extraction. For quantification of fungal growth, DNA from plant shoot was extracted using Kit. The relative amounts of B. cinerea and Arabidopsis DNA were determined by qPCR employing specific primers for cutinase A and SKII, respectively.

Pseudomonas syringae DC3000 inoculation was carried out by spaying *Pst* at 0.2 OD in 10 mM $MgCl_2$ on *A. thaliana* leaves of four weeks-old A. thaliana grown in the presence/absence of the BFO SynCom under either NC or LP. The entire infection processes were conducted under sterile clean bench. After plant leaves five days post pathogen inoculation in the FlowPot system, plant shoots were washed using 70% EtOH once and Milli-Q water twice. Plant shoots were dried with sterilized Whatman glass microfiber filters and weighted under sterile clean bench. Then plant shoots were put into 2 mL sterile Eppendorf tubes containing 1.5 mL 10 mM MgCl2/0.01% Silwet. Tubes were shaken with 650 rpm for 1 h at 28°C. For colony counting, 20 µl dilution series (10^{-1}, 10^{-2}, 10^{-3}, 10^{-4}, 10^{-5} with 10 mM $MgCl_2$) spot on NYGA plate, counting colonies after two days incubation at 28 °C.

6.2.9 Figures and Statistical Analysis

Data collection and analysis were performed blinded to conditions in all experiments. All figures and all statistical analyses were performed using the R environment (**R version 3.6.3**).

References

Achard, P., and Genschik, P. (2009). Releasing the brakes of plant growth: how GAs shutdown DELLA proteins. *J. Exp. Bot*. 60, 1085–1092. doi: 10.1093/jxb/ern301

Achard, P., Gong, F., Cheminant, S., Alioua, M., Hedden, P., and Genschik, P. (2008). The cold-inducible CBF1 factor-dependent signaling pathway modulates the accumulation of the growth-repressing DELLA proteins via its effect on gibberellin metabolism. *Plant Cell* 20, 2117–2129. doi: 10.1105/tpc.108.058941

Achkar NP, Cho SK, Poulsen C, Arce AL, Re DA, Giudicatti AJ, Karayekov E, Ryu MY, Choi SW, Harholt J, Casal J. J. (2018). A quick HYL1-dependent reactivation of microRNA production is required for a proper developmental response after extended periods of light deprivation. *Dev Cell* 46:236–247.

Acuña-Rodríguez, I.S., Newsham, K.K., Gundel, P.E., Torres-Díaz, C. and Molina-Montenegro, M.A. (2020), Functional roles of microbial symbionts in plant cold tolerance. *Ecol Lett*, 23: 1034-1048. doi:10.1111/ele.13502

Anders S, Pyl PT, Huber W. (2015). HTSeq--a Python framework to work with high-throughput sequencing data. *Bioinformatics* 31(2):166-169. doi:10.1093/bioinformatics/btu638.

Aroca, R., Porcel, R. and Ruiz-Lozano, J.M. (2007), How does arbuscular mycorrhizal symbiosis regulate root hydraulic properties and plasma membrane aquaporins in Phaseolus vulgaris under drought, cold or salinity stresses?. *New Phytologist*, 173: 808-816. doi:10.1111/j.1469-8137.2006.01961.x

Bai, Y., Müller, D., Srinivas, G. et al. (2015). Functional overlap of the Arabidopsis leaf and root microbiota. *Nature* 528, 364–369. https://doi.org/10.1038/nature16192.

Bailey-Serres J, Pierik R, Ruban A, Wingler A (2018) The dynamic plant: capture, transformation, and management of energy. *Plant Physiol* 176:961–966. https://doi.org/10.1104/pp.18.00041

Ballaré C.L. (2014) Light regulation of plant defense. *Annual Review of Plant Biology* **65**, 335–363.

Barka A. E., Nowak, J. & Clément, C. (2006). Enhancement of Chilling Resistance of Inoculated Grapevine Plantlets with a Plant Growth-Promoting Rhizobacterium, Burkholderia phytofirmans Strain PsJN. *Appl. Environ. Microbiol*. 72, 7246 LP – 7252.

Beattie G. A., Hatfield B. M., Dong H., McGrane R. S. (2018). Seeing the Light: The Roles of Red- and Blue-Light Sensing in Plant Microbes. *Annual Review of Phytopathology*. 56:1, 41-66

Berendsen, R.L., Vismans, G., Yu, K. *et al.* (2018). Disease-induced assemblage of a plant-beneficial bacterial consortium. *ISME J* **12,** 1496–1507. https://doi.org/10.1038/s41396-018-0093-1

Brown, J. H., Gillooly, J. F., Allen, A. P., Savage, V. M. & West, G. B. (2004). Toward a metabolic theory of ecology. Ecology 85, 1771–1789.

Buell, C.R. et al. (2003). The complete genome sequence of the Arabidopsis and tomato pathogen Pseudomonas syringae pv. tomato DC3000. *Proc. Natl. Acad. Sci*. USA 100, 10181–10186.

Campos M.L., Yoshida Y., Major I.T., de Oliveira Ferreira D., Weraduwage S.M., Froehlich J.E., … Howe G.A. (2016). Rewiring of jasmonate and phytochrome B signalling uncouples plant growth-defense tradeoffs. *Nature Communications* 7, 12570125.

Campos, M., Yoshida, Y., Major, I. et al. (2016). Rewiring of jasmonate and phytochrome B signalling uncouples plant growth-defense tradeoffs. *Nat Commun* 7, 12570.

Carrión, V. J., Perez-Jaramillo, J., Cordovez, V., Tracanna, V., de Hollander, M., Ruiz-Buck, D., … Raaijmakers, J. M. (2019). Pathogen-induced activation of disease-suppressive functions in the

endophytic root microbiome. *Science*, *366*(6465), 606 LP – 612. https://doi.org/10.1126/science.aaw9285

Castrillo, G., Teixeira, P., Paredes, S. et al. (2017). Root microbiota drive direct integration of phosphate stress and immunity. *Nature* 543, 513–518. https://doi.org/10.1038/nature21417

Cerrudo I., Caliri-Ortiz M.E., Keller M.M., Degano M.E., Demkura P.V. & Ballaré C.L. (2017) Exploring growth-defense tradeoffs in Arabidopsis. Phytochrome B inactivation requires JAZ10 to suppress plant immunity but not to trigger shade avoidance responses. *Plant, Cell & Environment*

Cerrudo I., Keller M.M., Cargnel M.D., Demkura P.V., Wit M. de, Patitucci M.S., Pierik R., Pieterse C.M., Ballare C.L. (2012). Low red/far-red ratios reduce Arabidopsis resistance to Botrytis cinerea and jasmonate responses via a COI1-JAZ10-dependent, salicylic acid-independent mechanism. *Plant Physiol*, 158, pp. 2042-2052

Chakraborty, M., Gangappa, S.N., Maurya, J.P., Sethi, V., Srivastava, A.K., Singh, A., Dutta, S., Ojha, M., Gupta, N., Sengupta, M., Ram, H. and Chattopadhyay, S. (2019), Functional interrelation of MYC2 and HY5 plays an important role in Arabidopsis seedling development. *Plant J*, 99: 1080-1097. doi:10.1111/tpj.14381

Chen, M., Chory, J., and Fankhauser, C. (2004). *Annu. Rev. Genet*. 38,87–117.

Cheng Y.T., Zhang L., He S.Y. (2019). Plant-Microbe Interactions Facing Environmental Challenge. *Cell Host & Microbe*. Volume 26, Issue 2, 14, Pages 183-192

Chini A., Fonseca S., Fernández G., Adie B., Chico J.M., et al. (2007). The JAZ family of repressors is the missing link in jasmonate signalling. *Nature*, 448, pp. 666-671

Christie JM, Blackwood L, Petersen J, Sullivan S. (2015). Plant flavoprotein photoreceptors. *Plant Cell Physiol*. 56:401-413.

Colebrook, E. H., Thomas, S. G., Phillips, A. L., and Hedden, P. (2014). The role of gibberellin signalling in plant responses to abiotic stress. *J. Exp. Bot.* 217, 67–75. doi: 10.1242/jeb.089938

Cortés L.E., Weldegergis B.T., Boccalandro H.E., Dicke M. & Ballaré C.L. (2016) Trading direct for indirect defense? Phytochrome B inactivation in tomato attenuates direct anti-herbivore defenses whilst enhancing volatile-mediated attraction of predators. *New Phytologist* **212**, 1057–1071.

Cui H. T., Qiu J. D., Zhou Y., et al. (2018). Antagonism of Transcription Factor MYC2 by EDS1/PAD4 Complexes Bolsters Salicylic Acid Defense in Arabidopsis Effector-Triggered Immunity. *Molecular Plant.* Volume 11, Issue 8, Pages 1053-1066

Cui H. T., Tsuda K., and Parker J. E. (2015). Effector-Triggered Immunity: From Pathogen Perception to Robust Defense. *Annual Review of Plant Biology*. Vol. 66:487-511.

Dechesne, A., Wang, G., Gulez, G., Or, D., and Smets, B.F. (2010). Hydration-controlled bacterial motility and dispersal on surfaces. *Proc. Natl. Acad. Sci*. USA 107, 14369–14372.

Degrave, A., Siamer, S., Boureau, T., and Barny, M.-A. (2015). The AvrE superfamily: ancestral type III effectors involved in suppression of pathogen-associated molecular pattern-triggered immunity. *Mol. Plant Pathol*. 16, 899–905.

Deveautour, C., Donn, S., Power, S. A., Bennett, A. E., & Powell, J. R. (2018). Experimentally altered rainfall regimes and host root traits affect grassland arbuscular mycorrhizal fungal communities. *Molecular Ecology*, 27(8), 2152– 2163. https://doi.org/10.1111/mec.14536

Dombrecht B., Xue G.P., Sprague S.J., Kirkegaard J.A., et al. (2007). MYC2 differentially modulates diverse jasmonate-dependent functions in Arabidopsis. *Plant Cell*, 19, pp. 2225-2245

Dubois, P. G., Olsefski, G. T., Flint-Garcia, S., Setter, T. L., Hoekenga, O. A. and Brutnell, T. P. (2010). Physiological and genetic characterization of end-of-day far-red light response in maize seedlings. *Plant physiology*, *154*(1), 173-186.

Durán P., Thiergart T., Garrido-Oter R., Agler M., Kemen E., Schulze-Lefert P., Hacquard S. (2018). Microbial Interkingdom Interactions in Roots Promote Arabidopsis Survival. *Cell*, Volume 175, Issue 4,

Fernandez-Calvo P, Chini A, Fernandez-Barbero G, Chico JM, Gimenez-Ibanez S, Geerinck J, et al. (2011). The Arabidopsis bHLH transcription factors MYC3 and MYC4 are targets of JAZ repressors and act additively with MYC2 in the activation of jasmonate responses. *Plant Cell*;23(2):701–15. Epub 2011/02/22. pmid:21335373; PubMed Central PMCID: PMC3077776.

Fitzpatrick, C.R., Copeland, J., Wang, P.W., Guttman, D.S., Kotanen, P.M. and Johnson, M.T.J. (2018) Assembly and ecological function of the root microbiome across angiosperm plant species. *Proc. Natl Acad. Sci*. U.S.A. 115, E1157–E1165

Franklin K. A., Whitelam G. C. (2005). Phytochromes and Shade-avoidance Responses in Plants. *Annals of Botany*, Volume 96, Issue 2, Pages 169–175, https://doi.org/10.1093/aob/mci165

Franklin, K.A. (2008), Shade avoidance. *New Phytologist*, 179: 930-944. doi:10.1111/j.1469-8137.2008.02507.x

Fung-Uceda J., Lee K., et al. (2018). The Circadian Clock Sets the Time of DNA Replication Licensing to Regulate Growth in Arabidopsis. *Developmental cell*. Volume 45, Issue 1, 9, Pages 101-113.e4

Gangappa, S.N., Prasad, V.B., and Chattopadhyay, S. (2010). Functional interconnection of MYC2 and SPA1 in the photomorphogenic seedling development of Arabidopsis. *Plant Physiol*. 154, 1210–1219.

Garcia-Pichel, F., Loza, V., Marusenko, Y., Mateo, M. P. & Potrafka, R. (2013) Temperature Drives the Continental-Scale Distribution of Key Microbes in Topsoil Communities. *Science* 340, 1574 LP – 1577.

Gendron JM, Pruneda-Paz JL, Doherty CJ, Gross AM, Kang SE, Kay SA. (2012). Arabidopsis circadian clock protein, TOC1, is a DNA-binding transcription factor. *Proceedings of the National Academy of Sciences*, USA 109: 3167– 3172.

Gillooly, J. F., Brown, J. H., West, G. B., Savage, V. M. & Charnov, E. L. (2001) Effects of size and temperature on metabolic rate. *Science* 293, 2248–2251.

Goodspeed D., Cheha E.W. b, Min-Venditti A., Braam J., Covington M.F. (2012). Arabidopsis synchronizes jasmonate-mediated defense with insect circadian behavior. *Proc Natl Acad Sci* USA, 109, pp. 4674-4677

Greenham K, McClung CR. (2015). Integrating circadian dynamics with physiological processes in plants. *Nat Rev Genet* 16: 598–610.

Guo Q., Major I. T., Howe G. A. (2018). Resolution of growth–defense conflict: mechanistic insights from jasmonate signaling. *Current Opinion in Plant Biology*. Volume 44, Pages 72-81

Hacquard S., Garrido-Oter R., González A., Spaepen S., Ackermann G.l, et al. (2015). Microbiota and Host Nutrition across Plant and Animal Kingdoms. *Cell Host & Microbe*, Volume 17, Issue 5, Pages 603-616, ISSN 1931-3128, https://doi.org/10.1016/j.chom.2015.04.009.

Hacquard, S., Kracher, B., Hiruma, K. et al. (2016). Survival trade-offs in plant roots during colonization by closely related beneficial and pathogenic fungi. *Nat Commun* 7, 11362. https://doi.org/10.1038/ncomms11362

Hacquard, S., Spaepen, S., Garrido-Oter, R., & Schulze-Lefert, P. (2017). Interplay Between Innate Immunity and the Plant Microbiota. *Annual Review of Phytopathology*, 55(1), 565–589.

https://doi.org/10.1146/annurev-phyto-080516-035623

Hammoudi V, Fokkens L, Beerens B, Vlachakis G, Chatterjee S, Arroyo-Mateos M, Wackers PF, Jonker MJ, van den Burg HA. (2018). The Arabidopsis SUMO E3 ligase SIZ1 mediates the temperature dependent trade-off between plant immunity and growth. *PLoS Genet*, 14:e1007157.

Harbort C. J., Hashimoto M., Inoue H., et al (2020). Root-Secreted Coumarins and the Microbiota Interact to Improve Iron Nutrition in Arabidopsis. *Cell Host & Microbes*, 28, 1–13. https://doi.org/10.1016/j.chom.2020.09.006

Hatfield J.L., Asrar G., Kanemasu E.T. (1984). Intercepted photosynthetically active radiation estimated by spectral reflectance. *Remote Sensing of Environment*, Volume 14, Issues 1–3, Pages 65-75

Hatfield, J.L., Prueger, J.H. (2015). Temperature extremes: Effect on plant growth and development. *Weather and Climate Extremes*. 10:4-10.

Heinz S, Benner C, Spann N, Bertolino E et al. (2010). Simple Combinations of Lineage-Determining Transcription Factors Prime cis-Regulatory Elements Required for Macrophage and B Cell Identities. *Mol Cell*, May 28;38(4):576-589.

Hinojosa, L, Matanguihan, JB, Murphy, KM. (2019). Effect of high temperature on pollen morphology, plant growth and seed yield in quinoa (*Chenopodium quinoa* Willd.). *J Agro Crop Sci*. ; 205: 33– 45. https://doi.org/10.1111/jac.12302

Hoch, B., and Körner, C. (2003). The carbon charging of pines at the climatic treeline: a global comparison. Oecologia 135, 10–21. doi: 10.1007/s00442-002-1154-7

Hoch, B., and Körner, C. (2009). Growth and carbon relations of tree line forming conifers at constant vs. variable low temperatures. *J. Ecol.* 97, 57–66. doi: 10.1111/j.1365-2745.2008.01447.x

Hoecker, U. (2017). The activities of the E3 ubiquitin ligase COP1/SPA, a key repressor in light signaling. *Current Opinion in Plant Biology*, 37, pp. 63-69.

Hong G. J., Xue X. Y., Mao Y. B., L. Wang J., Chen X. Y. (2012). Arabidopsis MYC2 interacts with DELLA proteins in regulating sesquiterpene synthase gene expression. *Plant Cell*, 24, pp. 2635-2648

Hou X., Lee L.Y.C., Xia K., Yan Y., Yu H. (2010). DELLAs modulate jasmonate signaling via competitive binding to JAZs. *Dev. Cell* 19: 884–894.

Hu, L., Robert, C.A.M., Cadot, S. et al. (2018). Root exudate metabolites drive plant-soil feedbacks on growth and defense by shaping the rhizosphere microbiota. *Nat Commun* 9, 2738. https://doi.org/10.1038/s41467-018-05122-7

Huang W, Pérez-García P, Pokhilko A, Millar AJ, Antoshechkin I, Riechmann JL, Más P. (2012). Mapping the core of the Arabidopsis circadian clock defines the network structure of the oscillator. *Science* 336: 75– 79.

Hubbard, C., Brock, M., van Diepen, L. et al. (2018). The plant circadian clock influences rhizosphere community structure and function. *ISME J* 12, 400–410. https://doi.org/10.1038/ismej.2017.172

Huot B, Castroverde CDM, Velásquez AC, Hubbard E, Pulman JA, Yao J, Childs KL, Tsuda K, Montg omery BL, He SY. (2017) Dual impact of elevated temperature on plant defence and bacterial virulence in Arabidopsis. *Nat Commun* **8**: 1808

Huot B, Yao J, Montgomery BL, He SY. (2014). Growth-defense tradeoffs in plants: a balancing act to optimize fitness. *Mol Plant*. 7(8):1267-1287. doi:10.1093/mp/ssu049

Huot, B., Castroverde, C.D.M., Velásquez, A.C. et al. (2017) Dual impact of elevated temperature on plant defence and bacterial virulence in Arabidopsis. *Nat Commun* 8, 1808.

Jenkins, G. I. (2009). *Annu. Rev. Plant Biol.* 60, 407–431.

Joo, Y, Schuman, MC, Goldberg, JK, Wissgott, A, Kim, S-G, Baldwin, IT. (2019). Herbivory elicits changes in green leaf volatile production via jasmonate signaling and the circadian clock. *Plant Cell Environ*. ; 42: 972– 982. https://doi.org/10.1111/pce.13474

Journot-Catalino N., Somssich I. E., Roby D., Kroj T. (2006). The Transcription Factors WRKY11 and WRKY17 Act as Negative Regulators of Basal Resistance in Arabidopsis thaliana. *The Plant Cell.* Volume: 18, Issue: 11, pages: 3289LP-3302

Kazan K. and Manners J. M. (2013). MYC2: The Master in Action. *Molecular Plant.* Volume 6, Issue 3, May 2013, Pages 686-703

Kazan K., Manners J.M. (2011). The interplay between light and jasmonate signalling during defence and development. *J Exp Bot*, 62, pp. 4087-4100

Kim, D., Pertea, G., Trapnell, C. et al. (2013). TopHat2: accurate alignment of transcriptomes in the presence of insertions, deletions and gene fusions. *Genome Biol* 14, R36 https://doi.org/10.1186/gb-2013-14-4-r36.

Kobayashi, Y., and Weigel, D. (2007). Genes Dev. 21, 2371–2384.

Kolde, R. (2015). pheatmap: Pretty Heatmaps. R package version 1.0. 8 http://CRAN.R-project.org/package=pheatmap.

Kremer et al., (2018). FlowPot axenic plant growth system for microbiota research. *bioRxiv*, 10.1101/254953.

Langmead, B., Salzberg, S. (2012). Fast gapped-read alignment with Bowtie 2. *Nat Methods* 9, 357–359. https://doi.org/10.1038/nmeth.1923.

Li H., Handsaker B., Wysoker A., Fennell T., Ruan J., Homer N., Marth G., Abecasis G., Durbin R. and 1000 Genome Project Data Processing Subgroup (2009) The Sequence alignment/map (SAM) format and SAMtools. Bioinformatics, 25, 2078-9.

Li Z., Liu H., Ding Z., et al. (2020). Low Temperature Enhances Plant Immunity via Salicylic Acid Pathway Genes That Are Repressed by Ethylene. *Plant Physiology*, 182 (1) 626-639; **DOI:** 10.1104/pp.19.01130

Liu, S., Ziegler, J., Zeier, J., Birkenbihl, R. P. and Somssich, I. E. (2017). Botrytis cinerea B05. 10 promotes disease development in Arabidopsis by suppressing WRKY33-mediated host immunity. *Plant, cell & environment*, *40*(10), 2189-2206.

Lomax, B.H., Woodward, F.I., Leitch, I.J., Knight, C.A. and Lake, J.A. (2009), Genome size as a predictor of guard cell length in *Arabidopsis thaliana* is independent of environmental conditions. *New Phytologist*, 181: 311-314. doi:10.1111/j.1469-8137.2008.02700.x

Major, I. T., Yoshida, Y., Campos, M. L., Kapali, G., Xin, X. F., Sugimoto, K., de Oliveira Ferreira, D., He, S. Y., & Howe, G. A. (2017). Regulation of growth-defense balance by the JASMONATE ZIM-DOMAIN (JAZ)-MYC transcriptional module. *The New phytologist*, 215(4), 1533–1547. https://doi.org/10.1111/nph.14638

Mandalari C, Losi A, Gärtner W. (2013). Distance-tree analysis, distribution and co-presence of bilin- and flavin-binding prokaryotic photoreceptors for visible light. Photochem. Photobiol. Sci. 12: 1144–57

Manfre A., Glenn M., Nunez A., Moreau R.A., Dardick C. (2011). Light quantity and photosystem function mediate host susceptibility to Turnip mosaic virus via a salicylic acid-independent mechanism. *Mol Plant Microbe Interact*, 24, pp. 315-327

Martin M (2011). Cutadapt removes adapter sequences from high-throughput sequencing reads. EMBnet Journal 17:10–12. https://doi.org/10.14806/ej.17.1.200.

Mockler, T.C., Guo, H., Yang, H., Duong, H., and Lin, C. (1999). Antagonistic actions of Arabidopsis cryptochromes and phytochrome B in the regulation of floral induction. *Development* 126, 2073–2082.

Molina-Montenegro, M. A., Gallardo-Cerda, J., Flores, T. S. M., and Atala, C. (2012). The trade-off between cold resistance and growth determines the Nothofagus pumilio treeline. *Plant Ecol.* 213, 133–142. doi: 10.1007/s11258-011-9964-5

Mwimba, M., Karapetyan, S., Liu, L. et al. (2018). Daily humidity oscillation regulates the circadian clock to influence plant physiology. *Nature Communication* 9, 4290. https://doi.org/10.1038/s41467-018-06692-2

Nagel DH, Kay SA. (2013). Complexity in the wiring and regulation of plant circadian networks. *Current Biology* 23: 95– 96.

Nakamichi N, Kiba T, Henriques R, Mizuno T, Chua NH, Sakakibara H. (2010). PSEUDO-RESPONSE REGULATORS 9, 7 and 5 are transcriptional repressors in the Arabidopsis circadian clock. *Plant Cell* 22: 594– 605.

Nusinow DA, Helfer A, Hamilton EE, King JJ, Imaizumi T, Schultz TF, Farré EM, Kay SA. (2011). The ELF4-ELF3-LUX complex links the circadian clock to diurnal control of hypocotyl growth. *Nature* 475: 398– 402.

Oldroyd GED, Murray JD, Poole PS, Downie JA. (2011). The rules of engagement in the legume-rhizobial symbiosis. *Annu. Rev. Genet*. 45:119–44.

Panchal S., Chitrakar R., Thompson B. K., et al. (2016). Regulation of Stomatal Defense by Air Relative Humidity. *Plant Physiology*. 172, 3: 2021-2032.

Park J., Nguyen K.T., Park E., Jeon J.S., Choi G. (2013). DELLA Proteins and Their Interacting RING Finger Proteins Repress Gibberellin Responses by Binding to the Promoters of a Subset of Gibberellin-Responsive Genes in Arabidopsis. *The Plant Cell*.

Penfield S. (2008) Temperature perception and signal transduction in plants. *New Phytol.*, 179, pp. 615-628

Ponnu, J., Riedel, T., Penner, E., Schrader, A., & Hoecker, U. (2019). Cryptochrome 2 competes with COP1 substrates to repress COP1 ubiquitin ligase activity during Arabidopsis photomorphogenesis. *Proceedings of the National Academy of Sciences*, 116(52), 27133 LP – 27141. https://doi.org/10.1073/pnas.1909181116

Pruneda-Paz JL, Kay SA. (2010). An expanding universe of circadian networks in higher plants. *Trends in Plant Science* 15: 259– 265.

Pusey PL, Stockwell VO, Mazzola M. (2009). Epiphytic bacteria and yeasts on apple blossoms and their potential as antagonists of Erwinia amylovora. *Phytopathology* 99(5): 571-581

Rasmussen, P. U., Hugerth, L. W., Blanchet, F. G., Andersson, A. F., Lindahl, B. D., & Tack, A. J. M. (2018). Multiscale patterns and drivers of AM fungal communities in the roots and root- associated soil of a wild perennial herb. *New Phytologist*, 222, 1248– 1261. https://doi.org/10.1111/nph.15088

Rasmussen, PU, Bennett, AE, Tack, AJM. (2020) The impact of elevated temperature and drought on the ecology and evolution of plant–soil microbe interactions. *J Ecol*.; 108: 337– 352. https://doi.org/10.1111/1365-2745.13292

Ritchie ME, Phipson B, Wu D, Hu Y, Law CW, Shi W, Smyth GK (2015). "limma powers differential expression analyses for RNA-sequencing and microarray studies." *Nucleic Acids Research*, 43(7), e47. doi: 10.1093/nar/gkv007.

Roberts M.R., Paul N.D. (2006). Seduced by the dark side: integrating molecular and ecological perspectives

on the influence of light on plant defence against pests and pathogens. *New Phytologist,* 170, pp. 677-699

Robson, F., Okamoto, H., Patrick, E., Sue-Re, H., Wasternack, C., Brearley, C., and Turner, J.G. (2010). Jasmonate and phytochrome A signaling in Arabidopsis wound and shade responses are integrated through JAZ1 stability. *Plant Cell.* 22, 1143–1160.

Roden L.C., Ingle R.A. (2009). Lights, rhythms, infection: the role of light and the circadian clock in determining the outcome of plant–pathogen interactions. *Plant Cell*, 21, pp. 2546-2552

Roden L.C., Ingle R.A. (2009). Lights, rhythms, infection: the role of light and the circadian clock in determining the outcome of plant–pathogen interactions. *Plant Cell*, 21, pp. 2546-2552

Saini, G. and Fricke, W. (2020), Photosynthetically active radiation impacts significantly on root and cell hydraulics in barley (*Hordeum vulgare* L.). *Physiol Plantarum,* 170: 357-372. doi:10.1111/ppl.13164

Schindelin, J., Arganda-Carreras, I., Frise, E. et al. (2012) Fiji: an open-source platform for biological-image analysis. *Na*t Methods 9, 676–682.

Schlenker W., Roberts M. J. (2009). Nonlinear temperature effects indicate severe damages to U.S. crop yields under climate change. *Proc. Natl. Acad. Sci.*, 106, pp. 15594-15598

Schmieder R, Edwards R (2011). Quality control and preprocessing of metagenomic datasets. *Bioinformatics* 27:863–864.https://doi.org/10.1093/bioinformatics/btr026.

Selosse M., Bessis A., Pozo M. J., et al. (2014). Microbial priming of plant and animal immunity: symbionts as developmental signals. *Trends in Microbiology*, 22 (11), 607-613, https://doi.org/10.1016/j.tim.2014.07.003.

Sheard L.B., Tan X., Mao H., Withers J., et al. (2010). Jasmonate perception by inositol-phosphate-potentiated COI1-JAZ co-receptor. *Nature*, 468, pp. 400-405

Shi, P., Körner, C., and Hoch, G. (2008). A test of the growth-limitation theory for alpine tree line formation in evergreen and deciduous taxa of the eastern Himalayas. *Funct. Ecol*. 22, 213–220. doi: 10.1111/j.1365-2435.2007.01370.x

Shin J., Heidrich K., Sanchez-Villarreal A., Parker J.E., Davis S.J. (2012). TIME FOR COFFEE represses MYC2 protein accumulation to provide time-of-day regulation of jasmonate signaling. *Plant Cell*, 24, pp. 2470-2482

Shin, J., Heidrich, K., Sanchez-Villarreal, A., Parker, J.E., and Davis, S.J. (2012). TIME FOR COFFEE represses accumulation of the MYC2 transcription factor to provide time-of-day regulation of jasmonate signaling in Arabidopsis. *Plant Cell* 24:2470–2482.

Shin, J., Heidrich, K., Sanchez-Villarreal, A., Parker, J.E., and Davis, S.J. (2012). TI ME FOR COFFEE represses MYC2 protein accumulation to provide time-of-day regulation of jasmonate signaling. *Plant Cell*. 24, 2470–2482.

Smakowska E., Kong J., Busch W. & Belkhadir Y. (2016) Organ-specific regulation of growth-defense tradeoffs by plants. *Current Opinion in Plant Biology* 29, 129–137.

Somers, D. E., and Fujiwara, S. (2009). *Trends Plant Sci*. 14, 206–213.

Staats, M. and van Kan, J.A.L. (2012) Genome update of Botrytis cinerea strains B05.10 and T4. *Eukaryotic Cell,* 11, 1413–1414.

Staley, C., Ferrieri, A.P., Tfaily, M.M. et al. (2017). Diurnal cycling of rhizosphere bacterial communities is associated with shifts in carbon metabolism. *Microbiome* 5, 65 https://doi.org/10.1186/s40168-017-0287-1

Subburaj S, Ha H-J, Jin Y-T et al (2017) Identification of γ-radiation-responsive microRNAs and their target genes in *Tradescantia* (BNL clone 4430). *J Plant Biol* 60:116–128. https://doi.org/10.1007/s12374-016-0433-5

Thiergart, T., Durán, P., Ellis, T. et al. (2020). Root microbiota assembly and adaptive differentiation among European Arabidopsis populations. *Nat Ecol Evol* 4, 122–131. https://doi.org/10.1038/s41559-019-1063-3

Thines B., Katsir L., Melotto M., Niu Y., Mandaokar A., et al. (2007). JAZ repressor proteins are targets of the SCF–COI1 complex during jasmonate signaling. *Nature*, 448, pp. 661-665

Tilbrook K, Arongaus AB, Binkert M, Heijde M, Yin R, Ulm R (2013). The UVR8 UV-B photoreceptor: perception, signaling and response. *Arabidopsis Book*, 11:e0164.

Turck, F., Fornara, F., and Coupland, G. (2008). *Annu. Rev. Plant Biol*. 59, 573–594.

Viczian A, Klose C, Adam E, Nagy F. (2017). New insights of red lightinduced development. *Plant Cell Environ*. http://dx.doi.org/10.1111/pce.12880.

von Malek, B., van der Graaff, E., Schneitz, K., Keller, B. (2002). The Arabidopsis male-sterile mutant dde2-2 is defective in the ALLENE OXIDE SYNTHASE gene encoding one of the key enzymes of the jasmonic acid biosynthesis pathway. *Planta* 216: 187–192.

Walitang, D.I., Kim, C., Kim, K. et al. (2018). The influence of host genotype and salt stress on the seed endophytic community of salt-sensitive and salt-tolerant rice cultivars. *BMC Plant Biol* 18, 51.

Wang W, Wang X, Huang M, Cai J, Zhou Q, Dai T, Cao W, Jiang D (2018) Hydrogen peroxide and abscisic acid mediate salicylic acid-induced freezing tolerance in wheat. Front. Plant Sci. 9

Wang W., Barnaby J.Y., Tada Y., Li H., Tor M., Caldelari D., Lee D.U., Fu X.D., Dong X. (2011). Timing of plant immune responses by a central circadian regulator. *Nature*, 470, pp. 110-114

Wang Y., Bao Z., et al. (2009) Analysis of temperature modulation of plant defense against biotrophic microbes. *Mol Plant Microbe Interact*, 22, pp. 498-506

Wang, C., Cai, X., and Zheng, Z. (2005). High humidity represses Cf-4/Avr4- and Cf-9/Avr9-dependent hypersensitive cell death and defense gene expression. *Planta* 222, 947–956.

Wang, F., Han, T., Song, Q., Ye, W., Song, X., Chu, J., et al. (2020). The Rice Circadian Clock Regulates Tiller Growth and Panicle Development Through Strigolactone Signaling and Sugar Sensing. *The Plant Cell*, 32(10), 3124 LP – 3138. https://doi.org/10.1105/tpc.20.00289

Wang, F., Zhang, L., Chen, X., Wu, X., Xiang, X., Zhou, J., … Zhou, Y. (2019). SlHY5 Integrates Temperature, Light, and Hormone Signaling to Balance Plant Growth and Cold Tolerance. *Plant Physiology*, 179(2), 749 LP – 760. https://doi.org/10.1104/pp.18.01140

Wang, J.; Song, L.; Gong, X.; Xu, J.; Li, M. (2020). Functions of Jasmonic Acid in Plant Regulation and Response to Abiotic Stress. *Int. J. Mol. Sci*., 21, 1446.

Wang, W., Wang, X., Zhang, X. *et al.* (2020). Involvement of salicylic acid in cold priming-induced freezing tolerance in wheat plants. *Plant Growth Regul* . https://doi.org/10.1007/s10725-020-00671-8

Wasternack C. (2007). Jasmonates, an update on biosynthesis, signal transduction and action in plant stress response, growth and development. *Ann. Bot*, 100, pp. 681-697

Wasternack C., Kombrink E. (2010). Jasmonates, structural requirements for lipid-derived signals active in plant stress responses and development. *ACS Chem. Biol*, 5, pp. 63-77

Wildermuth, M.C., Dewdney, J., Wu, G., Ausubel, F.M. (2001). Isochorismate synthase is required to synthesize salicylic acid for plant defence. *Nature* 414: 562–565.

Wu L., Yang H.Q. (2010). CRYPTOCHROME 1 is implicated in promoting R protein-mediated plant resistance to Pseudomonas syringae in Arabidopsis. *Mol Plant*, 3, pp. 539-548

Xin, X.-F., Nomura, K., Aung, K., Vela´ squez, A.C., Yao, J., Boutrot, F., Chang, J.H., Zipfel, C., and He, S.Y. (2016). Bacteria establish an aqueous living space in plants crucial for virulence. *Nature* 539, 524–529.

Xin, X., Nomura, K., Aung, K. et al. (2016). Bacteria establish an aqueous living space in plants crucial for virulence. *Nature* 539, 524–529. https://doi.org/10.1038/nature20166

Xu, H., Liu, Q., Yao, T., and Fu, X. (2014). Shedding light on integrative GA signaling. *Curr. Opin. Plant Biol.* 21, 89–95. doi: 10.1016/j.pbi.2014.06.010

Yan Y., Stolz S., Chételat A., Reymond P., et al. (2007). A downstream Mediator in the growth repression limb of the jasmonate pathway. *Plant Cell*, 19, pp. 2470-2483

Yang S.H., Hua J. (2004) A haplotype-specific Resistance gene regulated by BONZAI1 mediates temperature-dependent growth control in Arabidopsis. *Plant Cell*, 16, pp. 1060-1071

Yu G, Wang L, Han Y, He Q (2012). "clusterProfiler: an R package for comparing biological themes among gene clusters." OMICS: *A Journal of Integrative Biology*, 16(5), 284-287. doi: 10.1089/omi.2011.0118.

Zhang, C., Gao, M., Seitz, N.C. *et al.* (2019). LUX ARRHYTHMO mediates crosstalk between the circadian clock and defense in Arabidopsis. *Nat Commun* **10,** 2543. https://doi.org/10.1038/s41467-019-10485-6

Zhang, N., Meng, Y., Li, X., Zhou, Y., Ma, L., Fu, L., … Xiong, Y. (2019). Metabolite-mediated TOR signaling regulates the circadian clock in Arabidopsis. *Proceedings of the National Academy of Sciences*, 116(51), 25395 LP – 25397. https://doi.org/10.1073/pnas.1913095116

Zheng, M., Wang, Y., Liu, K., Shu, H., and Zhou, Z. (2012). Protein expression changes during cotton fiber elongation in response to low temperature stress. *J. Plant Physiol.* 169, 399–409. doi: 10.1016/j.jplph.2011.09.014

Zhou, J., Deng, Y., Shen, L. et al. (2016) Temperature mediates continental-scale diversity of microbes in forest soils. Nat Commun 7, 12083. https://doi.org/10.1038/ncomms12083

Zhu, D., Maier, A., Lee, J. H., Laubinger, S., Saijo, Y., Wang, H., Qu, L. J., Hoecker, U., and Deng, X. W. (2008). Biochemical Characterization of *Arabidopsis* Complexes Containing CONSTITUTIVELY PHOTOMORPHOGENIC1 and SUPPRESSOR OF PHYA Proteins in Light Control of Plant Development. *Plant Cell* 20, 2307–2323.

Zuther, E, Schaarschmidt, S, Fischer, A, et al. (2019). Molecular signatures associated with increased freezing tolerance due to low temperature memory in *Arabidopsis*. *Plant Cell Environ*. ; 42: 854– 873. https://doi.org/10.1111/pce.13502

Abbreviations

%	percent
:	to
~	approximately
<	less than
>	more than
®	registered trademark
°C	degrees Celsius
µM	micrometers
‰	permille
A. alpina	Arabis alpina
ABC	ATP-binding cassette transporter
AHL	N-acyl-l-homoserine lactone
Al	Aluminum
AMP	Arbuscular Mycorrhizal Fungi
Amp	ampicillin
As	Arsenic
B	bacteria
B	Boron
bbh	best blast hit
Be	Beryllium
bp	base pairs
BSA	bovine serum albumin
C	Comamonadaceae
Ca	Calcium (mg/kg)
Ca	Calcium
CAS	Cologne agricultural soil
Cd	Cadmium
c-di-GMP	cyclic diguanylate
CFUs	colony forming units
CFUs	Cytophaga-Flavobacterium
cm	centimeters
Co	Cobalt
CO_2	carbon dioxide
Col	Arabidopsis thaliana ecotype Columbia
Cq	quantification cycle
Cr	Chromium
Cs	Cesium
	Consejo Superior de Investigaciones Científicas
CSIC-CNB	*Centro Nacional de Biotecnología*

CSS	cumulative –sum scaling
Cu	Copper (mg/kg)
Cu	Copper
CxG	ClimatexGenotype
DF	dilution factor
DNA	Deoxyribonucleic acid
dNTP	desoxynucleotide
Dr.	doctor
e.g.	for example
EDTA	ethylendiaminetetraacetic acid
et al.	and colleagues
etc.	etcetera
F	fungi
FDR	false discovery rate
Fe	Iron (mg/kg)
Fe	Iron
g	grams
h	hour
H_2O	water/Dihydrogen oxide
i.e.	that is
INRA	Institut national de la recherche agronomique
iTOL	interactive tree of life
ITS	internal transcribed spacer
K	Potassium (mg/kg)
K	Potassium
KCl	Potassium chloride
kg	kilogram
KH_2PO_4	Monopotassium phosphate
Kn	kanamycin
L	liter
LP	Low PAR - photosynthetically active radiation
Li	Lithium
lmol m^2s^{-1}	light intensity measurement
max.	maximum
MES	2-(N-morpholino)ethanesulfonic acid
MF	microbe-free
Mg	Magnesium (mg/kg)
mg	miligrams
$MgCl_2$	magnesium chloride
min	minutes
mL	milliliters
mm	millimeters

Mn	Manganesium (mg/kg)
Mn	Manganese
Mo	Molybdenum
MPIPZ	Max Planck Institut fuer Pflanzenzuechtung Forschung
MS	Murashige and Skoog
Mya	million years ago
N.A	not available
Na	Sodium
Na_2HPO_4	Sodium phosphate dibasic
NaCl	Sodium chloride
NaClO	sodium hypochlorite
NC	Normal condition
NCBI	National Center for Biotechnology Information
ng	nanograms
NGS	next-generation sequencing
Ni	Nickel
nM	nanomol
NO_3	Nitrate (mg/kg)
O	oomycetes
OD	optical density
OTUs	operational taxonomic units
P	Phosphorous (mg/kg)
P	Pseudomonadaceae
P	Phosphorus
p.adj.method	p-value adjustment
PAR	photosynthetically active radiation
Pb	Lead
PBS	phosphate buffered saline
PCoA	Principal Coordinates Analysis
PCR	polymerase chain reaction
pep1	perpetual flowering 1
PERMANOVA	Permutational analysis of variance
PERT1	perturbation experiment 1
PERT1.2	perturbation experiment 1.2
PERT2	perturbation experiment 2
PERT3	perturbation experiment 3
PGA	Potato glucose agar
pH	negative decimal logarithm of H+ concentration
Prof.	Professor
pv.	pathovar
PyNAST	Python Nearest Alignment Space Termination
QIIME	quantitative insights into microbial ecology

qPCR	quantitative PCR
R	Coefficient of determination
R	reverse
RA	relative abundance
Rb	Rubidium
RDP	Ribosomal Database Project
Rimf	rifampicine
RP	Rhizoplane
rpm	Revolutions per minute
rRNA	ribosomal ribonucleic acid
RS	Rhizosphere
S	Sulfur
Se	Selenium
sec	seconds
SEM	scanning-electron microscopy
sp.	species (singular)
spp.	species (plural)
Sr	Strontium
Strep	stretomycin
SynCom/SC	synthetic community
Taq	Thermophilus aquaticus
Tc	tetracycline
TCUs	Taxonomic Community Units
TE	Tris-EDTA
TM	trademark
Tris	tris-(hydroxymethyl)-aminomethan
TSA	tryptic soy broth
U	units
UNITE	User-friendly Nordic ITS Ectomycorrhiza Database
V	volt
V	Vanadium
VOCs	Volatile Organic Compounds
w	watts
WGA	Wheat Germ Agglutinin
xg	times gravity
Zn	Zinc

Acknowledgement

I would like to thank everyone helping me finish my thesis.

I would like to thank my official supervisor Prof. Dr. Paul Schulze-Lefert for providing me this opportunity to study in the department of plant-microbe interactions at MPIPZ.

I would like to thank my direct supervisor Dr. Stéphane Hacquard for patient guidance and supervision. During four years' studies, I encountered numerous failures and difficulties in experiments especially at the beginning stage of my projects. Every time a failure or difficulty, I always could get helpful suggestions and encouragement from him. Without him, I could not finish my projects. Meanwhile, I learnt a lot during last four years under his supervision. He provided me many opportunities to learn experimental methods, RNAseq data analysis, and microbial profiling data analysis. He supported me to be a speaker in two international conferences. He helped me to improve my presentation one by one.

I would like to thank my thesis advisory committee members Dr. Kenichi Tsuda and Prof. Dr. Maria von Korff Schmising for helpful guidance.

I would like to thank all colleagues helping me. I would like to thank Dr. Thorstern Thiergart for helping me analyze microbial profiling data and helping me solve some errors. I would like to thank Dr. Nathan Vannier for helping me with the data model and providing me helpful suggestions. I would like to thank Fantin Mesny for helping me with the microbial data analysis and helpful suggestions. I would like to thank Brigitte Pickel for helping measure leaf traits. I would like to thank Dr. Christopher J. Harbort and Dr. Anthony Piro for helping me improve my English. I would like to thank Dr. Zhou Bo, Dr. He Gao, Dr. Yi Wang, Dr. Jingde Qiu, and Dr. Dmitry Lapin for helpful suggestions in my experiments. I would like to thank Dr. Yulong Niu, Dr. Wenbiao Jiao, Dr. Qichao Lian and Dr. Xiangchao Gan for helpful suggestions of data analysis. I would like to thank Dr. Rainer Birkenbihl for providing useful experimental stuff, helpful suggestions, and translating my thesis abstract to German.

Finally, I would like to thank my families for the support and encouragement. 感谢父母对我的理解与支持。感谢亲朋好友的鼓励和支持。

Erklärung zur Dissertation

Erklärung zur Dissertation
gemäß der Promotionsordnung vom 02. Februar 2006 mit den Änderungsordnungen vom 10. Mai 2012, 16. Januar 2013 und 21. Februar 2014

Diese Erklärung muss in der Dissertation enthalten sein

"Ich versichere, dass ich die von mir vorgelegte Dissertation selbständig angefertigt, die benutzten Quellen und Hilfsmittel vollständig angegeben und die Stellen der Arbeit − einschließlich Tabellen, Karten und Abbildungen −, die anderen Werken im Wortlaut oder dem Sinn nach entnommen sind, in jedem Einzelfall als Entlehnung kenntlich gemacht habe; dass diese Dissertation noch keiner anderen Fakultät oder Universität zur Prüfung vorgelegen hat; dass sie − abgesehen von unten angegebenen Teilpublikationen − noch nicht veröffentlicht worden ist, sowie, dass ich eine solche Veröffentlichung vor Abschluss des Promotionsverfahrens nicht vornehmen werde.
Die Bestimmungen der Promotionsordnung sind mir bekannt. Die von mir vorgelegte Dissertation ist von (*Name des anleitenden Dozenten oder der anleitenden Dozentin*) betreut worden."

Teilpublikationen:

Datum / Unterschrift 08.10.2020 Shyi Shou

Curriculum vitae

SHIJI HOU

CONTACT

Email
hou@mpipz.mpg.de

Phone
+49015908184771

Home
Ingendorfer Weg 34
50829 Cologne Germany

SKILLS

Biology:
DNA&RNA manipulation,
DNA library construction,
Real-time Quantitative PCR,
Protein extraction,
Chromatin immunoprecipitation

Bioinformatics:
R language,
Python language

Software:
Adobe Illustrate,
Adobe Photoshop,
Image J,
Microsoft Office

LANGUAGE

Mandarin: native language
English: IELTS 6.5
German: A1 level

EDUCATION

MASTER DEGREE University of the Chinese Academy of Sciences
Sep 2013 – Jun 2016 Master of Science in Ecology

BACHELOR DEGREE China Agricultural University
Sep 2009 – Jun 2013 Bachelor of Science in Agriculture

EXPERIENCE

International Conferences:

- 2018 Dec 4 – 6, International Phytobiomes Conference, Montpellier, France

Selected speaker talked about "the root microbiota coordinates trade-offs between shade and immune responses in *Arabidopsis*"

- 2019 Jun 16 – 21, the 30th International Conference on Arabidopsis Research, Wuhan, China

Selected speaker talked about "Root microbiota coordinates trade-offs between shade and immune responses in *Arabidopsis*"

Projects:

- Root microbiota functions in mitigating abiotic and biotic stresses in *Arabidopsis* (2016 – now)
- The ecological role of AMF in plant resistance to drought stress and the underlying mechanisms (National Natural Science Foundation of China, 41371264) (2014 – 2016)
- Diversity and multifunction of AM fungi in typical fragile ecosystems in North China (Chinese Academy of Sciences program, KZCX2-YW-BR-17) (2013 – 2014)
- The physical and chemical properties of humic acid and its effect on phosphorus availability in acid soil (2012 – 2013)

HONORS & AWARDS

2013 – 2016 Second Prize Scholarship, Chinese Academy of Sciences
2012 National Scholarship, China
2010 – 2012 First Prize Scholarship, China Agricultural University